Sleep control by TFAP2a and TFAP2b transcription factors in mice

Dissertation

for the award of the degree

‘‘Doctor rerum naturalium’’

(Dr. rer. nat)

of the Georg-August-Universtät Göttingen

within the doctoral program *Systems Neuroscience*

of the Georg-August-University School of Science (GAUSS)

submitted by

Yang Hu

from Xinjiang, China

Göttingen 2021

Thesis Committee Members

Prof. Dr. Henrik Bringmann	Biotechnology Center
(1st Reviewer)	Technical University of Dresden
Prof. Dr. Thomas Bayer	Division of Molecular Psychiatry
(2nd Reviewer)	University Medical Center Göttingen
Prof. Dr. Dr. Hannelore Ehrenreich	Clinical Neuroscience
	Max Planck Institute of Experimental Medicine, Göttingen

Examination Board Members

Prof. Dr. Gregor Eichele	Dept. of Genes and Behavior
	Max Planck Institute for Biophysical Chemistry, Göttingen
Prof. Dr. Klaus-Armin Nave	Dept. of Neurogenetics
	Max Planck Institute of Experimental Medicine, Göttingen
MD/PhD Arezoo Pooresmaeili	Research Group Perception and Cognition
	European Neuroscience Institute, Göttingen

Date of oral examination: 14.02.2022

Contents

Abstract

Sleep is a universal behavior that exists across species. We previously found that deletion of transcription factor *APTF-1* induces sleep loss in *C. elegans* and *Drosophila*. In mammals, sleep has two states: rapid eye movement sleep (REMS) and non-REM sleep (NREMS), which can be distinguished by EEG spectral power. There are five homologs of *APTF-1* in mammals, from *Tfap2a* to *e*. However, little is known about whether these homologs, *Tfap2a* and *b*, have a conserved role of regulating sleep in animals with a more complex brain. Therefore, I characterized the sleep and wakefulness of *Tfap2a* and *b* mutants in mice. Consistent with our previous finding, paralogs of *Tfap2a* and *b* control sleep in mice. However, *Tfap2a* and *b* control sleep in a bidirectional manner. EEG results showed that *Tfap2a*$^{+/-}$ mice exhibited higher sleep drive, whereas *Tfap2b*$^{+/-}$ mice showed a reduced sleep quality with shortened NREMS amount during baseline recording. As expected, sleep deprivation induced a stronger delta and theta power rebound in *Tfap2a* mutants, but a weaker response in *Tfap2b* mutants. This functional divergence was also observed in behaviors beyond sleep. *Tfap2b*$^{+/-}$ mice displayed depression-like behavior while *Tfap2a*$^{+/-}$ mice were hyperactive and showed more resistance to the stressful environment. With the decreased sleep quality, learning and memory were impaired in *Tfap2b* mutants. In addition, *Tfap2b* mutants exhibited a slightly shortened circadian period. In summary, *Tfap2a* and *b* control sleep in mice as well, but in a bidirectional way. It might support the hypothesis that, as nervous system evolved, the function of *Tfap2a* and *b* genes also diverged.

GABAergic neurons play a key role promoting sleep. The development of GABAergic neurons is regulated by various transcription factors. However, it is not clear whether or how *Tfap2a* and *b* are involved in the expression and function of GABAergic neurons. Here I measured the expression of the genes that control GABA synthesis and transportation in *Tfap2a*$^{+/-}$ and *Tfap2b*$^{+/-}$ mice. Results from qPCR has confirmed a role of *Tfap2b*, but not *TFap2a*, in regulating the GABAergic gene expression. However, the role of *Tfap2b* was complex. The expression of GAD65, GAD67, Vgat was decreased in cortex, brainstem, cerebellum, but increased in striatum. Further, using ISH, a decrease number of the GAD67 expressing GABAergic cells was detected in the parafacial zone, a sleep-promoting center located in the lower brainstem. Since the expression of *Tfap2b* in brain starts early at developmental stages, E14.5 brains were extracted and analyzed using RNA-seq. Results have revealed various differentially regulated genes from homeobox, *Slc* family and those related to neurotransmission function. Together with qPCR and ISH results, they provided molecular evidences implying a functional role of GABAergic neurons expressing *Tfap2b* gene. Next, I characterized the function of GABAergic neurons expressing *Tfap2b* in sleep in *Vgat-Tfap2b*$^{-/-}$ mice. EEG analysis showed that sleep quantity and intensity were reduced in female *Vgat-Tfap2b*$^{-/-}$ mice during baseline recording. Consistent with this observation, the homeostatic sleep response was also weakened in these mutants. These results

together suggest that *Tfap2b* plays a role in the GABAergic system at molecular and behavioral functional level.

In conclusion, my study has revealed a conserved role of *Tfap2b* and its paralog *Tfap2a* in sleep control. It is very likely that *Tfap2b* exerts its conserved function in sleep through GABAergic system.

1. Introduction

Sleep is many things. It is a behavioral state that animals in sleep maintain a distinct posture, stay inactive but are ready to wake up. Sleep is a neural concert that the conductor of neurons is active leading everyone else asleep in synchronized oscillation. Sleep is a physiological stage that mammals dream and twitch from time to time. Invoking a metaphor from Blumberg *et al.* [1], are these components of sleep like the varied tools in a Swiss army knife gathered in the same place, a gene and/or a brain area?

Over the evolutionary course, components of sleep expand from simple behaviors to complex physiological oscillations [2]. Genetics is the key to understand the common elements of sleep control shared between vertebrates and invertebrates [3]. Homeostatic regulation of sleep is a conserved function that sleep deprivation in *C. elegans* and mice can induce a rebound sleep to compensate for the lost [4, 5]. In the simple model of *C. elegans,* which has only 302 neurons, sleep behavior can be turned off either through deleting *APTF-1*, a transcription factor gene, or inactivating the GABAergic RIS neuron [6]. As sizes and complexity of nervous system grow, little is known about how the function of this conserved transcription factor evolved to support a more complex mammalian sleep.

1.1 NREM and REM sleep

In 1953, Aserinsky and Kleitman have reported a special state of sleep in humans where the electrooculograms (EOG) showed rapid, biocularly symmetrical eye movements [7], which is termed as rapid eye movement (REM) sleep. Since the discovery of the REM sleep, the two distinct sleep states have been defined in many other mammals and birds [8-10]. Nowadays, it is well accepted that the main physiological vigilance states in homeotherms are wakefulness, non-REM sleep (NREMS) and REM sleep (REMS) [10].

Mammals sleep in very different architectures. Sleep intensity (or depth), quantity, timing, stability are important measurements characterizing the sleep architecture [11]. Humans exhibit continuous monophasic sleep that, during a typical night, we cycle through all stages of NREMS and REMS 3-5 times with each cycle approximately 90 min [12, 13]. Mice are nocturnal animals that sleep in a discontinuously polyphasic architecture. In laboratory conditions (light-dark cycle of 12h : 12h), both wild-caught [14] and lab-bred *M. musculus* [5, 14, 15] sleep discontinuously for ~12.5h in total and shift through sleep-wake states in a 24-h day with most of the sleep states occurring in light phase [5]. In humans, NREMS can be further divided into 3 stages, N1 to N3, ranging from the lightest sleep in N1 to the deepest sleep in N3. Human-like sleep stages have been revealed in mice in a few studies [16, 17], but whether these stages have a physiological relevance remains to be explored. NREMS in mice, equivalent to human deep NREMS, is also termed as slow-wave sleep (SWS), with high-amplitude, low-frequency oscillations as the dominant spectral power state.

Studies in mammalian sleep rely heavily on monitoring physiological changes in cortical activity [18, 19]. In humans, a non-invasive scalp electroencephalogram (EEG) together with electromyogram (EMG) and EOG remains to be the essential method [19]. In mice, EEG signals are collected by electrodes implanted over the frontal/parietal cortex and EMG signals by a wire inserted into the neck muscle [18]. Slow and strong delta EEG power around 0.5-4Hz exists throughout the NREMS period in mice with a quiet muscle tone, whereas, in humans, slow wave activity (SWA) occurs only in the N3 deep sleep stage. Mouse REMS has a slow rhythmic theta wave ranging from 5-10Hz with musde atonia, but human EEG showed similar pattern to that of wakefulness where brain waves with low amplitude fast or mixed frequency exist [18, 19]. While REM and NREM sleep are clearly defined in birds and mammals, components of NREMS and REMS have also been identified in reptiles and jellyfish [20, 21].

EEG activity can occur in different time and space within the same brain during sleep. Birds share largely similar electrophysiological features of the two sleep states with mammals [22]. Based on EEG recording, unihemispheric NREMS (sleeping with one cerebral hemisphere at a time) or asymmetric NREMS (deeper within one hemisphere than the other) was described in birds [23]. Later, this phenomenon was also reported in marine mammals like dolphins. Even humans and mice that have symmetric sleep show spatiotemporal desynchronizations in sleep EEG [24, 25]. For example, anterior power in the NREMS EEG is predominant in lower-frequency power compared with that of posterior derivations [26]. Therefore, in this study, I collected EEG signals from both frontal and temporal areas of the same murine cortex (**Fig. 1**).

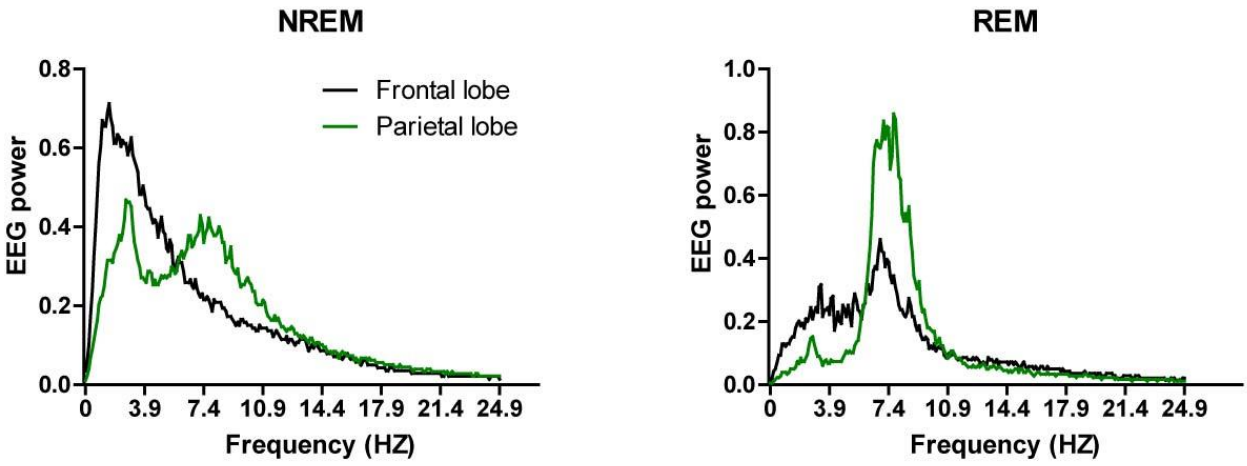

Figure 1. Example of EEG spectral power intensity in sleep.

EEG power spectra from frontal and parietal cortex recordings of a wild type mouse during NREMS (left) and REMS (right) in a 24-h day.

1.2 Regulations of Sleep

In 1982, Alexander Borbely proposed a two processes model that sleep is regulated through a homeostatic process (Process S) and the circadian oscillator (Process C) by studying human sleep architecture [27]. Process C determines the timing of sleep. For example, in humans, the light promote wake and night promotes sleep. Process S simulates the sleep pressure (or sleep need), which accumulates during the wakefulness and dissipates during sleep. The dynamics of the Process S is best characterized by the spectral analysis of SWA during sleep. Delta power accumulates proportionally to the duration of prior wakefulness [28], and progressively declines throughout the sleep period [29]. These two processes have been successfully applied in vertebrates with circadian system. When disentangled [30], based on the behavior to Process S, the dynamics of sleep was also interpreted in invertebrates under baseline level and after sleep deprivation (SD).

Sleep intensity is positively correlated with sleep pressure. In humans and mice, SWA or delta power is a metric of sleep intensity and homeostatic sleep respond. Delta power can be locally expressed within the same brain. In mice, within the overall vigilance state of NREM, delta signals (approx. 0.5 – 4Hz) derived from the frontal cortex is more intense than that from the somatosensory cortex [31]. On the contrary, under REM state, theta oscillation (approx. 5 – 10Hz) is more powerful in somatosensory cortex. Consistent with this observation, in my experiment, a stronger delta power derives from frontal EEG signal than parietal recording; and a higher theta oscillation from parietal electrodes (**Fig. 1**). The sleep pressure depends on the level of wakefulness that delta oscillation accumulates during baseline waking hours and increases further as the wakefulness prolongs [27]. The extension of waking hours is termed as sleep-deprived hours and the increased power of delta wave after SD is termed as a rebound of the delta power. For example, in humans on a 24-h baseline scale, sleep pressure is the highest before sleep onset [27]. After 12 to 36 hours of sleep deprivation, the power intensity in low frequency bands increases massively [28].

1.3 Methodology of sleep deprivation

Sleep deprivation refers to keep the subject awake when it shows signs of falling asleep. It is widely used in studies of the homeostatic regulation in sleep [32-34]. SD protocols defer in terms of length, frequency, stimuli, type of sleep state affected.

In humans, acute SD can be applied ranging from a few hours to a few days within healthy individuals to study sleep homeostasis. Total SD of ~72 hours is considered to have anti-depressant effect that it has been applied to treat patients with a major depressive disorder [35, 36]. However, chronic SD, as observed in patients having sleep disorders, links to a wide range of pathological symptoms, like Parkinson's disease, Attention-Deficit Hyperactivity Disorder (ADHD), as well as psychiatric disorders [37-39]. Similarly, chronic SD can also lead to long-term impairments in mouse behavior [40].

Procedures used to keep rodents awake include treadmills/rotating wheels, flowerpot and gentle handling. Major advantages and disadvantages of these methods were discussed in this review [41]. Further, treadmills and rotating wheels are based on forced locomotion, which might induce metabolic changes on top of sleep deprivation [42]. Flowerpot method requires animals to maintain wakefulness to remain on a platform, if not they fall into the water. These methods include forced locomotion, aversive stimulus or a combination of both. They are highly efficient strategies for an unsupervised SD but are more stressful to the animal compared to gentle handling, which can be applied in both chronic or acute SD for mouse pups [43] and adults. In this study, I aimed to apply the least stressful method to restrict total sleep while keeping its ability to induce a sleep rebound.

An acute SD of 6 h with gentle handling (GH) is considered to be the least stressful way to study the homeostatic sleep rebound. Such SD protocol usually starts after the lights-on when the sleep pressure is the highest to ensure a maximum efficiency. In mice, a 4-h SD by GH is enough to induce a rebound effect in REMS, whereas NREMS requires longer duration SD of at least 6h to ensure a rebound effect in commonly used mouse strains [5]. From the perspective of delta power intensity, the duration of acute SD seems to reach its upper limit after 6 h (approximately 55%). Longer restriction (e.g., 10h [5]) does not produce further delta power increased. A 6-h-SD procedure with GH is reported to have no significant effect on anxiety-like behavior [42], and evokes antidepressant effects [44]. While it has been reported to induce deficits in learning and memory, but these deficits are often reversible on a behavioral and molecular level within few hours of recovery sleep [45]. Therefore, in this study, I used 6-h-SD with GH protocol to investigate the homeostatic regulation of sleep with the smallest disruptions possible to other biological functions.

1.4 Genetic control of sleep

Sleep pattern is highly inheritable. Monozygotic twins share more similarities in sleep architecture such sleep quantity, EEG spectra, sleep timing than dizygotic twins [46]. Recently, studies based on family linkage analysis and genome-wide association studies (GWAS) reveal a conserved role of genes involved in sleep regulation across species. In familial natural short sleepers (FNSS), who need 4-6 hours of sleep, a point mutation in *ADRB1* gene has been identified to contribute to the short sleep feature. Consistent with the human phenotype, mice carrying the same mutation (*Adrb1–A187V*) also exhibit shorter sleep [47]. Similarly, a conserved role has also been identified for *Dec2* gene in human, mice and *Drosophila* [48].

Mice, sharing ~85% identity with human genome, display similar sleep states and EEG features to human sleep. Therefore, mouse models are important in studying the function of sleep genes. From the studies of genetic knockouts in mice (**Fig. 2**), it is implied that one gene can control different components of sleep and each component can be affected by multiple genes. The genetic control of one gene alone seems to be partial. For example, in terms of sleep quantity, genes affect around 10% to 30% of total sleep time. However, as sleep is crucial for survival, complete SD could lead to death of an animal [49]. Thus, it is also very likely that genes affect greater portion of sleep are also detrimental to survival when knocked down completely from an animal.

Circadian genes play a major role regulating the timing of sleep. Deletion of *Bmal1* [50] or *Vipr2* [51] completely disrupts the rhythm of sleep and T44A mutation of *CK1D* leads to advanced sleep phase syndrome [52]. Arrhythmic *Cry1/2* $^{-/-}$ mice exhibit faster sleep-wake cycles and more fragmented sleep [53]. Further, an altered circadian rhythm can also negatively affect components of sleep other than sleep timing. For example, arrhythmic *Per1/2* [54] knockouts, long period *Clock* $^{\Delta 19/\Delta 19}$ mutants [55], short period *Npas2* $^{-/-}$ mice [56], *Prok2* $^{-/-}$ mice[57] with attenuate circadian amplitude, all these mutations result in reduced NREMS time and an altered sleep rebound.

Serotonin, dopamine, norepinephrine (NE), orexin are main neurotransmitters/neuropeptide involved in arousal. Consistently, decreased NREMS is observed in *5-HT2c* [58] and *5-HT2a* [59] knockouts or *DAT* $^{-/-}$ mice [60, 61] which display elevated extracellular dopamine concentration. On the contrary, NREMS is increased in mice deprived of NE [62]. Although the overall sleep time in Orexin $^{-/-}$ mice[63] does not change, but these mutants showed sleep fragmentation (similar to *Dhc* $^{-/-}$ mutants[63, 64]) and narcolepsy when exposed to motor exercise.

Interestingly, compared with broad effects of circadian, neurotransmitter genes have imposed on sleep architecture, genes related to ion channels are targeting on slow wave EEG power, which is a marker of sleep homeostasis. Deletion of specific subunit in potassium channel (*Sk2*$^{-/-}$ [65]) or calcium channels (*Cacna1b* [66]; *Cacna1g* [67]) does not induce massive change in sleep quantity but lead to decreased NREMS power (marker of sleep homeostasis) and, therefore, less consolidated sleep.

A qualified sleep is important to the well-functioning of immune system, memory consolidation process and metabolism [68]. Reversely, genes associated with these functions also affect sleep behaviors. Mice lack of immune factors (TNF-a or IL-1b [69]), or are resistant to Leptin [70], growth hormone releasing hormone (GHRH) [71] have reduced sleep. Interestingly, increased NREMS was observed in mice lacking the α and Δ isoforms of CREB, which play an important role regulating memory consolidation [72]. This reflects a shared pathway between sleep and immune response/ memory/ metabolism.

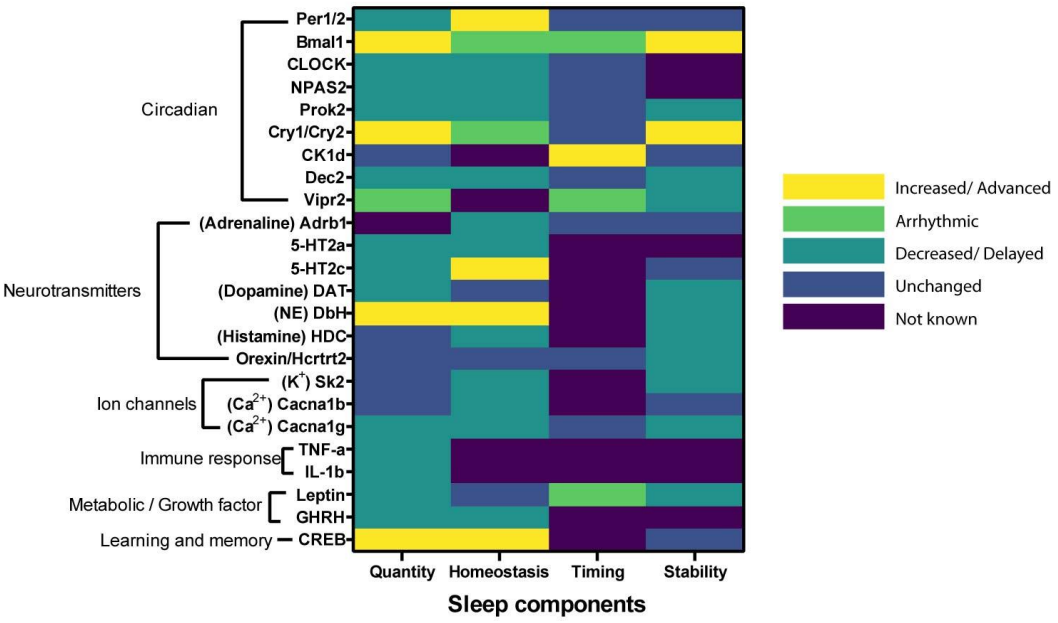

Figure 2. Heatmap of genes that control sleep with a focus on NREMS changes.

Genes were listed along the y-axis with their biological/cellular function added to their left side. Four components characterizing NREMS changes were listed along the x-axis. Legend to the right side described colors indicating changes of quantity/ homeostasis (marker: α wave power) / stability that were increased, arrhythmic (e.g. increased in light phase, but decreased in dark phase), decreased, unchanged or unknown; the legend also indicated the timing of sleep as advanced/ delayed NREMS onset, or with an arrhythmic schedule. All data were collected from literatures of mouse studies using homozygous knockout or point mutation, except for *CK1D*, which was from human studies.

1.5 Sleep-promoting brain areas

1.5.1 Preoptic area

Von Economo found that the damage in posterior hypothalamus area lead to insomnia 90 years ago, tremendous work has been made to find the central control of sleep ever since [73]. Seventy years later, a flip-flop model was proposed [74] and modified [75] to describe a brain circuitry that allows the organism (humans as the example) to switch between sleep and wakefulness. In the flip-flop model, the preoptic area (POA, **Fig. 3**) plays a key role in sleep-promoting circuitry whereas the lateral hypothalamus (LHA) is crucial for maintaining wakefulness [75]. Sleep-active GABAergic neurons [76, 77] in POA project to histaminergic tuberomammilary nucleus (TMN) in the LHA to inhibit wake active neurons and, therefore, promote sleep [78]. As expected, POA also has inputs from the arousal system [79] rendering the spatially intermingled and diffused expression of the sleep-promoting and the wake-promoting neurons [80]. POA is a functionally and molecularly heterogeneous area, for example, the sleep-active galaninergic neurons in ventrolateral preoptic nucleus (VLPO) also express glutamic acid decarboxylase (GAD) [78]. Within POA, VLPO has a denser expression of sleep-active neurons [81]. Studies have confirmed the sleep-promoting function of GABAergic neurons in POA that project to TMN [82] and galanin producing neurons in VLPO [83]. Although the neurotransmitters responsible for the mammalian sleep-promoting function remains elusive, a recent study in zebra fish larve reported that galanin is required in modulating sleep homeostasis [84]. Additionally, in search of a central commander of sleep, the inhibition of these sleep-active galaninergic neurons and lesions of VLPO reduce sleep of approximately 50% [83, 85]. Lesions of bilateral POA have produced sleeplessness in two cats, but with a large scale and severe (in some cases lethal) impairment upon other biological functions, such as motor function, sensory, temperature regulation, feeding behavior [49].

1.5.2 Parafacial zone

Parafacial zone (PZ), located in the medullary brainstem (**Fig. 3**), lies lateral and dorsal to the 7th facial nerve [86]. PZ is recognized as a delimited node of sleep-active neurons sending projections into medial parabrachial nucleus (MPB [87] , one of the pontine arousal systems) [86]. GABAergic cell-body-specific lesion in mouse PZ has induced a sustaining decrease in total sleep amount of around 40% without changing the sleep timing [86]. Chemogenetic activation of GABAergic neurons in PZ area promotes SWS with increased SWA and a more consolidated SWS bout length but not timing [88]. Further, the SWS sustaining effect is strong enough to counteract the wake-promoting effect of armodafinil [89], a psychostimulant used to treat narcolepsy.

1.5.3 Ventrolateral tegmental nucleus

Ventrolateral tegmental nucleus (VTA), locates in the ventral midbrain (**Fig. 3**), has a complex role in sleep-wake regulation. VTA has been considered as wake-promoting area for a long time because of the large presence of wake-promoting [90] or REMS-active [91] dopaminergic neurons, but it has also been uncovered that the dopaminergic neurons projected to the dorsal striatum has sleep-promoting effect [92]. Moreover, VTA contains a large population of GABAergic neurons that selective ablation induces wakefulness and activation results in long-lasting NREMS with higher delta power [93-95]. However, although ablation of GABAergic neurons in VTA has induced sustainable sleep loss similar to that resulted from lesions of GABAergic PZ [86, 95], the ablation also results in mania-like behaviors in mice such as hyperactivity, high risk-taking behaviors, distractability [96].

1.5.4 Emerging sleep-promoting areas

Adenosine receptor A_{2A} expressing neurons in nucleus accumbens (NAc, locates in the ventral striatum, **Fig. 3**) regulates SWS amount and bout duration, but does not affect sleep rebound or SWA [97, 98]. Conditional deletion of the homeobox transcription factor *Lhx6* from GABAergic neurons in zona incerta (ZI, lateral hypothalamus **Fig. 3**) induced a mild decrease of sleep amount (~ 10%) as well as delta power [99]. GABAergic/inhibitory neurons seem to play the key role in NREMS-promoting as more NREMS-regulating regions have been revealed, such as rostromedial tegmental nucleus [100] and central nucleus of the amygdala [101]. Since sleep-promoting and wake promoting areas innervate each other, it is not surprising to find NREMS promoting SOM-positive GABAergic neurons in the arousal center of basal forebrain [102]. REMS promoting brain areas are concluded in this review [103], including sublaterodorsal nucleus (SLD), ventromedial medulla, dorsomedial hypothalamus and LHA.

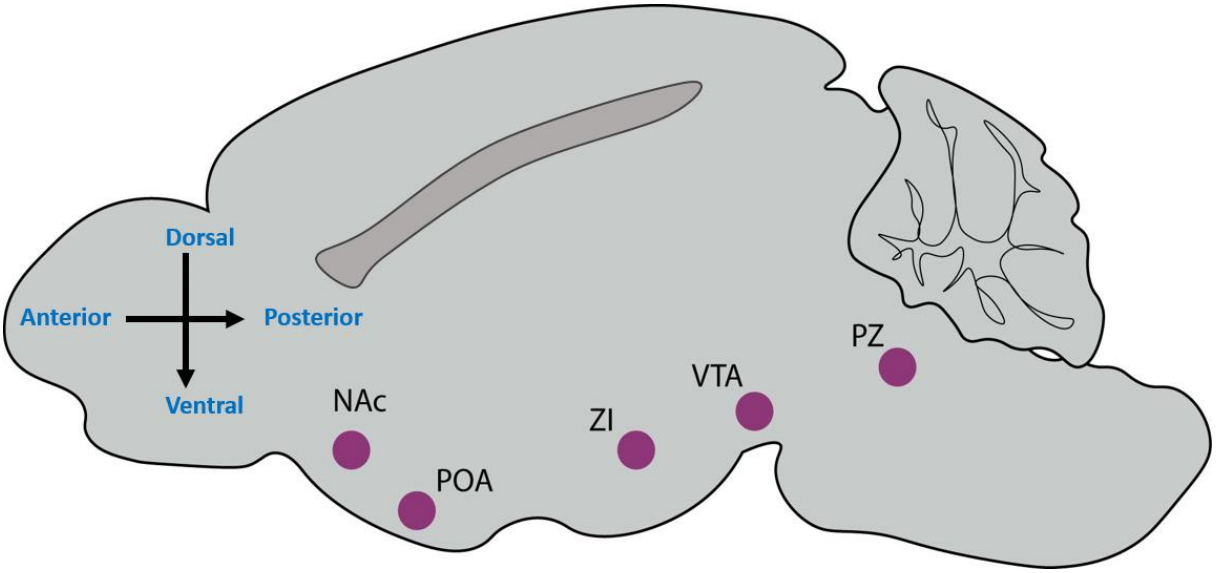

Figure 3. NREMS-promoting areas in adult mouse brain

NAc, nucleus accumbens; POA, preoptic area; ZI, zona incerta; VTA, ventrolateral tegmental nudeus; PZ, parafacial zone are marked in the graph.

1.6 AP-2 transcription factors

Transcription factor AP-2 family in mice and humans has five members from α to ε, each correspondently encoded by *Tfap2* genes from *a* to *e* [104]. AP-2 proteins consist of a transactivation domain rich in proline and glutamine at the amino terminus, a basic domain, a dimerization helix-span-helix motif at the carboxyl terminus [104]. The dimerization motif and the basic domain form the DNA binding site are highly conserved [105].

AP-2 proteins are crucial in neural crest cell, epidermal development, germ cell induction [106, 107]. In mouse, AP-2 proteins express early in neural crest (E9.5) and have rather restricted distribution in the head, peripheral nervous system and limbs [108, 109]. AP-2α, β, γ have overlaps in in the facial area, AP-2a and b in midbrain and hindbrain. AP-2α and β have prominent expression in diencephalon, midbrain, hindbrain from embryo (E11.5) to juvenile (P28) [Allen Developing Mouse Brain Atlas, Gene paint]. AP-2δ is almost exclusively but very diffusely expressed throughout the midbrain [109]. *Tfap2e* expression was restricted to the developing olfactory bulb from E11.5 to an undetectable level in P14 [110], which made this gene a less promising candidate for sleep regulation. I focused on *Tfap2a* and *b* because of their abundant expression in the midbrain/hindbrain which become brainstem where sleep-promoting centers locate [86]. Deletion of *Tfap2d* produces viable animals [111], whereas deletion of either *Tfap2a* or *b* is perinatal-lethal [112, 113]. Therefore, we used heterozygous deletion of *Tfap2a* and *b*, as partial mutations of these genes result in detectable phenotypes. For example, two families with heterozygous loss of *Tfap2b* have CHAR syndrome (CHAR, OMIM#169100) [114].

As *Tfap2a-Tfap2b* heterodimer promotes neuro crest specification [115], the function of AP-2a and AP-2b has been extensively investigated in the peripheral system of mammals. Deletion of *Tfap2* paralogs causes abnormalities in craniofacial, renal, retinal function and they play a key role in sympathetic nervous system development [112, 113]. Patients carries *Tfap2b* mutation have mild abnormalities in anterior body patterning, such as facial dysmorphism and shortened or absent 5th finger [116]. Except for typical syndromes of heart, face, limbs abnormalities, they are also reported to have parasomnia symptoms [114]. Our previous studies showed that *Tfap2* homologs in *C. elegans* and *Drosophila* control sleep behavior [6, 117]. Therefore, I explored the molecular change in *Tfap2a* and *b* mutant brain from both embryo and adult mouse using RNA-seq. Since GABAergic neurons play a major role regulating sleep in the brainstem sleep centers, expression of GABAergic genes was quantified using qPCR and ISH within specific brain areas.

1.7 Amis of this project

Sleep can be described in behavioral and electrophysiological terms. Behavioral sleep is universal in the animal kingdom, while electrophysiological sleep has only been defined in homeothermic vertebrates. Our previous studies showed that *APTF-1* deletion results in sleep loss in *C. elegans*, this gene is conserved in mammals where there are 5 subtypes (*Tfap2b* to *e*). Thus, further validation is required through genetic studies in mammals, like mouse, which allow the study of a complex brain. This could also be beneficial since the involvement of both REM and NREM states in a mouse model. Moreover, this may shed light on the evolution of sleep.

Aim 1 - Validate and characterize function of *Tfap2a* and *Tfap2b* in mice on a molecular and behavioral level to elucidate if they have implications on sleep circuitry

To achieve the first goal, I used heterozygous knockout mouse lines of *Tfap2a* and *Tfap2b* to characterize: (1) biophysical features of sleep by EEG/EMG recordings combined with sleep deprivation experiments; (2) circadian, behavioral psychological and cognitive features of these mouse lines; (3) gene expression patterns in brain using RNA-seq.

Aim 2 – Investigate how *Tfap2b* affect GABAergic system

GABAergic neurons play an essential role promoting sleep in mammals. My previous study has confirmed a role of Tfap2b in the shortened sleep phenotype. Thus, the next focus of my thesis is to study the correlation between *Tfap2b* and GABAergic system. To achieve this second goal, I aimed (1) to investigate the GABAergic gene expression using RT-qPCR in *Tfap2b*$^{+/-}$ adult mouse brain; (2) to analyze the distribution of GABAergic neurons in the sleep promoting parafacial zone using ISH; (3) to examine gene expression pattern in developing mutant brains.

Aim 3 – Explore whether deletion of *Tfap2b* in GABAergic neurons affect sleep

Based on the previous results revealing that deletion of *Tfap2b* affected the GABAergic gene expression, I determined to test its function in sleep behavior. To achieve this third goal, I aimed (1) to generate a mouse line with *Tfap2b* specific knockout in GABAergic neurons (2) characterize the sleep behavior using EEG/EMG recordings combined with sleep deprivation experiments.

2. Results

2.1 Part 1: Publication

All results from this part was published in:

Hu, Y., Korovaichuk, A., Astiz, M., Schroeder, H., Islam, R., Barrenetxea, J., Fischer, A., Oster, H., and Bringmann, H. (2020). Functional Divergence of Mammalian TFAP2a and TFAP2b Transcription Factors for Bidirectional Sleep Control. Genetics *216*, 735-752.

DOI: https://doi.org/10.1534/genetics.120.303533

Functional Divergence of Mammalian TFAP2a and TFAP2b Transcription Factors for Bidirectional Sleep Control

Yang Hu,* Alejandra Korovaichuk,* Mariana Astiz,† Henning Schroeder,‡ Rezaul Islam,‡ Jon Barrenetxea,* Andre Fischer,‡,§, Henrik Oster,† and Henrik Bringmann*,††,‡‡,1**

*Max Planck Research Group "Sleep and Waking", Max Planck Institute for Biophysical Chemistry, Göttingen 37077, Germany, †Institute of Neurobiology, University of Lübeck, 23562, Germany, ‡German Center for Neurodegenerative Diseases, Göttingen 37075, Germany, §Department for Psychiatry and Psychotherapy, University Medical Center, Göttingen 37075, Germany, **Cluster of Excellence "Multiscale Bioimaging: from Molecular Machines to Networks of Excitable Cells" (MBExC), University of Göttingen, 37073, Germany, ††Department of Animal Physiology/Neurophysiology, Philipps University Marburg, Marburg 35043, Germany, and ‡‡BIOTEC of the Technical University Dresden, Dresden 01307, Germany

ORCID IDs: 0000-0002-2515-4458 (Y.H.); 0000-0001-9912-1686 (M.A.); 0000-0002-1414-7068 (H.O.); 0000-0002-7689-8617 (H.B.)

ABSTRACT Sleep is a conserved behavioral state. Invertebrates typically show quiet sleep, whereas in mammals, sleep consists of periods of nonrapid-eye-movement sleep (NREMS) and REM sleep (REMS). We previously found that the transcription factor AP-2 promotes sleep in *Caenorhabditis elegans* and *Drosophila*. In mammals, several paralogous AP-2 transcription factors exist. Sleep-controlling genes are often conserved. However, little is known about how sleep genes evolved from controlling simpler types of sleep to govern complex mammalian sleep. Here, we studied the roles of *Tfap2a* and *Tfap2b* in sleep control in mice. Consistent with our results from *C. elegans* and *Drosophila*, the AP-2 transcription factors *Tfap2a* and *Tfap2b* also control sleep in mice. Surprisingly, however, the two AP-2 paralogs play contrary roles in sleep control. *Tfap2a* reduction of function causes stronger delta and theta power in both baseline and homeostasis analysis, thus indicating increased sleep quality, but did not affect sleep quantity. By contrast, *Tfap2b* reduction of function decreased NREM sleep time specifically during the dark phase, reduced NREMS and REMS power, and caused a weaker response to sleep deprivation. Consistent with the observed signatures of decreased sleep quality, stress resistance and memory were impaired in *Tfap2b* mutant animals. Also, the circadian period was slightly shortened. Taken together, AP-2 transcription factors control sleep behavior also in mice, but the role of the *AP-2* genes functionally diversified to allow for a bi-directional control of sleep quality. Divergence of AP-2 transcription factors might perhaps have supported the evolution of more complex types of sleep.

KEYWORDS TFAP2; sleep; behavior; EEG; *Mus musculus*

SLEEP is a fundamental state that is defined by behavioral criteria that include the absence of voluntary movement, an increased arousal threshold, relaxed body posture, reversibility, and homeostatic regulation (Campbell and Tobler 1984). By these criteria, sleep has been identified not only in mammals, but also in other vertebrates as well as in invertebrates (Campbell and Tobler 1984; Tobler 1995; Joiner 2016; Bringmann 2018; Keene and Duboue 2018). Sleep in invertebrates is characterized mostly as quiet sleep, with a reduction of neuronal and behavioral activity (Raizen and Zimmerman 2011; Miyazaki *et al.* 2017). In the more complex brains of mammals, two major stages of sleep have been defined. Rapid eye movement sleep (REMS) is characterized by a relatively active brain and muscle paralysis and is also called active sleep. Non-REM sleep (NREMS) is a type of quiet sleep characterized by a strong reduction of brain and muscle activity (Campbell and Tobler 1984). This suggests that sleep appeared first in evolution as a type of quiet sleep

doi: https://doi.org/10.1534/genetics.120.303533
Manuscript received April 29, 2020; accepted for publication July 20, 2020; published Early Online August 7, 2020.
Available freely online through the author-supported open access option.
Supplemental material available at figshare: https://doi.org/10.6084/m9.figshare.12738545.v1.
[1]Corresponding author: Max Planck Research Group Sleep and Waking, Max Planck Institute for Biophysical Chemistry, 37077 Göttingen, Germany. E-mail: Henrik.Bringmann@mpibpc.mpg.de

and then diversified into two types of sleep, which are manifested as NREMS and REMS in mammals (Miyazaki *et al.* 2017).

The molecular biology of sleep has been studied in all major genetic model animals such as mice, zebrafish, fruit flies, and nematodes (Joiner 2016; Miyazaki *et al.* 2017). Genetic analysis indicates that many genes play evolutionarily conserved roles in sleep control (Roberts and Hudson 2009). Thus, genes can be studied across model organisms to solve underlying molecular mechanisms of sleep regulation. For example, a gain-of-function mutation of salt-inducible kinase 3 (SIK-3) called *sleepy* increased NREM sleep in mice (Funato *et al.* 2016). Whereas a loss-of-function mutation of *SIK-3* is lethal in mice, deletion of the *Caenorhabditis elegans SIK-3* homolog *KIN-29* is not lethal, but reduces sleep (Funato *et al.* 2016). It was shown that SIK-3 impacts sleep in *C. elegans* by controlling energy metabolism (Grubbs *et al.* 2019). We previously showed that knockout of the AP-2 transcription factor APTF-1 results in sleep loss in *C. elegans* (Turek *et al.* 2013). The AP-2 family of transcription factors is evolutionarily conserved in both invertebrates and vertebrates (Bringmann 2018). The basic and helix-span-helix (HSH) domains are necessary for DNA binding and dimerization functions, and are highly conserved among all TFAP2 orthologs and paralogues. The N-terminal portion of the protein contains the transactivation domain, which has an amino acid sequence that is poorly conserved among the AP-2 proteins (Williams and Tjian 1991).

AP-2 transcription factors are best known to control ontogenetic processes such as the development of face, limbs, and organs (Moser *et al.* 1997b; Werling and Schorle 2002; Zhao *et al.* 2003; Lin *et al.* 2018). We showed that, in *C. elegans*, APTF-1 is required for the functioning of the sleep-inducing RIS (Ring Interneuron S) neuron. Without APTF-1, crucial sleep-inducing neuropeptides are not expressed in RIS, and, thus, sleep is virtually abolished (Turek *et al.* 2013). Consistent with a conserved role in sleep control, neuronal knockdown of the sole AP-2 homolog in adult *Drosophila* almost completely abolishes night sleep but without affecting day sleep (Kucherenko *et al.* 2016).

In mammals, the AP-2 family consists of five paralogs, AP-2α–AP-2ε, encoded by genes *Tfap2a–Tfap2e*, respectively (Eckert *et al.* 2005). Here, we focus on *Tfap2a* and *b*, which are expressed prominently in neural crest cells starting around embryonic day 8 (E8) during early development of the central nervous system and are still detectable in adult brains (Chazaud *et al.* 1996; Moser *et al.* 1997b; Zhao *et al.* 2003). In humans, mutations affecting the basic domain in AP-2 can lead to the loss of function of these transcription factors. Heterozygous mutation of *Tfap2a* causes branchio-oculo-facial syndrome (BOFS; OMIM#113620) by a mechanism that mostly involves the loss of function of transcription factor activity (Li *et al.* 2013). BOFS is associated with multiple craniofacial abnormalities as well as eye, hearing, and skin defects. To our knowledge, no sleep abnormalities have been reported for BOFS individuals. Loss of *Tfap2a* causes severe developmental problems of the heart, brain, and skeletal systems leading to lethality (Schorle *et al.* 1996; Zhang *et al.* 1996; Brewer *et al.* 2004). *Tfap2a*$^{+/-}$ mice are viable and fertile. Heterozygous deletion is associated with mild developmental defects in craniofacial and brain development, providing a mouse model to study BOFS (Schorle *et al.* 1996; Zhang *et al.* 1996; Kohlbecker *et al.* 2002; Green *et al.* 2015). To our knowledge, *Tfap2a*$^{+/-}$ mice have not yet been tested for sleep abnormalities.

Heterozygous mutation of *Tfap2b* causes Char syndrome (CHAR, OMIM#169100) by either dominant negative or haploinsufficiency mechanisms (Satoda *et al.* 2000; Zhao *et al.* 2001; Mani *et al.* 2005). CHAR is characterized by developmental defects that include facial dysmorphism, abnormalities of the fifth finger, and failure of *ductus arteriosus* closure (patent *ductus arteriosus*, PDA) (Satoda *et al.* 1999). In two families with heterozygous loss of *Tfap2b* function, CHAR individuals showed self-reported sleep abnormalities. In the first family, sleepwalking was reported, whereas in the second family individuals reported shortened nocturnal sleep. However, the nature of these sleep changes remains unclear as these phenotypes were not confirmed using polysomnography (Mani *et al.* 2005). Homozygous deletion of *Tfap2b* in mice causes early lethality. By contrast, heterozygous deletion in mice causes PDA and fifth finger digit abnormalities but no obvious facial anomalies, providing a model of CHAR (Moser *et al.* 1997a; Satoda *et al.* 1999). However, sleep has not yet been studied in *Tfap2b*$^{+/-}$ mice.

AP-2 transcription factors have diverged in mammals to play nonredundant roles in development. In invertebrates, AP-2 plays a key role in sleep induction. Hence, AP-2 transcription factors provide a unique chance to study how sleep genes evolved from controlling simpler types of sleep in invertebrates to more complex types of sleep in mammals. Multiple hypotheses are conceivable for how AP-2 transcription factors may have evolved to control sleep. Three hypotheses may seem most plausible. (1) A sleep-promoting role might be present in one of the AP-2 paralogs, but such a role is not found in other AP-2 paralogs. (2) Multiple AP-2 paralogs might play a redundant role in promoting sleep. (3) Different AP-2 paralogs might serve specialized subfunctions in promoting sleep.

In this study, we studied sleep in *Tfap2a*$^{+/-}$ and *Tfap2b*$^{+/-}$ mice. Surprisingly, we found that *Tfap2a* and *Tfap2b* play opposing roles in sleep control. *Tfap2a*$^{+/-}$ causes an increase in sleep quality, and is also associated with hyperactivity during a stress test. By contrast, *Tfap2b*$^{+/-}$ reduces sleep time and quality and is associated with altered circadian rhythms, mildly depressive-like symptoms, and a learning defect. Thus, AP-2 transcription factors appear to have diverged to allow bidirectional control of sleep.

Materials and Methods

Animals

Neofloxed-*Tfap2a* conditional knockout mice were obtained from Trever Williams (Brewer *et al.* 2004) and bred with

CMV-Cre mice to delete exons 5–6 of *Tfap2a*. Mice that are homozygous for this allele were perinatal lethal in our colony probably due to neural tube closure defects and cleft secondary palate (Zhang *et al.* 1996). Thus, heterozygous mice (*Tfap2a*$^{+/-}$) were used in this study and their wild-type littermates (*Tfap2a*$^{+/+}$) were used as controls.

Tfap2b knockout mice were provided by Markus Moser [Max Planck Institute (MPI) for Biochemistry] with PGK-neo cassette inserted into exon four of the *Tfap2b* gene. *Tfap2b*$^{-/-}$ mice die shortly after birth due to polycystic kidney disease (Moser *et al.* 1997a). Thus, heterozygous mice (*Tfap2b*$^{+/-}$) were used in this study and their wild-type littermates (*Tfap2b*$^{+/+}$) were used as controls.

Adult (2–6 M) males were used in this study, except for the running-wheel test (see section *Wheel-running activity and circadian analysis*). Mice were kept at the animal facility of the MPI of Biophysical Chemistry in accordance to Lower-Saxony animal welfare laws. All animal experiments were carried out in compliance with the German Law on Animal Welfare and were approved by the Office for Consumer Protection and Food Safety of the State of Lower Saxony. All animal experiments were approved by the Animal Experiments Ethical Committee of the Max Planck Institute for Biophysical Chemistry (Göttingen, Germany) and Laves, and were carried out in accordance with European Union (EU) Directive 2010/63/EU on the protection of animals used for scientific reasons. Mice were entrained in a 12:12 hr light-dark cycle from 6:00 to 18:00. For the entire behavioral testing, adult male mice were singly housed with *ad libitum* access to water and food pellets, in controlled constant temperature and humidity. The animals were individually housed at least 1 week prior to the experiment.

Genotyping

Ear biopsies of mice were collected and genomic DNA was extracted through incubation in PBND lysis buffer (PCR buffer with nonionic detergents: 50 mM KCl, 10 mM Tris HCl pH 8.3, 2.5 M $MgCl_2$, 0.1 mg/ml Gelatin, 1 mg/ml proteinase K, 0.45% NP-40, 0.45% Tween) for at least 6 hr at 55°, followed by 45 min at 85° to deactivate the Proteinase K. Genotyping primers and conditions are listed in Supplemental material, Table S1.

Surgeries

Mice were anesthetized using isoflurane (1–2% in 100% O_2) during the surgery. Miniature screw electrodes (2.16 mm diameter, Bilaney Consultants GmbH) with wire (5 mm) attached were implanted. Two electrodes were placed over the right and left frontal cortex [anteroposterior (AP) +1.5 mm from bregma; mediolateral (ML) 1.7 mm). One electrode was placed over the right parietal (AP +1.5 mm from lambda, ML, 1.7 mm) cortex. Two electrodes were placed bilaterally over the cerebellum (AP -1.5 mm from lambda, ML, 1.7 mm) as reference (left) and ground signal (right). One subcutaneous electrode (12 mm, Bilaney Consultants GmbH) was placed in the nuchal muscle for the electromyogram (EMG) recording. All attached wires were assembled in a plastic pedestal (MS363, PlasticsOne, Bilaney Consultants GmbH), which was fixed to the skull with dental cement. The mice were housed individually and left to recover for at least 8 days before they were attached to the recording cable. Mice were given a 2-day acclimation period to adjust to the cable before recording.

Electroencephalogram recording setups and schedule

The recording room was kept under 12 hr light/12 hr dark cycles and room temperature. Light was delivered from ZT0 (6 AM) to ZT12 every day. All electrodes were gathered into a light weight and flexible cable and connected to the recording system (Multi Channel Systems MCS GmbH). Electroencephalogram (EEG) and Electromyography (EMG) signals were collected continuously at a sampling rate of 2000 Hz. To examine the sleep–wake behavior under the baseline conditions, the EEG/EMG recordings were performed for two consecutive days, beginning at ZT0. By the end of the baseline recording, all mice were sleep-deprived (Bernard *et al.* 2015) by gentle handling and novel object interaction protocols for six consecutive hours started from ZT0 to ZT6 (Colavito *et al.* 2013). Any direct contact of the experimenter with the animals was avoided. At the end of the sleep deprivation (SD) period, the animals were left to move and sleep freely with free access to food and water, and recording was continued for the next 48 hr.

EEG data analysis

A MatLab-based, custom-written auto-score system was first trained with EEG/EMG data by a human scorer. The EEG/EMG data were then analyzed by the auto-score system (Gao *et al.* 2016), followed by visual inspection by the same human scorer. In brief, a training set was selected for every 24 hr of data based on a random REMS epoch and preceding 90 epochs (15 min) as well as the following 90 epochs. This process was repeated until a total of 720 epochs (2 hr) of training was selected. The remaining 7920 epochs (22 hr) were subjected to short-time Fourier transformation and auto-scored with a multiple classifier system at a 5% rejection threshold using MatLab. Training and rejected epochs were scored using Sirenia Sleep Pro (Pinnacle Technologies, Lawrence, KS). Manual scoring of three vigilance states were performed for each 10-s epoch as either wake, NREMS and REMS. Wake was scored based on the presence of low amplitude, fast EEG, and high amplitude, variable EMG. NREMS was characterized by high-amplitude delta (0.5–4 Hz) EEG but low frequency EMG activity. REMS was characterized by low-amplitude rhythmic theta waves (6–10 Hz) with EMG atonia. The scorer was blind to the genotype within all the scoring process. The power for each 0.1-Hz bin (between 0.5 and 25 Hz) within the 10-s segment was calculated. For 48 hr of baseline recording, average values were calculated and plotted on a 24 hr-scale. Time spent per hour or total hours in wake/NREMS/REMS stages was calculated over ZT or during the 24 hr light/dark phase for each genotype. To

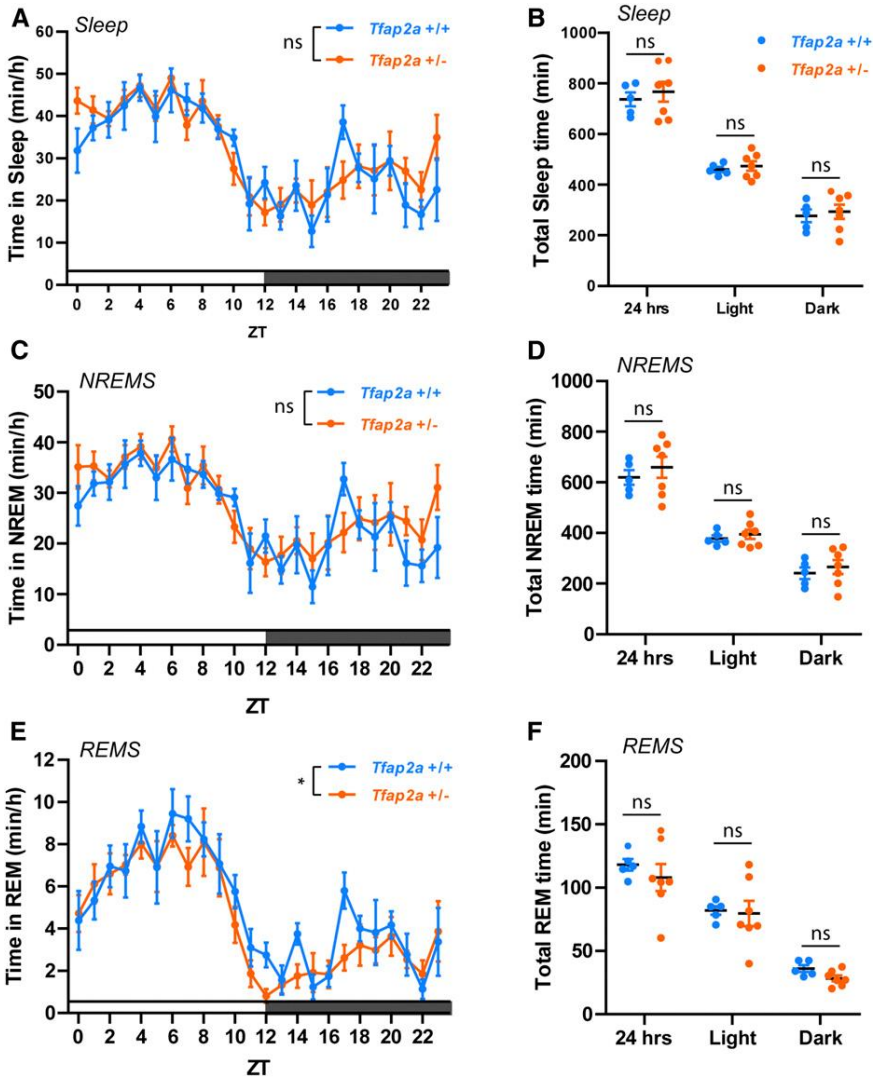

Figure 1 Sleep amount is not significantly altered in *Tfap2a*$^{+/-}$ mice. (A) Total sleep quantification over *Zeitgeber* times (ZT), two-way ANOVA followed by Sidak's multiple comparisons test, the main effect of genotype, F (1,240) = 0.941, P = 0.333. (B) Total sleep time quantification, P = 0.576; light, P = 0.574; dark, P = 0.687. (C) NREMS quantification over ZT, two-way ANOVA followed by Sidak's multiple comparisons test, the main effect of genotype, F (1,10) = 0.526, P = 0.485. (D) NREMS time quantification, P = 0.446; light, P = 0.521; dark, P = 0.543. (E) REMS quantification over ZT, two-way ANOVA followed by Sidak's multiple comparisons test, the main effect of genotype, F (1,239) = 0.492, *P = 0.0353. (F) REMS time quantification, P = 0.466; light, P = 0.852; dark, P = 0.053. n = 5 for *Tfap2a*$^{+/+}$, n = 7 for *Tfap2a*$^{+/-}$. Two-tailed unpaired *t*-tests were used for (B, D, and F). Averaged data are shown as the mean ± SEM.

evaluate the effect of SD, changes in time or bout length of NREMS/REMS during recovery sleep were calculated. In power spectral analysis, the EEG time series were decomposed into a voltage by frequency spectral graph, with power calculated as the square of the EEG magnitude, and magnitude being the integral average of the amplitude of the EEG signal (Kent *et al.* 2018). During baseline recording, derived power data were further grouped and analyzed based on frequency and vigilance states. Here, we presented the raw power data based on the vigilance state in combination with either the distribution of power in 0.1-Hz windows or frequency classes. After SD, the NREMS/REMS/wake powers during recovery sleep were expressed as percentage to the mean of the same ZT from basal recording. Mean values of power spectrum data were calculated for each genotype and the values were submitted to Wilcoxon signed rank tests to make comparison between the genotypes. All power data were expressed as averaged values from measurement of frontal and temporal lobes. For delta and theta power analysis following SD, Z06-12, Z12-18, Z18-24 time zones following the end of SD were used.

Behavioral testing

All behavioral tests were conducted between 08:30 AM and 06:00 PM during the light phase. The order of testing was as follows: elevated plus maze (EPM), rotarod, Morris water maze (MWM), sucrose preference test (SPT), forced swim test (FST), tail suspension test (TST), and fear conditioning (FC).

Elevated plus maze

The EPM consisted of four arms, each 30 cm long and 9.7 cm wide, elevated 50 cm off the ground. Two arms were enclosed by walls 25 cm high and the other two arms were exposed. Mice were placed on the central platform. The behavior of each subject was tracked by an overhead camera and a computer equipped with VideoMot (TSE Systems GmbH, Germany), and recorded for 5 min. VideoMot was

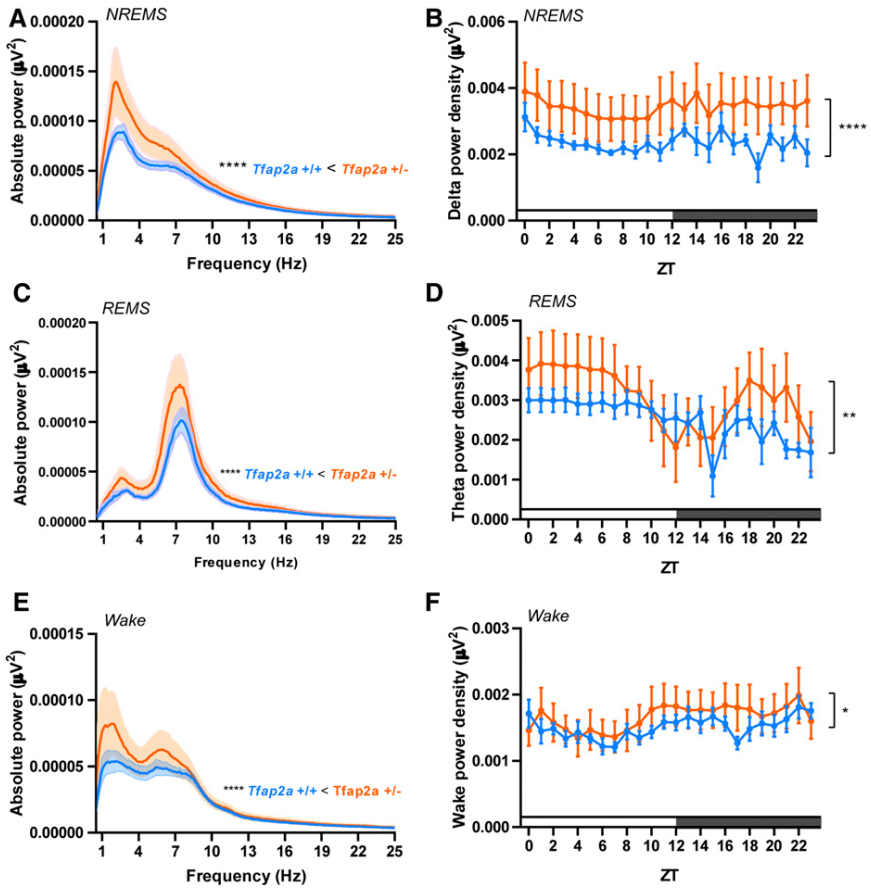

Figure 2 EEG delta and theta power are increased in *Tfap2a*$^{+/-}$ mice. (A) EEG power spectra in NREMS. (B) NREMS delta power (1–4 Hz), two-way ANOVA followed by Sidak's multiple comparisons test, the main effect of genotype, $F(1,240) = 29.58$, $^{****}P < 0.0001$. (C) EEG power spectra in REMS. (D) REMS theta power (6–10 Hz): two-way ANOVA followed by Sidak's multiple comparisons test, the main effect of genotype, $F(1,240) = 7.558$, $^{**}P = 0.0064$. (E) EEG power spectra during wakefulness. (F) Power analysis during wake (0.5–4 Hz), two-way ANOVA followed by Sidak's multiple comparisons test, the main effect of genotype, $F(1,240) = 4.028$, $^{*}P = 0.0459$. All data are shown as the mean ± SEM $n = 5$ for *Tfap2a*$^{+/+}$, $n = 7$ for *Tfap2a*$^{+/-}$. *P* values for 1–25 Hz were calculated using Wilcoxon two-sided signed-rank test, $^{****}P < 0.0001$. All data are shown as the mean ± SEM.

used to calculate the time spent in the open or closed arm. Time spent in open arm or central platform was used to evaluate exposure aversion.

Rotarod test

Motor functions and coordination were examined on the rotarod machine with automatic falling sensors (RotaRod Advanced, TSE Systems GmbH, Germany). For the habituation, mice were trained with the rotating speed of 10 rpm twice a day for two consecutive days. In each trial, mice were placed back to the rod immediately after falling off. After training, mice were tested under continuous acceleration from 5 rpm to 40 rpm with two sessions per day for two consecutive days. The latency to fall was recorded with a computer equipped with RotaRod software. Each measurement lasted 180 s with at least 6-hr intervals.

MWM test

A circular pool of 1.0 m in diameter was used for the MWM. The water (21°), made opaque by addition of nontoxic tempera paint, was 20 cm deep, and the wall of the pool extended 15 cm above the surface of the water. A square hidden platform (13 × 13 cm) was located 1 cm below the water surface approximately in the middle of one of the pool quadrants. Distal visual cues surrounding the pool included four colored labels of different shapes fixed around the edge of the water tank, as well as a door and a wall of cabinets. The test consisted of three phases: visible platform task, hidden platform task and probe test for a total of 11 consecutive days. To exclude mice with visual or motivational impairments and habituate them to the testing conditions, we performed visible platform task during the first 2 days. In this phase, mice were trained to swim to a visible platform placed 1 cm above water surface and in the middle of the water tank. Next, mice were tested with a hidden platform task where a fixed platform was hidden 1.0 cm below the water surface. Mice that failed to locate the platform within 90 sec were guided to it, and all mice were allowed to rest on the platform for at least 15 sec before being returned to their cage. On probe test day, the platform was removed, and mice were allowed to swim in the pool for up to 90 sec. The time spent in each quadrant was measured. On each of the 11 days, mice were given four trials per day starting from each of the four cardinal directions (N, S, E, W) in a pseudorandom order that changed every day. In each trial, mice were gently held close to the water surface facing the wall and then placed in the pool. The swim patterns were monitored by the video-tracking system VideoMot (TSE Systems GmbH). The escape latency, swim speed, path length, and

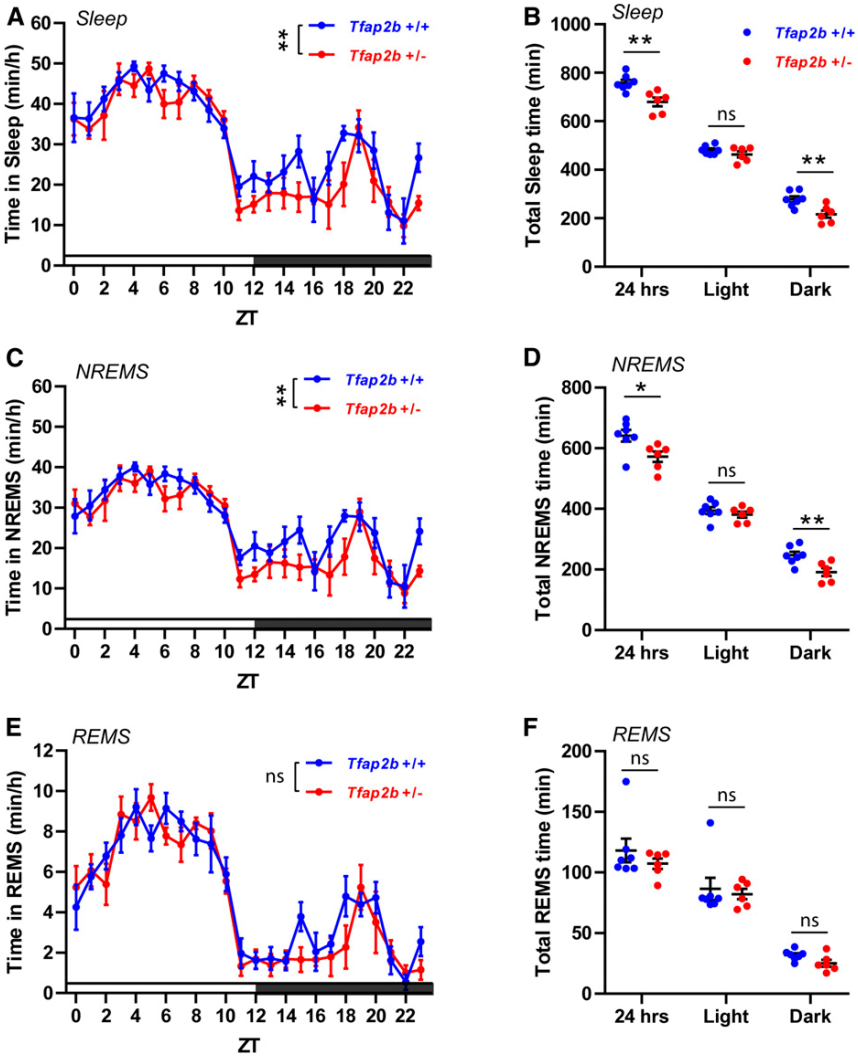

Figure 3 Sleep during the dark phase is reduced in *Tfap2b*$^{+/-}$ mice. (A) Total sleep time quantification over ZT, two-way ANOVA followed by Sidak's multiple comparisons test, the main effect of genotype, F (1,264) = 10.01, $^{**}P$ = 0.002. (B) Total sleep time quantification, $^{**}P$ = 0.004; light, P = 0.222; dark, $^{**}P$ = 0.007. (C) NREMS quantification over ZT, two-way ANOVA followed by Sidak's multiple comparisons test, the main effect of genotype, F (1,264) = 10.26, $^{**}P$ = 0.002. (D) NREMS total time quantification, $^{*}P$ = 0.024; light, P = 0.411; dark, $^{**}P$ = 0.008. (E) REMS quantification over ZT, two-way ANOVA followed by Sidak's multiple comparisons test, the main effect of genotype, F (1,263) = 1.492, P = 0.223. (F) REMS total time quantification, P = 0.668; light, P = 1.000; dark, P = 0.055. n = 7 for *Tfap2b*$^{+/+}$, n = 6 for *Tfap2b*$^{+/-}$. Two-tailed unpaired t-tests were used for (B, D, and F). All data are shown as the mean ± SEM.

trajectory of swimming were recorded for each mouse. Mice that were swimming slower than 60% of the average speed of wild type, *Tfap2a*, and *Tfap2b* mutants during each phase were classified as floaters. Two floaters were removed from the *Tfap2a*$^{+/-}$, eight from *Tfap2b*$^{+/+}$, six from *Tfap2b*$^{+/-}$.

Sucrose preference test

The whole experiment was carried out in the home cage of the mice in the breeding area. Two identical bottles were used for each cage and placed in left and right sides of the cage. Mice were allowed to habituate to the bottles with standard drinking water for 48 hr. In the second 24 hr of the habituation period, weights of the bottles were recorded. Then, mice were given 48 hr of free choice between two bottles of either 2% sucrose or standard drinking water. At the end of the period the bottles were weighed again and the consumption was calculated. No previous food or water deprivation was applied before the test. The percentage of sucrose preference was calculated using the following formula: Sucrose preference = V(sucrose solution)/[V(sucrose solution)+V(water)] × 100%.

Forced swim test

The test apparatus consisted of an inescapable transparent cylinder (25 cm height × 15 cm diameter) containing 20 cm of water (23°). Dividers (35 cm height × 22 cm width) were used between cylinders to prevent mice from seeing each other during the test. Mice were individually placed into the cylinders, and the immobility was recorded over a 6-min test period. Immobility was analyzed by an observer according to the following criteria. Each mouse was judged to be immobile when it ceased struggling and remained floating motionlessly in the water, making only those movements necessary to keep its head above water.

Tail suspension test

The TST (Gibney *et al.* 2013) was performed as described previously (Can *et al.* 2012). Each mouse was suspended

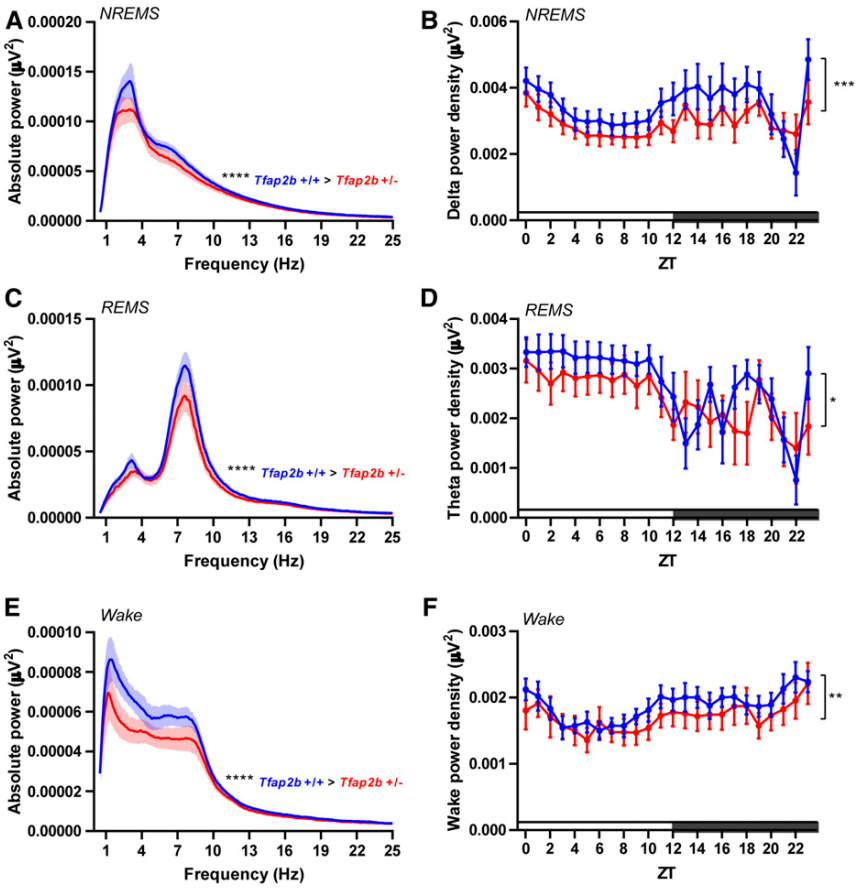

Figure 4 EEG delta and theta power are decreased in *Tfap2b*$^{+/-}$ mice. (A) EEG power spectra in NREMS. (B) NREMS delta power (1–4 Hz), two-way ANOVA followed by Sidak's multiple comparisons test, the main effect of genotype, $F(1,264) = 13.68$, $^{***}P = 0.0003$. (C) EEG power spectra in REMS. (D) REMS theta power (6–10 Hz), two-way ANOVA followed by Sidak's multiple comparisons test, the main effect of genotype, $F(1,264) = 5.525$, $^{*}P = 0.0195$. (E) EEG power spectra during wakefulness. (F) Wake power analysis (0.5–4 Hz), two-way ANOVA followed by Sidak's multiple comparisons test, the main effect of genotype, $F(1,264) = 9.126$, $^{**}P = 0.0028$. All data are shown as the mean ± SEM, $n = 7$ for *Tfap2b*$^{+/+}$, $n = 6$ for *Tfap2b*$^{+/-}$. *P* values for 1–25 Hz were calculated using Wilcoxon two-sided signed-rank test, $^{****}P < 0.0001$. All data are shown as the mean ± SEM.

30 cm above the floor by the tail with a 16 cm long piece of tape. Dividers (35 cm height × 15 cm width) were hanged between tapes to prevent mice from seeing each other during the test. The behavior was recorded for 6 min. Immobility was analyzed by an observer.

Contextual FC test

The contextual FC test was performed as described previously (Fischer *et al.* 2004; Sananbenesi *et al.* 2007). In brief, FC was carried out with a computerized fear conditioning system (TSE Systems GmbH) using a computer, equipped with Freeze Scan software (Clever Systems), connected to a control unit containing a shock and a noise generator. Animals were allowed to explore the training cage for 3 min followed by a mild electric shock (2 sec, 0.5 mA). Context-dependent freezing, defined as the absence of movements other than those required for breathing, was assessed for the following 2 days with a 24-hr interval without the electric shock. Freezing behavior and average movement were recorded for each mouse.

Wheel-running activity and circadian analysis

The setup included six controls and six mutant mice (three males and three females for each genotype of *Tfap2a* and *Tfap2b*) at the age of 2–5 months. Mice were placed in single cages with running wheels connected to a computer running ClockLab (Actimetrics) data collection software. Genotypes and sexes were evenly distributed over two boxes. Animals were not disturbed during the entire experiment. Wheel counts were checked every day to assess well-being of the animal. The experiment consisted of five phases: training phase, entrainment phase, phase advance (jetlag), light pulse at ZT14, and free-running phase. During the training phase, animals were in a 12 hr light: 12 hr dark (LD) cycle for >7 days with a light phase light intensity of 300 lux to habituate to the running-wheel. Next, daily activities were recorded and calculated as an average of 10 days. After the entrainment period in LD, mice were subjected to an abrupt shift in the light schedule by advancing the "lights off" time by 6 hr (jetlag paradigm). The number of days needed to completely re-entrain to the shifted LD cycle was compared between the genotypes. After mice were completely re-entrained to the new LD cycle, a light pulse was delivered at ZT14 for 30 min at 300 lux and mice released into constant darkness (DD), and phase shifts were calculated for activity onsets on the day after the light pulse. Mice were retained in DD for another 2 weeks to assess free-running period lengths by χ^2 periodogram analysis. One female in

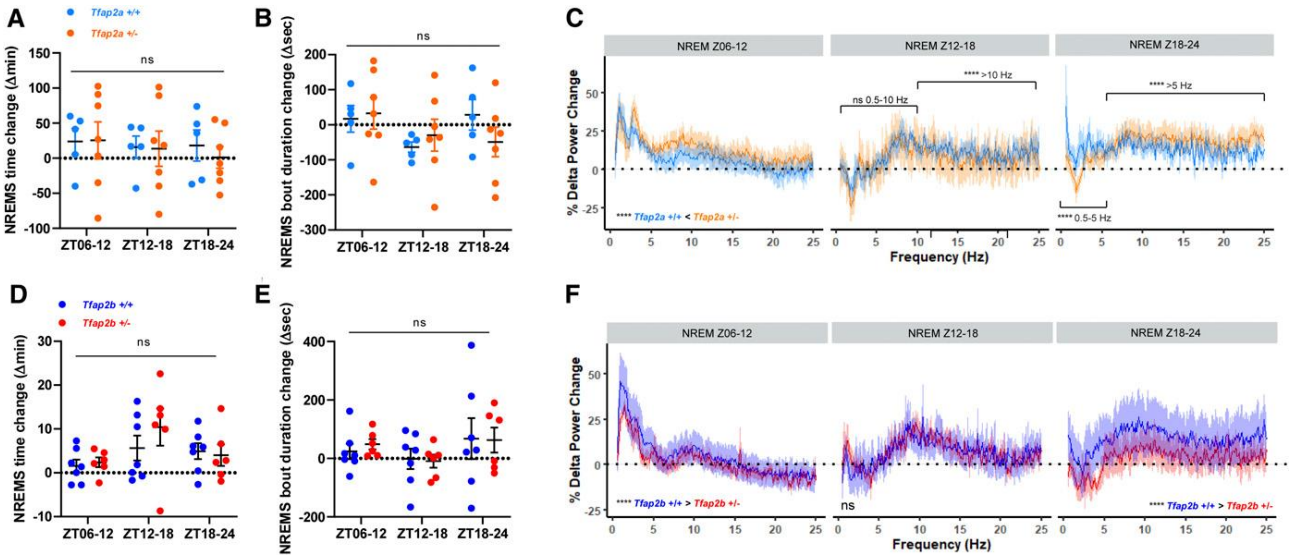

Figure 5 NREMS delta power following sleep deprivation is increased more strongly in *Tfap2a*$^{+/-}$ mice but less strongly in *Tfap2b*$^{+/-}$ mice. (A) NREMS time change in *Tfap2a*$^{+/-}$, two-way ANOVA tests followed by Sidak's pairwise comparison, the main effect of genotype: F(1, 30) = 0.103, P = 0.750; the main effect of time, F(2, 30) = 0.791, P = 0.791. (B) Average NREMS bout duration change in *Tfap2a*$^{+/-}$, two-way ANOVA tests followed by Sidak's pairwise comparison, the main effect of genotype: F(1, 30) = 0.072, P = 0.790; the main effect of time, F(2, 30) = 1.407, P = 0.261. (C) NREMS delta power changes (0.5–25 Hz) in *Tfap2a*$^{+/-}$ mice. Z06-12: 0.5–25 Hz, ****$P < 0.0001$. Z12-18: 0.5–10 Hz, P = 0.334; 10–25 Hz, ****$P < 0.0001$. Z18–24: 0.5–5 Hz, P = 0.334; 5–25 Hz, ****$P < 0.0001$. (D) NREMS time change in *Tfap2b*$^{+/-}$, two-way ANOVA tests followed by Sidak's pairwise comparison, the main effect of genotype: F(1, 33) = 0.595, P = 0.446; the main effect of time, F(2, 33) = 3.008, P = 0.063. (E) Average NREMS bout duration change in *Tfap2b*$^{+/-}$, two-way ANOVA tests followed by Sidak's pairwise comparison, the main effect of genotype: F(1, 33) = 0.014, P = 0.906; the main effect of time, F(2, 33) = 1.476, P = 0.243. (F) NREMS delta power changes (0.5–25 Hz) in *Tfap2b*$^{+/-}$ mice. Z06–12: 0.5–25Hz, ****$P < 0.0001$. Z12–18: 0.5–25 Hz, P = 0.715. Z18–24: 0.5–25 Hz, ****$P < 0.0001$. n = 5 for *Tfap2a*$^{+/+}$, n = 7 for *Tfap2a*$^{+/-}$, n = 7 for *Tfap2b*$^{+/+}$, n = 6 for *Tfap2b*$^{+/-}$. Wilcoxon two-sided signed-rank tests were used for power changes in (C and F). BSL, baseline sleep; R, recovery sleep. All data are shown as the mean ± SEM.

Tfap2a$^{+/+}$ was identified as an outlier using ROUT (Q = 1%) method and was removed from further analyses.

RNA-sequencing

RNA isolation and sequencing were carried out by Bernd Timmermann and Stefan Börno at the sequencing facility of the Max Planck Institute for Molecular Genetics, Berlin, according to their protocol: RNA was isolated from 20 to 80 mg of mouse brain tissue from B6N, *Tfap2a*$^{+/-}$ and *Tfap2b*$^{+/-}$ (stored in RNAlater) following the Qiagen RNeasy protocol. First, the tissue samples were homogenized with the TissueLyser (Qiagen) at 25 Hz for 2 × 2 min in Qiazol lysis buffer; 140 µl chloroform was added, and, after 15 min centrifugation at 12,000 × g, the aqueous phase containing the RNA was extracted. Ethanol (1.5 volumes) was added and the samples were washed with Qiagen's RWT buffer on a Qiagen RNeasy spin column. RNA was treated with 10 µl of DNase I on column for 15 min followed by a wash with RWT. After further washes with RPE buffer, the purified RNA was eluted with 50 µl water, yielding between 5 and 22 µg RNA.

After quality control using Agilent's Bioanalyzer, sequencing libraries were prepared from 500 ng of total RNA per sample following Roche's stranded "KAPA RNA HyperPrep" library preparation protocol for single indexed Illumina libraries: First, the polyA-RNA fraction was enriched using oligo-dT-probed paramagnetic beads. Enriched RNA was heat-fragmented and subjected to first-strand synthesis using random priming. The second strand was synthesized incorporating dUTP instead of dTTP to preserve strand information. After A-tailing, Illumina sequencing compatible adapters were ligated. Following bead-based clean-up steps, the libraries were amplified using 11 cycles of PCR. Library quality and size was checked with qBit, Agilent Bioanalyzer, and quantitative PCR (qPCR). Sequencing was carried out on an Illumina HiSeq 4000 system in PE75bp mode, yielding between 27 and 37 million fragments per sample.

Data analysis of RNA-sequencing

Following base calling, adaptor clipping was performed using cutadapt 2.4 (Martin 2011). Data were mapped against the GRCm38.p6 genome using STAR v 2.6.1d (Dobin *et al.* 2013) and differentially expressed genes were analyzed using EdgeR.

Statistics

Statistical analysis was performed using GraphPad Prism 8.3.0 and IBM SPSS (Version 22). All data were subjected to a Shapiro-Wilk normality test for Gaussian distribution and Levene's test for equality of variances. For the dataset that showed a Gaussian distribution ($P > 0.05$ in normality test), we performed parametric tests such as two-tailed

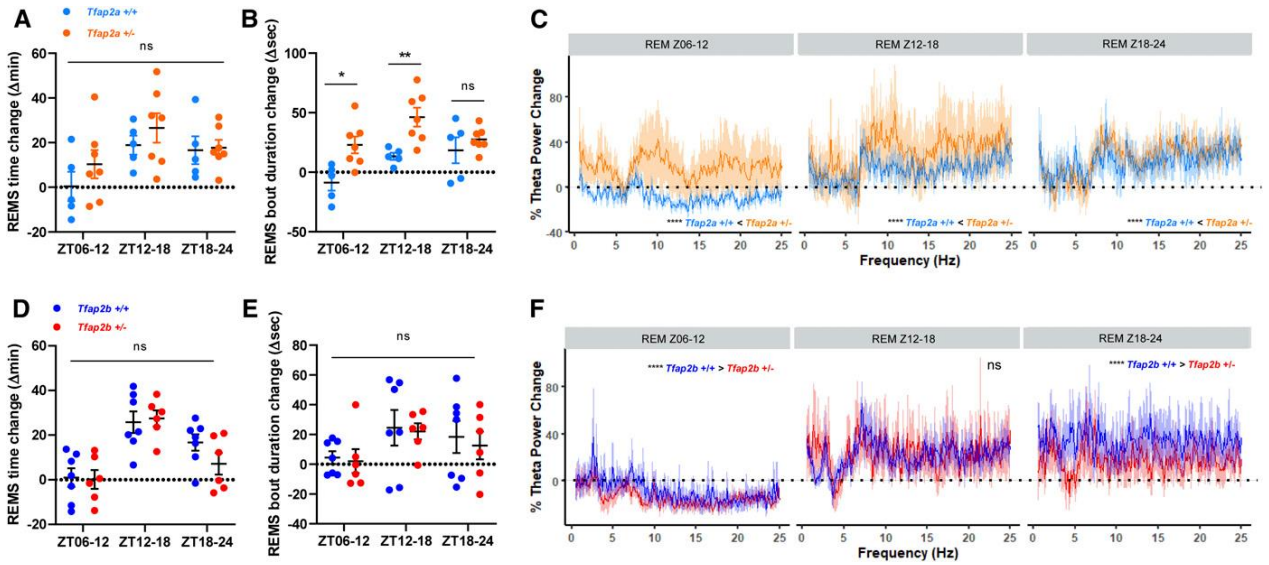

Figure 6 REMS theta power following sleep deprivation is increased more strongly in *Tfap2a*$^{+/-}$ mice but less strongly in *Tfap2b*$^{+/-}$ mice compared with wild-type controls. (A) REMS time change in *Tfap2a*$^{+/-}$, two-way ANOVA tests followed by Sidak's pairwise comparison, the main effect of genotype: $F(1, 30) = 1.698$, $P = 0.202$; the main effect of time, $F(2, 30) = 4.585$, $P = 0.018$. (B) Average REMS bout duration change in *Tfap2a*$^{+/-}$, two-way ANOVA tests followed by Sidak's pairwise comparison, the main effect of genotype: $F(1, 30) = 17.95$, $P = 0.010$; the main effect of time, $F(2, 30) = 5.365$, $P = 0.0002$. ZT06–12: $^{*}P = 0.011$. Z12–18: $^{**}P = 0.0079$. Z18–24: $P = 0.749$. (C) Rebound differences of REMS in theta power (0.5–25 Hz) in *Tfap2a*$^{+/-}$. Z06–12: 0.5–25 Hz, $^{****}P < 0.0001$. Z12–18: 0.5–25 Hz, $^{****}P < 0.0001$. Z18–24: 0.5–25 Hz, $^{****}P < 0.0001$. (D) REMS time change in *Tfap2b*$^{+/-}$, two-way ANOVA tests followed by Sidak's pairwise comparison, the main effect of genotype: $F(1, 33) = 0.673$, $P = 0.418$; the main effect of time, $F(2, 33) = 16.86$, $P < 0.0001$. (E) Average REMS bout duration in *Tfap2b*$^{+/-}$, two-way ANOVA tests followed by Sidak's pairwise comparison, the main effect of genotype: $F(1, 33) = 0.234$, $P = 0.632$; the main effect of time, $F(2, 33) = 2.521$, $P = 0.096$. (F) Rebound differences of REMS in theta power (0.5–25 Hz) in *Tfap2b*$^{+/-}$. Z06–12: 0.5–25 Hz, $^{****}P < 0.0001$. Z12–18: 0.5–25 Hz, $P = 0.119$. Z18–24: 0.5–25 Hz, $^{****}P < 0.0001$. $n = 5$ for *Tfap2a*$^{+/+}$, $n = 7$ for *Tfap2a*$^{+/-}$, $n = 7$ for *Tfap2b*$^{+/+}$, $n = 6$ for *Tfap2b*$^{+/-}$. Wilcoxon two-sided signed-rank tests were used for power changes in (C and F). BSL, baseline sleep; R, recovery sleep. All data are shown as the mean ± SEM.

paired/unpaired *t*-test and ANOVA followed by Sidak's multiple comparisons. For the dataset that failed to show a Gaussian distribution, we performed nonparametric tests, such as a Mann-Whitney test and Wilcoxon signed-rank test. Significance levels in the figures are represented as $^{*}P < 0.05$, $^{**}P < 0.01$, $^{***}P < 0.001$, and $^{****}P < 0.0001$. Error bars in the graphs represent mean ± SEM.

Quantitative PCR

To assess the mRNA reduction of AP-2α and β in *Tfap2a* and *b* mice, total RNA was extracted from the cortex using an RNA extraction kit (Qiagen GmbH). Total RNA was reverse transcribed into cDNA using the high capacity cDNA RT kit (Applied Biosystems) according to the manufacturer's instructions. Subsequently, the mRNA expression levels of AP-2α and β were quantified by qPCR using the Fast SYBR Green Master Mix (Applied Biosystems) using specific primers for each gene (Table S2). cDNA amplification was performed following a PCR program of 40 cycles, with denaturation at 94° for 1 min and annealing at 62° for 30 sec, followed by elongation at 72° for 1 min using an ABI 7500 qPCR cycler. mRNA expression was analyzed using the $2^{-\Delta\Delta Cq}$ method where the control was normalized to 1, and the treated samples were compared with their control. Primers and conditions are listed in Table S2.

Data availability

The authors state that all data necessary for confirming the conclusions presented in the article are represented fully within the article. All data are available at Dryad: https://doi.org/10.5061/dryad.rv15dv45r. Raw RNA-seq data are available at GEO: https://www.ncbi.nlm.nih.gov/geo/query/acc.cgi?acc=GSE155629. EEG-autoscore code is available at GitHub: https://zenodo.org/badge/latestdoi/240526669.

Results

Increased sleep pressure in Tfap2a$^{+/-}$ *mice*

We first analyzed sleep in *Tfap2a* mice. To quantify sleep and wake, we used EEG and EMG recordings (Mang and Franken 2012). As homozygous knockouts of *Tfap2a* are not viable (Zhang *et al.* 1996), we studied *Tfap2a* heterozygous animals. qPCR showed that these mutants had a reduced *Tfap2a* mRNA amount by about half (Supplemental Material, Figure S1). We first analyzed the amount of NREMS and REMS from the electrophysiological recordings. Total sleep time was not significantly affected (Figure 1, A and B). We observed a trend toward increased NREMS (Figure 1, C and D), which did not, however, reach statistical significance. REMS time was decreased slightly (Figure 1, E and F). Sleep

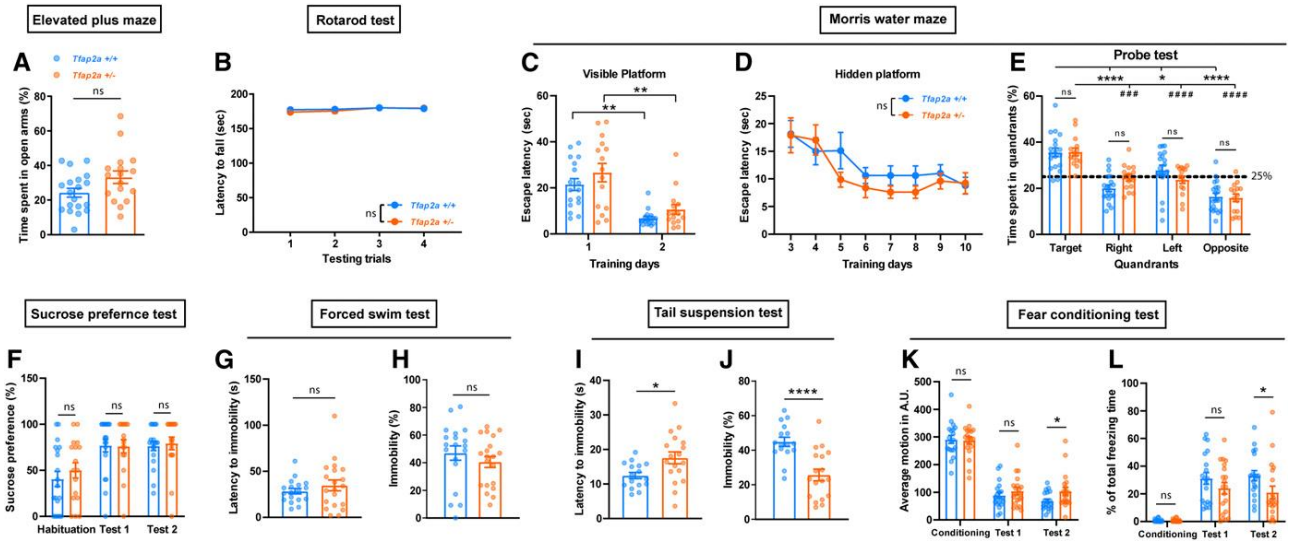

Figure 7 Behavioral phenotyping of *Tfap2a*$^{+/-}$ mice reveals signs of mild hyperactivity. (A) Elevate plus maze, two-tailed unpaired *t*-test, $P = 0.136$. (B) Rotarod test, two-way ANOVA test, the main effect of genotype: $F(1, 148) = 0.927$, $P = 0.337$; the main effect of time, $F(3, 148) = 2.512$, $P = 0.061$. (C) Morris water maze (MWM), time spent searching for visible platform during two consecutive training days: to compare mutants and their controls, unpaired Student *t*-test was used for day 1, $P = 0.274$; Mann-Whitney *U*-test for day 2, $P = 0.096$. Wilcoxon two-sided signed-rank tests for two related samples were used for day 1 and day 2 within each genotype: *Tfap2a*$^{+/+}$, $^{**}P = 0.001$; *Tfap2a*$^{+/-}$, $^{**}P = 0.004$. (D) MWM, time spent searching for hidden platform during eight consecutive training days from day 3 to day 10. Two-way ANOVA tests followed by Sidak's pairwise comparison, the main effect of genotype: $F(1, 256) = 1.049$, $P = 0.307$; the main effect of time, $F(7, 256) = 8.652$, $P < 0.0001$. (E) MWM, time spent in each quadrant during probe test: one-way ANOVA followed by Sidak's pairwise comparison, $F = 21.125$, $P < 0.0001$. *Tfap2a*$^{+/+}$ *vs.* *Tfap2a*$^{+/-}$: target, $P = 1.000$; right, $P = 0.819$; left, $P = 0.918$; opposite, $P = 1.000$. Target *vs.* right/left/opposite quadrant in *Tfap2a*$^{+/+}$: $^{****}P < 0.0001$, $^{*}P = 0.024$, $^{****}P < 0.0001$. Target *vs.* right/left/opposite in *Tfap2a*$^{+/-}$: $^{\#\#\#}P = 0.001$, $^{\#\#\#\#}P < 0.0001$, $^{\#\#\#\#}P < 0.0001$. (F) Sucrose preference test: habituation, $P = 0.379$; test 1, $P = 0.781$; test 2, $P = 0.415$, Mann Whitney test. (G) Forced swim test (FST), latency to immobility, $P = 0.830$, Mann Whitney test. (H) FST, time spent immobile, $P = 0.147$, Mann Whitney test. (I) Tail suspension test (TST), latency to immobility, $^{*}P = 0.039$, Mann Whitney test. (J) TST, time spent immobile, $^{****}P < 0.0001$, Mann Whitney test. (K) Fear conditioning test, average motion, training, $P = 0.296$; test 1, $P = 0.428$; test 2, $^{*}P = 0.028$, Mann Whitney test. (L) Total freezing time, training, $P = 0.771$; test 1, $P = 0.258$; test 2, $^{*}P = 0.018$, Mann Whitney test. Data are shown as the mean ± SEM $n \geq 16$ for *Tfap2a*$^{+/+}$, $n \geq 15$ for *Tfap2a*$^{+/-}$.

bout analysis did not show any significant changes in sleep architecture (Figure S2). We next investigated sleep quality using power spectrum analysis. *Tfap2a*$^{+/-}$ mice exhibited significantly increased delta power in NREMS (Figure 2, A and B) and theta power in REMS (Figure 2, C and D). Additionally, EEG spectral analysis of *Tfap2a*$^{+/-}$ mice during wakefulness showed increased low-frequency power (1–7 Hz) (Figure 2, E and F). Increased delta power in NREMS and increased theta power in REMS suggests that sleep intensity in *Tfap2a*$^{+/-}$ mice was increased.

Sleep loss and reduced sleep quality in Tfap2b$^{+/-}$ *mice*

We next determined sleep amount and quality of *Tfap2b*$^{+/-}$ mice by EEG/EMG recordings. Heterozygous deletion of *Tfap2b* led to a reduction of mRNA by about half (Figure S1). Total sleep time was significantly reduced, an effect that was caused by a specific reduction of sleep during the dark phase (Figure 3, A and B). Analysis of NREMS showed that the reduction of total sleep was due mainly to a reduction in NREMS during the dark phase (Figure 3, C and D). By contrast, no difference could be detected for REMS (Figure 3, E and F). We next analyzed the distribution of sleep bouts in *Tfap2b*$^{+/-}$ mice. Longer sleep bouts were reduced, an effect that was particularly pronounced in the dark phase (Figure S3, A–D). NREMS bouts, particularly long ones, were significantly reduced, again most strongly in the dark phase (Figure S3, E–H). The distribution of REMS bouts remained unchanged (Figure S3, I–L). Power analysis showed that *Tfap2b*$^{+/-}$ mice had significantly decreased delta power in NREMS (Figure 4, A and B), as well as reduced theta power in REMS (Figure 4, C and D). Delta power was already reduced during wakefulness (Figure 4, E and F). In summary, these findings suggest that, in contrast to *Tfap2a*$^{+/-}$ mutants, *Tfap2b*$^{+/-}$ mice have reduced total sleep, which primarily is a consequence of reduced or shortened NREMS bouts in the dark phase. *Tfap2b*$^{+/-}$ mice have less NREMS/REMS power, suggesting a reduction not only of sleep amount, but also of sleep quality.

Opposing effects of Tfap2a$^{+/-}$ *and Tfap2b*$^{+/-}$ *on homeostatic responses to SD*

Baseline sleep characterization showed that reductions in the function of *Tfap2a* and *Tfap2b* have opposing roles in sleep regulation. To test whether these different roles of the two transcription factors extend to sleep homeostasis, we tested the response of *Tfap2a*$^{+/-}$ and *Tfap2b*$^{+/-}$ mice to SD. Using

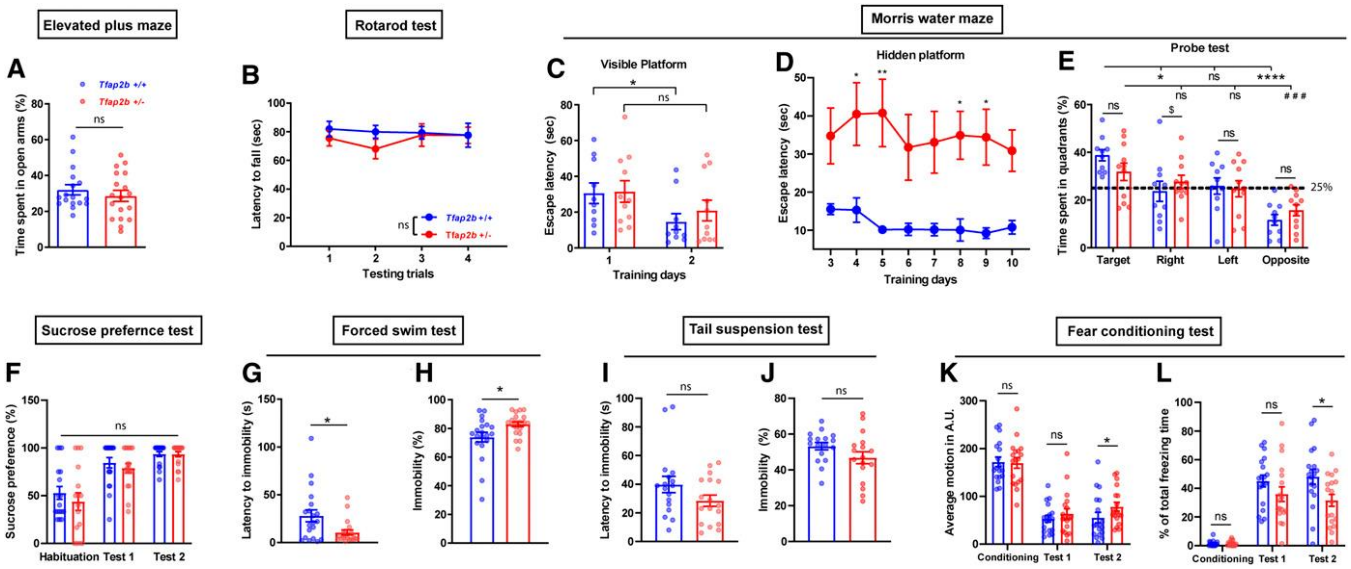

Figure 8 Behavioral phenotyping of *Tfap2b*$^{+/-}$ mice reveals signs of mild depressive-like symptoms. (A) Elevated plus maze, $P = 0.463$, Mann Whitney test. (B) Rotarod test, two-way ANOVA test, the main effect of genotype: F(1, 136) = 1.313, $P = 0.254$; the main effect of time, F(3, 136) = 0.249, $P = 0.862$. (C) Morris water maze (MWM), time spent searching for visible platform during two consecutive training days: to compare mutants and their controls, unpaired Student *t*-test was used for day 1, $P = 0.908$; Mann-Whitney *U*-test for day 2, $P = 0.557$. Wilcoxon two-sided signed-rank tests for two related samples were used for day 1 and day 2 within each genotype: *Tfap2b*$^{+/+}$, $^{*}P = 0.028$; *Tfap2b*$^{+/-}$, $P = 0.091$. (D) MWM, time spent searching for hidden platform during eight consecutive training days, Two-way ANOVA tests, the main effect of genotype: F(1, 148) = 63.40, $P < 0.0001$; the main effect of time, F(7, 148) = 0.377, $P = 0.915$; Sidak's pairwise comparison between genotype,$^{*}P < 0.05$,$^{**}P < 0.01$. (E) MWM, time spent in each quadrant during probe test, one-way ANOVA followed by Sidak's pairwise comparison, F = 7.381, $P < 0.0001$. *Tfap2b*$^{+/+}$ *vs.* *Tfap2b*$^{+/-}$: target, $P = 1.000$; right, $\$P = 0.034$; left, $P = 0.141$; opposite, $P = 1.000$. Target *vs.* right/left/opposite quadrant in *Tfap2b*$^{+/+}$: $^{*}P = 0.034$, $P = 0.141$, $^{****}P < 0.0001$. Target *vs.* right/left/opposite in *Tfap2b*$^{+/-}$: $P = 1.000$, $P = 0.950$, $^{\#\#\#}P = 0.009$. (F) Sucrose preference test, habituation, $P = 0.465$; test 1, $P = 0.372$; test 2, $P = 0.961$, Mann Whitney test. (G) Forced swim test (FST), latency to immobility, $^{*}P = 0.039$, Mann-Whitney test. (H) FST, time spent immobile, $^{*}P = 0.020$, Mann-Whitney test. (I) Tail suspension test, latency to immobility, $P = 0.231$, Mann-Whitney test. (J) Tail suspension test, time spent immobile, $P = 0.087$, Mann-Whitney test. (K) Fear conditioning test, average motion, training, $P = 0.815$; test 1, $P = 0.673$; test 2, $^{*}P = 0.047$, Mann Whitney test. (L) Fear conditioning test, total freezing time, training, $P = 0.696$; test 1, $P = 0.152$; test 2, $^{*}P = 0.027$. Mann Whitney test. All data are shown as the mean ± SEM $n \geq 10$ for *Tfap2b*$^{+/+}$, $n \geq 11$ for *Tfap2b*$^{+/-}$.

gentle handling (Colavito *et al.* 2013), we kept mice awake for 6 hr starting from light onset and measured and quantified the increase in sleep amount and quality by EEG.

Sleep time and delta power increased after SD in all conditions tested (Figures S4 and S5), but the magnitude of delta power responses differed in the different mutants. *Tfap2a*$^{+/-}$ mutant and control animals did not show statistically significant differences in sleep time and bout length (Figure 5, A and B). However, mutant animals exhibited higher rebound delta power compared to control animals within the first 6 hr after SD (Z06–12) (Figure 5C). The delta power rebound diminished during the next (Z12–18) and following 6 hr periods (Z18–24) in both control and mutant animals (Figure 5C). *Tfap2b*$^{+/-}$ animals also showed no difference in NREMS time (Figure 5D) or bout duration (Figure 5E) after SD compared to control animals, but lower rebound delta power during Z06–12 (Figure 5F). During Z12–18, no rebound was observed in both control and mutant animals, but the power change was smaller in mutants during Z18–24 (Figure 5F).

We next quantified REMS time and theta power following SD. A delayed REMS rebound was observed in both *Tfap2a* and *Tfap2b* mutants for REMS time as well as for theta power (Figure S6 and S7). REMS bout duration increased more strongly in *Tfap2a*$^{+/-}$ compared to wild-type littermates ($P < 0.01$) (Figure 6, A and B). *Tfap2a*$^{+/-}$ also showed a higher theta power rebound compared to their littermates (Figure 6C). In contrast, REMS time and REMS bout duration increased less in *Tfap2b*$^{+/-}$ after SD compared to wild-type controls during ZT18-24, although these differences were not significant (Figure 6, D and E). Supporting this trend, the theta power rebound after SD in *Tfap2b*$^{+/-}$ mice was significantly weaker compared to wild-type control animals during Z06-12 and Z18-24 (Figure 6F). Thus, *Tfap2a*$^{+/-}$ mice respond more strongly to SD, whereas *Tfap2b*$^{+/-}$ animals exhibit a weaker response to SD compared to wild-type controls.

Divergent behavioral changes in Tfap2a$^{+/-}$ *and Tfap2b*$^{+/-}$ *mice*

Sleep loss is correlated with emotional instability, anxiety (Verbitsky 2017), depression (Matsuda *et al.* 2017), and cognitive defects (Bezdicek *et al.* 2018). We hence tested how reduction of function of *Tfap2a* and *Tfap2b* affects anxiety, depression, as well as learning and memory (Figures 7 and 8). To assess anxiety-associated behavior, we performed the EPM test (Walf and Frye 2007). Explorative behavior assayed

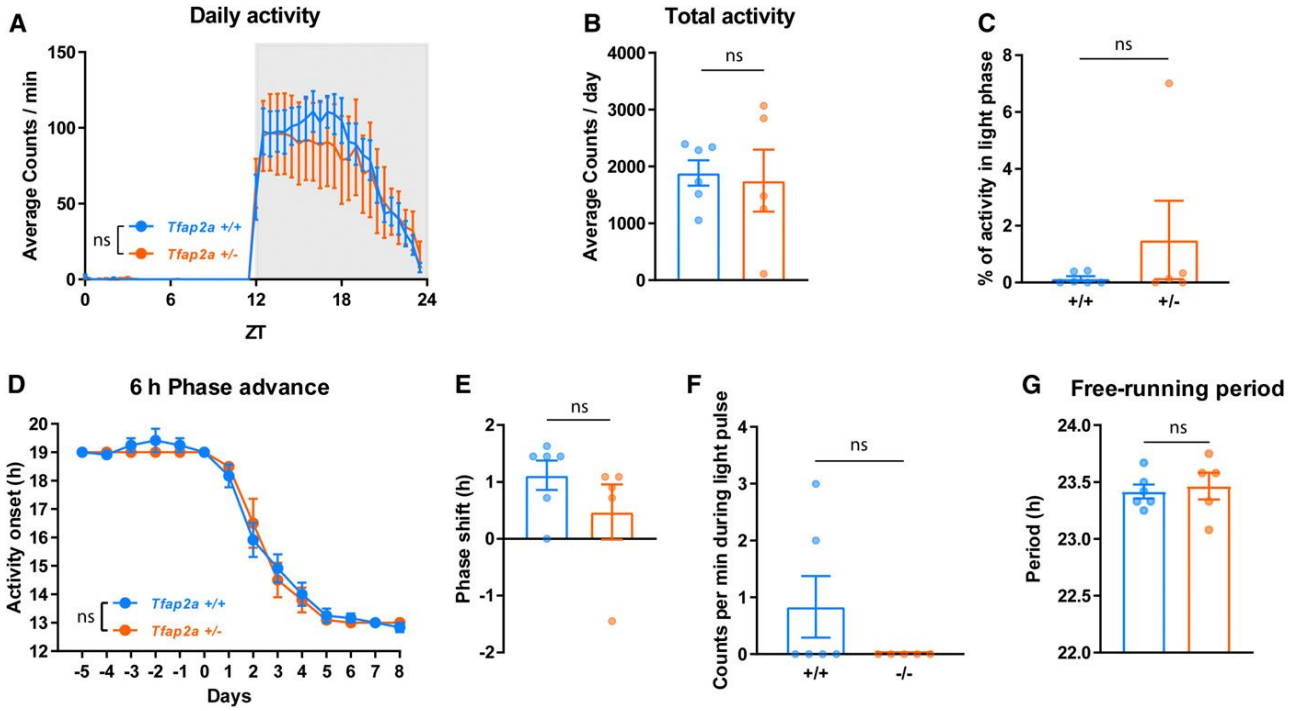

Figure 9 Circadian rhythms are comparable to wild-type controls in *Tfap2a*$^{+/-}$ mice. (A) Daily activity, two-way ANOVA tests followed by Sidak's pairwise comparison, the main effect of genotype: F(1, 432) = 1.133, $P = 0.288$; the main effect of time, F(47, 432) = 21.64, $P < 0.0001$. (B) Total activity, $P = 0.931$, Mann-Whitney test. (C) Activity in light phase, $P = 0.784$, Mann-Whitney test. (D) Six hours phase advance, Two-way ANOVA tests followed by Sidak's pairwise comparison, the main effect of genotype: F(1, 126) = 0.169, $P = 0.682$; the main effect of time, F(13, 126) = 156.8, $P < 0.0001$. (E) Phase shift, $P = 0.197$, Mann-Whitney test. (F) Locomotor activity during light pulse, $P = 0.455$, Mann-Whitney test. (G) Free-running period during constant darkness, $P = 0.626$, Mann-Whitney test. All data are shown as the mean ± SEM $n = 6$ for *Tfap2a*$^{+/+}$, $n = 5$ for *Tfap2a*$^{+/-}$.

in the EPM was similar across groups (Figure S8, A–D). The time spent in open arms and entries into the open arms were not changed relative to the corresponding littermates. Thus, we could not detect altered anxiety-associated exploration behavior in *Tfap2a*$^{+/-}$ *or Tfap2b*$^{+/-}$ (Figures 7A and 8A). Accelerating rotarod tests (Deacon 2013) showed that there was no difference in latency to fall during four testing trials in both mutants compared to their respective littermates (Figures 7B and 8B), indicating that motor coordination and balance in both mutants are not affected. Interestingly, *Tfap2b*$^{+/-}$ showed minor motor learning deficiency during the training trials, but this was not observed in *Tfap2a*$^{+/-}$ (Figure S8, E and F).

To assess spatial learning and memory, we performed the MWM test (Radyushkin *et al.* 2009). *Tfap2a*$^{+/-}$ mice as well as controls required similar times to reach the visible platform during the 2 days of training, and the latency was significantly shortened on the second training day (Figure 7C). *Tfap2b*$^{+/-}$ and control mice did not differ significantly when exposed to the visual water maze paradigm (Figure 8C). The mice were next subjected to an 8-day hidden platform training test. Over time, the latency to locate the hidden platform decreased, and the learning pattern in *Tfap2a*$^{+/-}$ mice was comparable to wild-type litter mates (Figure 7D). By contrast, *Tfap2b*$^{+/-}$ mice had severe problems finding the hidden platform (Figure 8D). Finally, the platform was removed in the probe test, and the percentage of time spent in the target quadrant where the platform was previously located was examined in comparison to other quadrants. *Tfap2a*$^{+/-}$ mice and their littermates spent most of the time in the target quadrant, suggesting that they learnt and remembered the previous location of the platform (Figure 7E). By contrast, *Tfap2b*$^{+/-}$ mice did not show the preference for the target quadrant as clearly as the wild type (Figure 8E). Together, these data suggest that spatial learning and memory might be impaired in *Tfap2b*$^{+/-}$ but not in *Tfap2a*$^{+/-}$ mice.Depression-associated behavior was assessed by SPT (Alkhlaif *et al.* 2017), FST (Yankelevitch-Yahav *et al.* 2015) and TST (Can *et al.* 2012). In *Tfap2a*$^{+/-}$ and *Tfap2b*$^{+/-}$ mice, no difference was observed in sucrose preference across all days of the experiment (Figures 7F and 8F). This result suggests that both *Tfap2a*$^{+/-}$ and *Tfap2b*$^{+/-}$ mice are able to experience pleasure from the reward (sucrose water). In the FST, there was no significant difference in latency to immobility and time spent immobile in *Tfap2a*$^{+/-}$ mice, but *Tfap2b*$^{+/-}$ mice showed a reduced immobility latency and spent more time immobile (Figures 7, G–H and 8, G–H). During the TST, increased immobilization latency and less immobility time were observed in *Tfap2a*$^{+/-}$ mutants but not in *Tfap2b*$^{+/-}$ mice (Figures 7, I and J and 8, I and J). Taken together, *Tfap2a*$^{+/-}$ mice showed signs of hyperactive

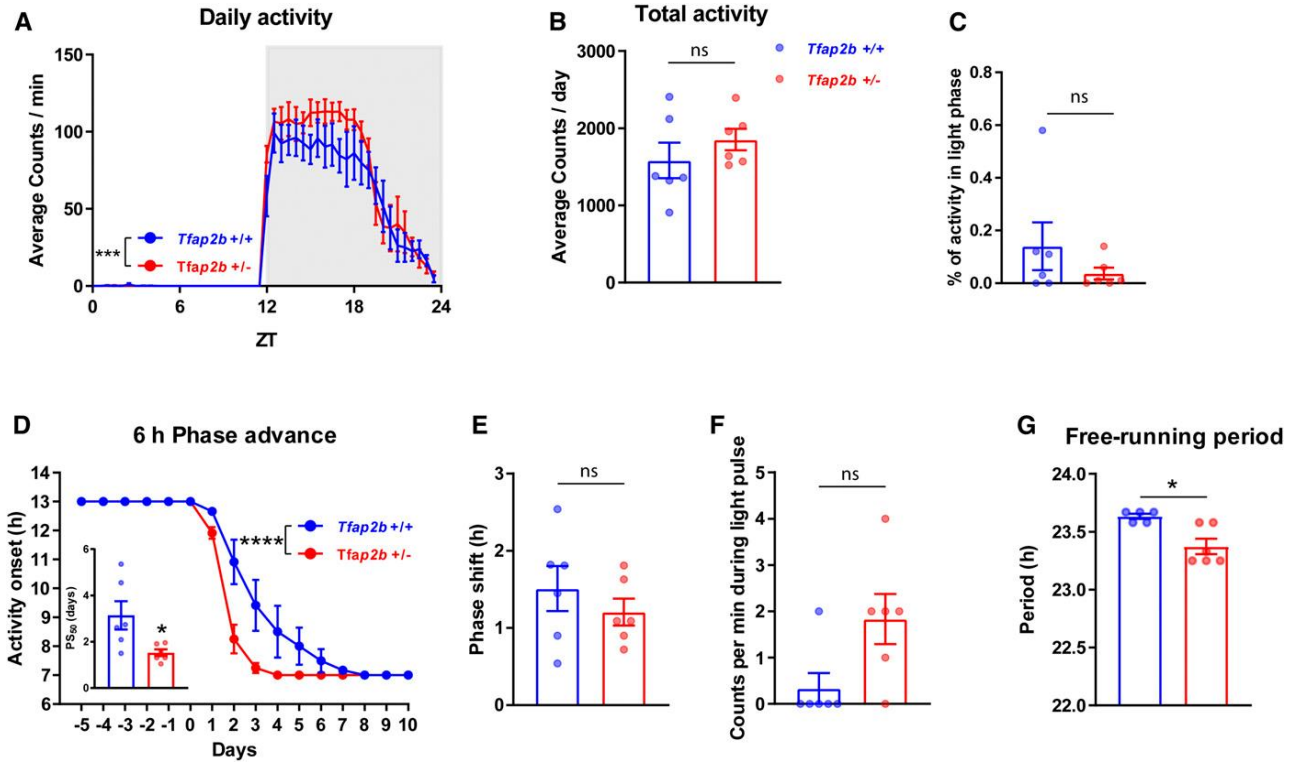

Figure 10 Circadian period is shortened and jetlag re-entrainment is accelerated in *Tfap2b*$^{+/-}$ mice. (A) Daily activity, two-way ANOVA test followed by Sidak's pairwise comparison, the main effect of genotype: F(1, 480) = 13.12, ***P = 0.0003; the main effect of time, F(47, 480) = 65.66, $P <$ 0.0001. (B) Total activity, P = 0.310, Mann-Whitney test. (C) Activity in light phase, P = 0.558, Mann-Whitney test. (D) Six hours phase advance two-way ANOVA test followed by Sidak's pairwise comparison, the main effect of genotype, F(1, 160) = 24.82, ****$P <$ 0.0001; the main effect of time, F(15, 160) = 161.1, $P <$ 0.0001; 50% phase shift (PS_{50}): two-tailed unpaired *t*-test, *P = 0.0273. (E) Phase shift, P = 0.452, Mann-Whitney test. (F) Locomotor activity during light pulse, P = 0.558, Mann-Whitney test. (G) Free-running period during constant darkness, *P = 0.022, Mann-Whitney test. All data are shown as the mean ± SEM n = 6 for *Tfap2b*$^{+/+}$, n = 6 for *Tfap2b*$^{+/-}$.

behavior in the TST. By contrast, *Tfap2b*$^{+/-}$ mice showed longer periods of immobility in the FST.

We next performed the contextual FC test (Fischer *et al.* 2004). In the conditioning session, average motion and freezing did not differ significantly between mutants and controls in both *Tfap2a*$^{+/-}$ and *Tfap2b*$^{+/-}$ mice. On the first test day after conditioning, both groups of mice showed signs of fear memory as evidenced by increased freezing time. On the second test day, both *Tfap2a*$^{+/-}$ and *Tfap2b*$^{+/-}$ mice exhibited higher motions and less freezing time compared to the respective controls, indicating impaired reconsolidation (Figures 7, K and L and 8, K and L).

In summary, motor function and balance in both *Tfap2a*$^{+/-}$ and *Tfap2b*$^{+/-}$ mice are comparable to wild-type controls. Emotion-associated behavior, assayed by the response to positive sensation (sucrose water) or mild environmental stress (*e.g.*, EPM), in both *Tfap2a*$^{+/-}$ and *Tfap2b*$^{+/-}$ mice also appears to be comparable to wild-type controls. In MWM tests, *Tfap2b*$^{+/-}$ mice showed severe impairment in finding the platform during training. However, the difference between *Tfap2b*$^{+/-}$ and controls was less severe in the probe test, where *Tfap2b*$^{+/-}$ still showed preference of the target quadrant, even though this preference did not reach statistical significance to the neighboring left quadrant. This suggests that, perhaps, spatial memory in *Tfap2b*$^{+/-}$ is less accurate. In addition, the lack of platform arrival might have stimulated expanded search behavior also in other quadrants. Interestingly, *Tfap2a*$^{+/-}$ mice appear to be less stressed when exposed to the TST, whereas *Tfap2b*$^{+/-}$ mice tend to react negatively in this test. *Tfap2b*$^{+/-}$ mice have impaired spatial as well as contextual fear memory. *Tfap2a*$^{+/-}$ mutants have reduced freezing time during FC, but this might be due to the hyperactivity rather than impaired fear memory. These results suggest that the different AP-2 mutants display at least partially divergent behavioral characteristics.

The free-running period of the circadian rhythm is shortened in Tfap2b$^{+/-}$ *mice*

Sleep is strongly regulated by the circadian system. We thus explored circadian rest-activity regulation in *Tfap2a*$^{+/-}$ and *Tfap2b*$^{+/-}$ mice. We measured wheel-running activity under baseline conditions (12 hr light: 12 hr dark - LD), during re-entrainment to a 6 hr phase advance of the LD cycle, in response to a nocturnal light pulse, and under constant dark (DD) conditions (Zheng *et al.* 2001) (Figures 9 and 10). Under LD conditions, *Tfap2a*$^{+/-}$ and *Tfap2b*$^{+/-}$ mice did not show

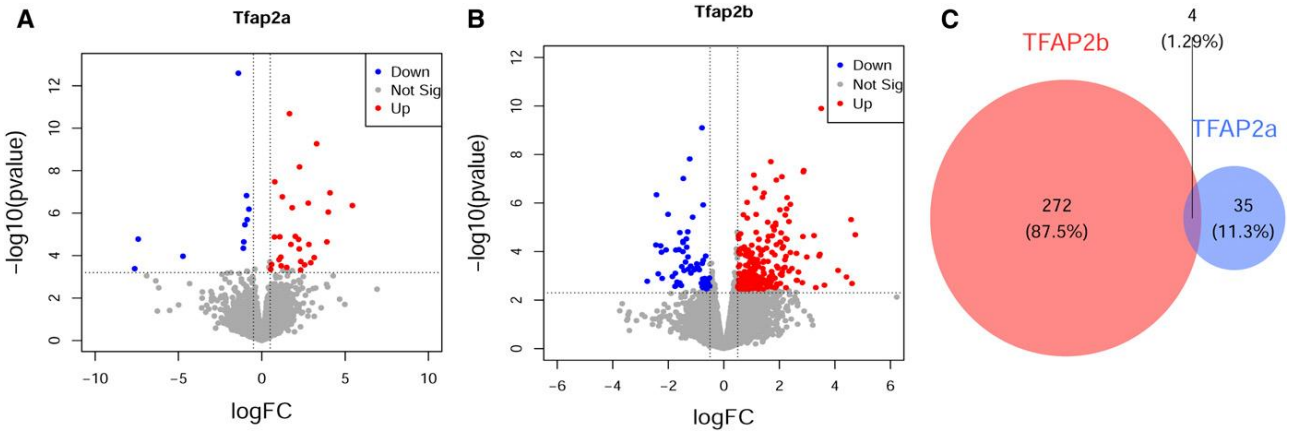

Figure 11 Divergent gene expression changes in *Tfap2a*$^{+/-}$ and *Tfap2b*$^{+/-}$. (A) Volcano plot of genes that are differentially expressed in *Tfap2a*$^{+/-}$ mice. (B) Volcano plot of genes that are differentially expressed in *Tfap2b*$^{+/-}$ mice. (C) Venn diagram showing distinct and overlapping genes that are differentially expressed [false discovery rate (FDR) < 0.20] in *Tfap2a*$^{+/-}$ and *Tfap2b*$^{+/-}$. The overlapping *P* value was calculated using Fischer's Exact tests, $P = 0.005$. $n = 3$ for B6N, $n = 3$ for *Tfap2a*$^{+/-}$, $n = 3$ for *Tfap2b*$^{+/-}$. Genes that are differentially expressed at FDR < 0.20 and logFC > 0.5 are highlighted and labeled in the volcano plot.

significant differences in their rest-activity patterns compared to controls (Figures 9, A–C and 10, A–C). We next measured the response of *Tfap2a*$^{+/-}$ and *Tfap2b*$^{+/-}$ mice to a shift in the LD cycle by advancing the dark phase by 6 hr (jetlag paradigm). Re-entrainment to the new cycle was normal in *Tfap2a*$^{+/-}$ mice compared with wild-type controls (Figure 9D), but it was significantly faster in *Tfap2b*$^{+/-}$ mice (Figure 10D).

To measure the capacity of light to phase reset the circadian clock system of *Tfap2a*$^{+/-}$ and *Tfap2b*$^{+/-}$ mice, a 30-min light pulse was delivered at ZT14 (2 hr after "lights off") and mice were released into DD, which, in wild-type mice, normally induces a phase delay in their rest-activity rhythm (Schwartz and Zimmerman 1990). Light induced similar amounts of phase delays in both *Tfap2a*$^{+/-}$ and *Tfap2b*$^{+/-}$ mice, and the acute reduction of activity during the 30-min light pulse (a.k.a. negative light masking) was not significantly different between mutants and controls (Figures 9, E and F and 10, E and F). There was no difference in DD free-running periods in *Tfap2a*$^{+/-}$ mice, but a shorter period length was observed in *Tfap2b*$^{+/-}$ mice (Figures 9G and 10G). In summary, circadian rhythms in *Tfap2a*$^{+/-}$ mice were comparable to wild-type controls. In *Tfap2b*$^{+/-}$ mice, a shorter intrinsic clock period may have facilitated the faster entrainment in the jetlag paradigm. Speculatively, the observed reduction in sleep amount in these mice might also facilitate such clock acceleration.

Divergent differential gene expression in Tfap2a$^{+/-}$ *and Tfap2b*$^{+/-}$ *mice*

The divergent effects of *Tfap2a*$^{+/-}$ and *Tfap2b*$^{+/-}$ on behavior might stem from different gene expression caused by reduction of the amount of the respective transcription factor. We thus measured gene expression changes in the brain in *Tfap2a*$^{+/-}$, *Tfap2b*$^{+/-}$, and wild type controls. For this, we took brain samples from these mutants and controls, determined their transcriptomes using RNA sequencing, and extracted differentially expressed genes. We found 276 genes to be significantly differentially expressed in *Tfap2b*$^{+/-}$ compared with wild types, whereas only 39 genes were found to be differentially expressed in *Tfap2a*$^{+/-}$. Thus, the more severe behavioral and sleep phenotypes in *Tfap2b*$^{+/-}$ correlate with increased differences in gene expression (Figure 11). Only one gene was downregulated and three genes were upregulated in both *Tfap2a*$^{+/-}$ and *Tfap2b*$^{+/-}$ (Supplemental excel workbook), while all other genes were unique to either of the mutants. This broad divergence in gene expression is consistent with the divergence in sleep and behavior. The differentially expressed genes could potentially explain the sleep and behavioral phenotypes observed in *Tfap2a*$^{+/-}$ and *Tfap2b*$^{+/-}$. We hence searched the literature for these genes to find phenotypes associated with sleep and the behavioral tests that we have performed. Only one gene that is differentially expressed in *Tfap2a*$^{+/-}$ has been previously associated with sleep and none of the genes has been described to have phenotypes in the behavioral tests. By contrast, four genes that are differentially expressed in *Tfap2b*$^{+/-}$ have been associated with sleep phenotypes, and eight genes have been associated with phenotypes in the behavioral tests that we have performed (see details in Table 1). Future studies will be required to establish causality and to solve mechanisms by which *Tfap2a*$^{+/-}$ and *Tfap2b*$^{+/-}$ affect behavior.

Discussion

Divergent phenotypes in sleep, behavior, circadian rhythms, and gene expression in Tfap2a$^{+/-}$ *and Tfap2b*$^{+/-}$

After gene duplication events, paralogs can take on different functions. In mice, both *Tfap2a* and *b* genes play an important role during the development of the neural crest (Mander *et al.* 2013) that gives rise to most of the peripheral nervous system (PNS) and to several non-neural cell types, including

Table 1 Association of *Tfap2b and Tfap2a*-controlled genes with sleep and behavioral phenotypes

Assay	Phenotype	*Tfap2a*$^{+/-}$ DE genes	*Tfap2b*$^{+/-}$ Phenotype	*Tfap2b*$^{+/-}$ DE genes
EEG/EMG recording	Normal sleep amount but increased sleep power	Slc5a5[a]	Shortened sleep amount and impaired sleep quality	Fos[a], Fosb[a], Slc5a5[a] Slc18a2[b]
EPM	Normal anxiety-associated behavior	—	Normal anxiety-associated behavior	—
Rotarod	Normal motor function	—	Normal motor function	—
MWM	Normal spatial learning and memory	—	Impaired spatial learning and memory	Arc[a], Fos[a], Fosb[a], Vgf[a]
SPT, FST, TST	Hyperactive in TST, but normal in SPT or TST	—	Depression-like behavior only in FST, but normal in SPT or TST	Fosb[a], Dusp1[a] Slc6a4[b]
Contextual fear conditioning	Shortened freezing behavior	—	Shortened freezing behavior	Arc[a], Vgf[a] Slc6a4[b]
Wheel-running	Normal circadian activity	—	Shortened circadian period and accelerated re-entrainment	Vgf[a]

Literature analysis of genes that are differentially expressed in *Tfap2a*$^{+/-}$ and *TFAP2b*$^{+/-}$. All interpretations are purely speculative. *Fos* and *Fosb* from the *Fos* family of transcription factors as well as *Slc5a5* and *Slc18a2* from the solute carrier (SLC) group of membrane transport proteins were found to be differentially regulated in *Tfap2b*$^{+/-}$ mice, which might contribute to the shortened sleep (Figure 3). *Slc5a5*, which encodes a sodium/iodide symporter (NIS), was down regulated in both *Tfap2a*$^{+/-}$ and *Tfap2b*$^{+/-}$ mice. The NIS plays a fundamental role in the first step in thyroid hormone biosynthesis (Dohán *et al.* 2003). Multiple phenotypes relating to neurological features, skeleton, vision, and metabolism have been discovered in *Slc5a5* knockouts. Among those phenotypes, abnormal sleep behavior, such as shorter sleep bout duration during the dark phase, has been found in male *Slc5a5*$^{-/-}$ mice (Dickinson *et al.* 2016). *Fos* (*c-fos*) is a nuclear proto-oncogene, whose expression is used as an indirect marker of neuronal activity. *Fosb* expression is induced often in the same cells as *Fos*, but at a later time (Gass *et al.* 1992; Peters *et al.* 1994). In *Tfap2b*$^{+/-}$ mice, *Fos* and *Fosb* were downregulated. Abnormal sleep has been found in *Fos* or Fosb-deficient mice such that *Fos-null* mice have less NREMS and normal REM sleep, but *Fosb*-deficient mice have less REMS but unchanged NREMS (Shiromani *et al.* 2000). Dopamine is transported into synaptic vesicles by the vesicular monoamine transporter (VMAT2), which is encoded by *Slc18a2*. VMAT2-deficient mice are used as a model of Parkinson's Disease (PD) that exhibits shorter latency to sleep and lower circadian activity except for a major phenotype of the motor dysfunction (Taylor *et al.* 2009). In *Tfap2b*$^{+/-}$ animals, *Slc18a2* was upregulated, and overexpression of this gene was reported to have neuroprotective effects, such as antidepressive and anxiolytic activity and increased ambulation during the dark phase (Lohr *et al.* 2014). The downregulation of *Arc*, *Fos*, *Fosb*, and *Vgf* might be associated with the impaired spatial learning and memory that we found in *Tfap2b*$^{+/-}$ animals (Figure 8, C–E). The deletion of either *Arc*, *Fos*, *Fosb*, or *Vgf* in mice result in impaired spatial learning (Paylor *et al.* 1994; Plath *et al.* 2006; Bozdagi *et al.* 2008; Ohnishi *et al.* 2011). Increased immobility was observed in *Tfap2b*$^{+/-}$ mice (Figure 8H), which is consistent with downregulation of *Fosb* and *Duspt1* as well as upregulation of *Slc6a4*. *Fosb* null mice have increased immobility in FST compared with their controls (Ohnishi *et al.* 2011). On the contrary, overexpression of *Dusp1* causes depressive behaviors and mice lacking *Dusp-1* are resilient to stress (Duric *et al.* 2010). *Slc6a4* encodes the serotonin transporter (SERT) in mice. It is reported that mice that are more susceptible to stress have increased expression of SERT and exhibit longer immobility in FST (Couch *et al.* 2013). In addition, SERT overexpression (5-HTTOE) mice have reduced freezing time in the cued fear conditioning test (McHugh *et al.* 2015). In *Tfap2b*$^{+/-}$ mice, we found a shortened freezing time in the contextual fear conditioning test (Figure 8L). The downregulation of *Arc* and *Vgf* might also contribute to this fear-related phenotype, as *Arc* and *Vgf* null mice exhibit shortened freezing time in the contextual fear conditioning test (Plath *et al.* 2006; Bozdagi *et al.* 2008). Moreover, *Vgf*$^{-/-}$ mice have a slightly shortened circadian period length (Hahm *et al.* 1999), which might help explain the similar phenotype we observed in *Tfap2b*$^{+/-}$ mice (Figure 10).

[a] Upregulated genes.

[b] Downregulated genes. "—" indicates that no information was found.

smooth muscle cells of the cardiovascular system, pigment cells in the skin, and craniofacial bones (Moser *et al.* 1997b). Despite their common expression pattern during early embryonic stages, deletion of *Tfap2a* or *Tfap2b* produces strikingly different phenotypes (Zhang *et al.* 1996). The loss of *Tfap2a* causes neuronal, craniofacial, skeletal, and body wall defects, whereas *Tfap2b*-deficient mice show brain development, *ductus arteriosus*, and renal impairments (Zhang *et al.* 1996; Moser *et al.* 1997a; Brewer *et al.* 2004).

Functional divergence in AP-2 is also seen for sleep phenotypes. *Tfap2a*$^{+/-}$ displays a rather increased sleep quality, whereas sleep length and quality in *Tfap2b*$^{+/-}$ are reduced. Homeostatic regulation exists in both *Tfap2a*$^{+/-}$ *and Tfap2b*$^{+/-}$, but a stronger response was found in the former and a weaker one in the latter. Our work from *C. elegans* and *Drosophila* indicated that the ancient function of AP-2 appears to be to promote sleep (Turek *et al.* 2013; Kucherenko *et al.* 2016). This suggests that *Tfap2b*$^{+/-}$ may have kept the original sleep-promoting function, whereas *Tfap2a*$^{+/-}$ may have taken on a new, opposing function in sleep control. Thus, as sleep evolved in more complex brains, there might have emerged a need for negative control of sleep that favored the divergence of AP-2 transcription factors.

We show that this functional divergence extended to additional behaviors. *Tfap2a*$^{+/-}$ was more robust in the behavioral assays, at least in the TST, which indicated a mild hyperactivity. By contrast, the performance of *Tfap2b*$^{+/-}$ revealed mildly depressive-like symptoms. Consistent with diverging roles in development and behavior, our RNA-sequencing data of *Tfap2a*$^{+/-}$ and *Tfap2b*$^{+/-}$ mice revealed divergent patterns of gene expression. The divergent behavioral changes observed in *Tfap2a*$^{+/-}$ *and Tfap2b*$^{+/-}$ mice may, thus, speculatively result from the modulation of expression of *Tfap2a* and *Tfap2b* target genes. Consistent with this view, *Tfap2a* and *Tfap2b* have been shown to play distinct roles in the specification of GABAergic neurons (Zainolabidin *et al.* 2017). This finding is intriguing as sleep-active, sleep-inducing neurons typically are GABAergic. Alternatively, changes in depressive-like symptoms in the mutants may be the consequence of sleep quality alterations. As poor sleep quality impairs memory consolidation (Mander *et al.* 2013; Bezdicek *et al.* 2018), the memory deficits shown in *Tfap2b*$^{+/-}$ mice might be the result

of a loss of sleep time or quality. *Tfap2a*$^{+/-}$ mice showed less freezing in FC despite a better sleep quality. However, since *Tfap2a*$^{+/-}$ mice exhibited hyperactive behavior in a stressful situation (TST), this effect might speculatively have blunted the freezing response in FC.

Different phenotypes were also found in circadian rhythm regulation for *Tfap2a*$^{+/-}$ *and Tfap2b*$^{+/-}$ mice. Circadian rhythmicity was unaffected in *Tfap2a*$^{+/-}$, whereas *Tfap2b*$^{+/-}$ showed a shortened period of the internal clock system. The circadian period shortening in *Tfap2b*$^{+/-}$ most likely is too mild to be the cause of the sleep impairment. For example, mice lacking the clock gene *Per1* with 1 hr shorter intrinsic period and preserved homeostatic responses do not exhibit overall sleep changes (Kopp *et al.* 2002).

Our results suggest that AP-2 transcription factors have diverged to take on divergent control of sleep and other behaviors. To our knowledge, this is the first instance where a sleep gene is shown to have diversified in evolution from a sleep-promoting role in invertebrates to serve bidirectional control of sleep in mammals.

Acknowledgments

We thank Ahmed Mansouri, Mayumi Kimura, Anja Ronnenberg, Ulrike Teichmann, and Sara Kimmina for advice on electroencephalogram (EEG), animal experimentation, and help with obtaining permits. We are grateful to Gregor Eichele for providing laboratory space and resources. We thank Markus Moser and Trever Williams for mouse strains. Sequencing was carried out by Bernd Timmermann and Stefan Börno, Max Planck Institute for Molecular Genetics, Berlin. This work was supported by the Max Planck Society (Max Planck Research Group "Sleep and Waking"), by a European Research Council Starting Grant (ID: 637860, SLEEPCONTROL), and by Deutsche Forschungsgemeinschaft (DFG) grants AS547/1-1 and OS353-10/1.

Literature Cited

Alkhlaif, Y., D. Bagdas, A. Jackson, A. J. Park, and I. M. Damaj, 2017 Assessment of nicotine withdrawal-induced changes in sucrose preference in mice. Pharmacol. Biochem. Behav. 161: 47–52. https://doi.org/10.1016/j.pbb.2017.08.013

Bernard, K., N. J. Logsdon, S. Ravi, N. Xie, B. P. Persons *et al.*, 2015 Metabolic reprogramming is required for myofibroblast contractility and differentiation. J. Biol. Chem. 290: 25427–25438. https://doi.org/10.1074/jbc.M115.646984

Bezdicek, O., T. Nikolai, J. Nepozitek, P. Perinova, D. Kemlink *et al.*, 2018 Prospective memory impairment in idiopathic REM sleep behavior disorder. Clin. Neuropsychol. 32: 1019–1037. https://doi.org/10.1080/13854046.2017.1394493

Bozdagi, O., E. Rich, S. Tronel, M. Sadahiro, K. Patterson *et al.*, 2008 The neurotrophin-inducible gene Vgf regulates hippocampal function and behavior through a brain-derived neurotrophic factor-dependent mechanism. J. Neurosci. 28: 9857–9869. https://doi.org/10.1523/JNEUROSCI.3145-08.2008

Brewer, S., W. Feng, J. Huang, S. Sullivan, and T. Williams, 2004 Wnt1-Cre-mediated deletion of AP-2alpha causes multiple neural crest-related defects. Dev. Biol. 267: 135–152. https://doi.org/10.1016/j.ydbio.2003.10.039

Bringmann, H., 2018 Sleep-active neurons: conserved motors of sleep. Genetics 208: 1279–1289. https://doi.org/10.1534/genetics.117.300521

Campbell, S. S., and I. Tobler, 1984 Animal sleep: a review of sleep duration across phylogeny. Neurosci. Biobehav. Rev. 8: 269–300. https://doi.org/10.1016/0149-7634(84)90054-X

Can, A., D. T. Dao, C. E. Terrillion, S. C. Piantadosi, S. Bhat *et al.*, 2012 The tail suspension test. J. Vis. Exp. 59: e 3769. https://doi.org/10.3791/3769

Chazaud, C., M. Oulad-Abdelghani, P. Bouillet, D. Decimo, P. Chambon *et al.*, 1996 AP-2.2, a novel gene related to AP-2, is expressed in the forebrain, limbs and face during mouse embryogenesis. Mech. Dev. 54: 83–94. https://doi.org/10.1016/0925-4773(95)00463-7

Colavito, V., P. F. Fabene, G. Grassi-Zucconi, F. Pifferi, Y. Lamberty *et al.*, 2013 Experimental sleep deprivation as a tool to test memory deficits in rodents. Front. Syst. Neurosci. 7: 106. https://doi.org/10.3389/fnsys.2013.00106

Couch, Y., D. C. Anthony, O. Dolgov, A. Revischin, B. Festoff *et al.*, 2013 Microglial activation, increased TNF and SERT expression in the prefrontal cortex define stress-altered behaviour in mice susceptible to anhedonia. Brain Behav. Immun. 29: 136–146 [Corrigenda: Brain Behav. Immun. 36: 215 (2014)]. https://doi.org/10.1016/j.bbi.2012.12.017

Deacon, R. M., 2013 Measuring motor coordination in mice. J. Vis. Exp. 75: e 2609. https://doi.org/10.3791/2609

Dickinson, M. E., A. M. Flenniken, X. Ji, L. Teboul, M. D. Wong *et al.*, 2016 High-throughput discovery of novel developmental phenotypes. Nature 537: 508–514 [Corrigenda: Nature 551: 398 (2017)]. https://doi.org/10.1038/nature19356

Dobin, A., C. A. Davis, F. Schlesinger, J. Drenkow, C. Zaleski *et al.*, 2013 STAR: ultrafast universal RNA-seq aligner. Bioinformatics 29: 15–21. https://doi.org/10.1093/bioinformatics/bts635

Dohán, O., A. De la Vieja, V. Paroder, C. Riedel, M. Artani *et al.*, 2003 The sodium/iodide Symporter (NIS): characterization, regulation, and medical significance. Endocr. Rev. 24: 48–77. https://doi.org/10.1210/er.2001-0029

Duric, V., M. Banasr, P. Licznerski, H. D. Schmidt, C. A. Stockmeier *et al.*, 2010 A negative regulator of MAP kinase causes depressive behavior. Nat. Med. 16: 1328–1332. https://doi.org/10.1038/nm.2219

Eckert, D., S. Buhl, S. Weber, R. Jager, and H. Schorle, 2005 The AP-2 family of transcription factors. Genome Biol. 6: 246. https://doi.org/10.1186/gb-2005-6-13-246

Fischer, A., F. Sananbenesi, C. Schrick, J. Spiess, and J. Radulovic, 2004 Distinct roles of hippocampal de novo protein synthesis and actin rearrangement in extinction of contextual fear. J. Neurosci. 24: 1962–1966. https://doi.org/10.1523/JNEUROSCI.5112-03.2004

Funato, H., C. Miyoshi, T. Fujiyama, T. Kanda, M. Sato *et al.*, 2016 Forward-genetics analysis of sleep in randomly mutagenized mice. Nature 539: 378–383. https://doi.org/10.1038/nature20142

Gao, V., F. Turek, and M. Vitaterna, 2016 Multiple classifier systems for automatic sleep scoring in mice. J. Neurosci. Methods 264: 33–39. https://doi.org/10.1016/j.jneumeth.2016.02.016

Gass, P., T. Herdegen, R. Bravo, and M. Kiessling, 1992 Induction of immediate early gene encoded proteins in the rat hippocampus after bicuculline-induced seizures: differential expression of KROX-24, FOS and JUN proteins. Neuroscience 48: 315–324. https://doi.org/10.1016/0306-4522(92)90493-L

Gibney, P. A., C. Lu, A. A. Caudy, D. C. Hess, and D. Botstein, 2013 Yeast metabolic and signaling genes are required for heat-shock survival and have little overlap with the heat-in-

duced genes. Proc. Natl. Acad. Sci. USA 110: E4393–E4402. https://doi.org/10.1073/pnas.1318100110

Green, R. M., W. Feng, T. Phang, J. L. Fish, H. Li *et al.*, 2015 Tfap2a-dependent changes in mouse facial morphology result in clefting that can be ameliorated by a reduction in Fgf8 gene dosage. Dis. Model. Mech. 8: 31–43. https://doi.org/10.1242/dmm.017616

Grubbs, J. J., L. L. Lopes, A. M. van der Linden, and D. M. Raizen, 2019 Sik-Hdac4 signaling is required for the metabolic regulation of sleep. Sleep 42: A11.

Hahm, S., T. M. Mizuno, T. J. Wu, J. P. Wisor, C. A. Priest *et al.*, 1999 Targeted deletion of the Vgf gene indicates that the encoded secretory peptide precursor plays a novel role in the regulation of energy balance. Neuron 23: 537–548. https://doi.org/10.1016/S0896-6273(00)80806-5

Joiner, W. J., 2016 Unraveling the evolutionary determinants of sleep. Curr. Biol. 26: R1073–R1087. https://doi.org/10.1016/j.cub.2016.08.068

Keene, A. C., and E. R. Duboue, 2018 The origins and evolution of sleep. J. Exp. Biol. 221: jeb159533. https://doi.org/10.1242/jeb.159533

Kent, B. A., S. M. Strittmatter, and H. B. Nygaard, 2018 Sleep and EEG power spectral analysis in three transgenic mouse models of Alzheimer's disease: APP/PS1, 3xTgAD, and Tg2576. J. Alzheimers Dis. 64: 1325–1336. https://doi.org/10.3233/JAD-180260

Kohlbecker, A., A. E. Lee, and H. Schorle, 2002 Exencephaly in a subset of animals heterozygous for AP-2alpha mutation. Teratology 65: 213–218. https://doi.org/10.1002/tera.10037

Kopp, C., U. Albrecht, B. Zheng, and I. Tobler, 2002 Homeostatic sleep regulation is preserved in mPer1 and mPer2 mutant mice. Eur. J. Neurosci. 16: 1099–1106. https://doi.org/10.1046/j.1460-9568.2002.02156.x

Kucherenko, M. M., V. Ilangovan, B. Herzig, H. R. Shcherbata, and H. Bringmann, 2016 TfAP-2 is required for night sleep in Drosophila. BMC Neurosci. 17: 72. https://doi.org/10.1186/s12868-016-0306-3

Lin, J. M., E. Z. M. Taroc, J. A. Frias, A. Prasad, A. N. Catizone *et al.*, 2018 The transcription factor Tfap2e/AP-2ε plays a pivotal role in maintaining the identity of basal vomeronasal sensory neurons. Dev. Biol. 441: 67–82. https://doi.org/10.1016/j.ydbio.2018.06.007

Li, H., R. Sheridan, and T. Williams, 2013 Analysis of TFAP2A mutations in Branchio-Oculo-Facial Syndrome indicates functional complexity within the AP-2alpha DNA-binding domain. Hum. Mol. Genet. 22: 3195–3206. https://doi.org/10.1093/hmg/ddt173

Lohr, K. M., A. I. Bernstein, K. A. Stout, A. R. Dunn, C. R. Lazo *et al.*, 2014 Increased vesicular monoamine transporter enhances dopamine release and opposes Parkinson disease-related neurodegeneration in vivo. Proc. Natl. Acad. Sci. USA 111: 9977–9982. https://doi.org/10.1073/pnas.1402134111

Mander, B. A., V. Rao, B. Lu, J. M. Saletin, J. R. Lindquist *et al.*, 2013 Prefrontal atrophy, disrupted NREM slow waves and impaired hippocampal-dependent memory in aging. Nat. Neurosci. 16: 357–364. https://doi.org/10.1038/nn.3324

Mang, G. M., and P. Franken, 2012 Sleep and EEG phenotyping in mice. Curr. Protoc. Mouse Biol. 2: 55–74.

Mani, A., J. Radhakrishnan, A. Farhi, K. S. Carew, C. A. Warnes *et al.*, 2005 Syndromic patent ductus arteriosus: evidence for haploinsufficient TFAP2B mutations and identification of a linked sleep disorder. Proc. Natl. Acad. Sci. USA 102: 2975–2979. https://doi.org/10.1073/pnas.0409852102

Martin, M., 2011 Cutadapt removes adapter sequences from high-throughput sequencing reads. 17: 3.

Matsuda, R., T. Kohno, S. Kohsaka, R. Fukuoka, Y. Maekawa *et al.*, 2017 The prevalence of poor sleep quality and its association with depression and anxiety scores in patients admitted for cardiovascular disease: a cross-sectional designed study. Int. J. Cardiol. 228: 977–982. https://doi.org/10.1016/j.ijcard.2016.11.091

McHugh, S. B., C. Barkus, J. Lima, L. R. Glover, T. Sharp *et al.*, 2015 SERT and uncertainty: serotonin transporter expression influences information processing biases for ambiguous aversive cues in mice. Genes Brain Behav. 14: 330–336. https://doi.org/10.1111/gbb.12215

Miyazaki, S., C. Y. Liu, and Y. Hayashi, 2017 Sleep in vertebrate and invertebrate animals, and insights into the function and evolution of sleep. Neurosci. Res. 118: 3–12. https://doi.org/10.1016/j.neures.2017.04.017

Moser, M., A. Pscherer, C. Roth, J. Becker, G. Mucher *et al.*, 1997a Enhanced apoptotic cell death of renal epithelial cells in mice lacking transcription factor AP-2beta. Genes Dev. 11: 1938–1948. https://doi.org/10.1101/gad.11.15.1938

Moser, M., J. Ruschoff, and R. Buettner, 1997b Comparative analysis of AP-2 alpha and AP-2 beta gene expression during murine embryogenesis. Dev. Dyn. 208: 115–124. https://doi.org/10.1002/(SICI)1097-0177(199701)208:1<115::AID-AJA11>3.0.CO;2-5

Ohnishi, Y. N., Y. H. Ohnishi, M. Hokama, H. Nomaru, K. Yamazaki *et al.*, 2011 FosB is essential for the enhancement of stress tolerance and antagonizes locomotor sensitization by DeltaFosB. Biol. Psychiatry 70: 487–495. https://doi.org/10.1016/j.biopsych.2011.04.021

Paylor, R., R. S. Johnson, V. Papaioannou, B. M. Spiegelman, and J. M. Wehner, 1994 Behavioral assessment of c-fos mutant mice. Brain Res. 651: 275–282. https://doi.org/10.1016/0006-8993(94)90707-2

Peters, R. V., N. Aronin, and W. J. Schwartz, 1994 Circadian regulation of Fos B is different from c-Fos in the rat suprachiasmatic nucleus. Brain Res. Mol. Brain Res. 27: 243–248. https://doi.org/10.1016/0169-328X(94)90006-X

Plath, N., O. Ohana, B. Dammermann, M. L. Errington, D. Schmitz *et al.*, 2006 Arc/Arg3.1 is essential for the consolidation of synaptic plasticity and memories. Neuron 52: 437–444. https://doi.org/10.1016/j.neuron.2006.08.024

Radyushkin, K., K. Hammerschmidt, S. Boretius, F. Varoqueaux, A. El-Kordi *et al.*, 2009 Neuroligin-3-deficient mice: model of a monogenic heritable form of autism with an olfactory deficit. Genes Brain Behav. 8: 416–425. https://doi.org/10.1111/j.1601-183X.2009.00487.x

Raizen, D. M., and J. E. Zimmerman, 2011 Non-mammalian genetic model systems in sleep research. Sleep Med. Clin. 6: 131–139. https://doi.org/10.1016/j.jsmc.2011.04.005

Roberts, G. G., 3rd, and A. P. Hudson, 2009 Rsf1p is required for an efficient metabolic shift from fermentative to glycerol-based respiratory growth in S. cerevisiae. Yeast 26: 95–110. https://doi.org/10.1002/yea.1655

Sananbenesi, F., A. Fischer, X. Wang, C. Schrick, R. Neve *et al.*, 2007 A hippocampal Cdk5 pathway regulates extinction of contextual fear. Nat. Neurosci. 10: 1012–1019. https://doi.org/10.1038/nn1943

Satoda, M., M. E. Pierpont, G. A. Diaz, R. A. Bornemeier, and B. D. Gelb, 1999 Char syndrome, an inherited disorder with patent ductus arteriosus, maps to chromosome 6p12-p21. Circulation 99: 3036–3042. https://doi.org/10.1161/01.CIR.99.23.3036

Satoda, M., F. Zhao, G. A. Diaz, J. Burn, J. Goodship *et al.*, 2000 Mutations in TFAP2B cause Char syndrome, a familial form of patent ductus arteriosus. Nat. Genet. 25: 42–46. https://doi.org/10.1038/75578

Schorle, H., P. Meier, M. Buchert, R. Jaenisch, and P. J. Mitchell, 1996 Transcription factor AP-2 essential for cranial closure and craniofacial development. Nature 381: 235–238. https://doi.org/10.1038/381235a0

Schwartz, W. J., and P. Zimmerman, 1990 Circadian timekeeping in BALB/c and C57BL/6 inbred mouse strains. J. Neurosci. 10: 3685–3694. https://doi.org/10.1523/JNEUROSCI.10-11-03685.1990

Shiromani, P. J., R. Basheer, J. Thakkar, D. Wagner, M. A. Greco *et al.*, 2000 Sleep and wakefulness in c-fos and fos B gene knockout mice. Brain Res. Mol. Brain Res. 80: 75–87. https://doi.org/10.1016/S0169-328X(00)00123-6

Taylor, T. N., W. M. Caudle, K. R. Shepherd, A. Noorian, C. R. Jackson *et al.*, 2009 Nonmotor symptoms of Parkinson's disease revealed in an animal model with reduced monoamine storage capacity. J. Neurosci. 29: 8103–8113. https://doi.org/10.1523/JNEUROSCI.1495-09.2009

Tobler, I., 1995 Is sleep fundamentally different between mammalian species? Behav. Brain Res. 69: 35–41. https://doi.org/10.1016/0166-4328(95)00025-O

Turek, M., I. Lewandrowski, and H. Bringmann, 2013 An AP2 transcription factor is required for a sleep-active neuron to induce sleep-like quiescence in C. elegans. Curr. Biol. 23: 2215–2223. https://doi.org/10.1016/j.cub.2013.09.028

Verbitsky, E. V., 2017 Anxiety and sleep in experiment and clinic. Zh. Nevrol. Psikhiatr. Im. S. S. Korsakova 117: 12–18. https://doi.org/10.17116/jnevro20171174212-18

Walf, A. A., and C. A. Frye, 2007 The use of the elevated plus maze as an assay of anxiety-related behavior in rodents. Nat. Protoc. 2: 322–328. https://doi.org/10.1038/nprot.2007.44

Werling, U., and H. Schorle, 2002 Transcription factor gene AP-2 gamma essential for early murine development. Mol. Cell. Biol. 22: 3149–3156. https://doi.org/10.1128/MCB.22.9.3149-3156.2002

Williams, T., and R. Tjian, 1991 Characterization of a dimerization motif in AP-2 and its function in heterologous DNA-binding proteins. Science 251: 1067–1071. https://doi.org/10.1126/science.1998122

Yankelevitch-Yahav, R., M. Franko, A. Huly, and R. Doron, 2015 The forced swim test as a model of depressive-like behavior. J. Vis. Exp. 97: 52587. https://doi.org/10.3791/52587

Zainolabidin, N., S. P. Kamath, A. R. Thanawalla, and A. I. Chen, 2017 Distinct activities of Tfap2A and Tfap2B in the specification of GABAergic interneurons in the developing cerebellum. Front. Mol. Neurosci. 10: 281. https://doi.org/10.3389/fnmol.2017.00281

Zhang, J., S. Hagopian-Donaldson, G. Serbedzija, J. Elsemore, D. Plehn-Dujowich *et al.*, 1996 Neural tube, skeletal and body wall defects in mice lacking transcription factor AP-2. Nature 381: 238–241. https://doi.org/10.1038/381238a0

Zhao, F., C. G. Weismann, M. Satoda, M. E. Pierpont, E. Sweeney *et al.*, 2001 Novel TFAP2B mutations that cause Char syndrome provide a genotype-phenotype correlation. Am. J. Hum. Genet. 69: 695–703. https://doi.org/10.1086/323410

Zhao, F., T. Lufkin, and B. D. Gelb, 2003 Expression of Tfap2d, the gene encoding the transcription factor Ap-2 delta, during mouse embryogenesis. Gene Expr. Patterns 3: 213–217. https://doi.org/10.1016/S1567-133X(02)00067-4

Zheng, B., U. Albrecht, K. Kaasik, M. Sage, W. Lu *et al.*, 2001 Nonredundant roles of the mPer1 and mPer2 genes in the mammalian circadian clock. Cell 105: 683–694. https://doi.org/10.1016/S0092-8674(01)00380-4

Communicating editor: J. Schimenti

Supplementary materials for "Functional divergence of mammalian TFAP2a and TFAP2b transcription factors for bidirectional sleep control"

Table S1. Genotyping protocols

Gene	Primer names	Primer sequence 5' - 3'	PCR conditions	Products
Tfap2a_fl; *Tfap2a*_WT	ALFGF5	GCCAAGTTCTAATTCCATCAGAAGCTTATCGATACCGTCG	45s at 95°, 45s at 68°, 1min at 72° for 35 cycles	flox allele 245bp; flp allele 600bp; wildtype allele 510bp
	ALFLPF4	CCCAAAGTGCCTGGGCTGAATTGACTTCTCTAGG		
	ALFLPR1	GCTCAGAATTTATGTAAGAATCTAGCTTGGAGGCTTATGTC		
Tfap2a$^{+/-}$	ALFLPF1	GCTCTCTCTTTTCCTGCCTTGGAACCATGACCCTCAG	45s at 95°, 45s at 68°, 1min at 72° for 35 cycles	*Tfap2a*-190bp; wildtype allele no band
	ALFLPR1	GCTCAGAATTTATGTAAGAATCTAGCTTGGAGGCTTATGTC		
Tfap2b$^{+/-}$; *Tfap2b*$^{+/+}$	PGK-PolyA DW	CTGCTCTTTACTGAAGGCTCTTT	30s at 95°, 45s at 61°, 1min at 72° for 40 cycles	*Tfap2b*-380bp; *Tfap2b*+ 221bp
	4 Exon Rev	TTCTGAGGACGCCGCCCAGG		
	4 Exon DW	CCTCCCAAATCTGTGACTTCT		

Table S2. qPCR protocols

Gene	Forward	Reverse	PCR conditions
Tfap2a	GCTCACTCCAGAAGGGGTTG	GTGCGGGCCTGAAGAGGTTA	1 min at 94°, 30s at 62°, 1min at 72° for 40 cycles
Tfap2b	GGAGAGGAGCGTCGGATTTG	CGTCGTGACGGTCCATAGC	
eef1a1	TGCCCCAGGACACAGAGACTTCA	AATTCACCAACACCAGCAGCAA	

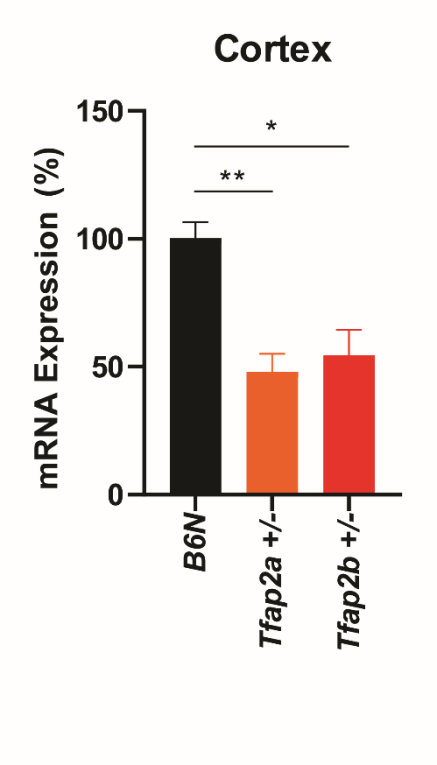

Fig.S1. Reduction of mRNA expression in the cortex of *Tfap2a*$^{+/-}$ and *Tfap2b*$^{+/-}$ mutants.

Male B6N (n=3), *Tfap2a*$^{+/-}$ (n=3), *Tfap2b*$^{+/-}$ (n= 3), mRNA expression examined by qPCR, reduction rates were calculated as fold changes normalized to the mean of the control (B6N) and were analyzed using one-way ANOVA followed by Dunnett's multiple comparisons. F = 15.11, p = 0.0066; *Tfap2a*$^{+/-}$ vs. B6N, ** p =0.0061; *Tfap2b*$^{+/-}$ vs. B6N, * p = 0.0114. All data are shown as the mean ± SEM.

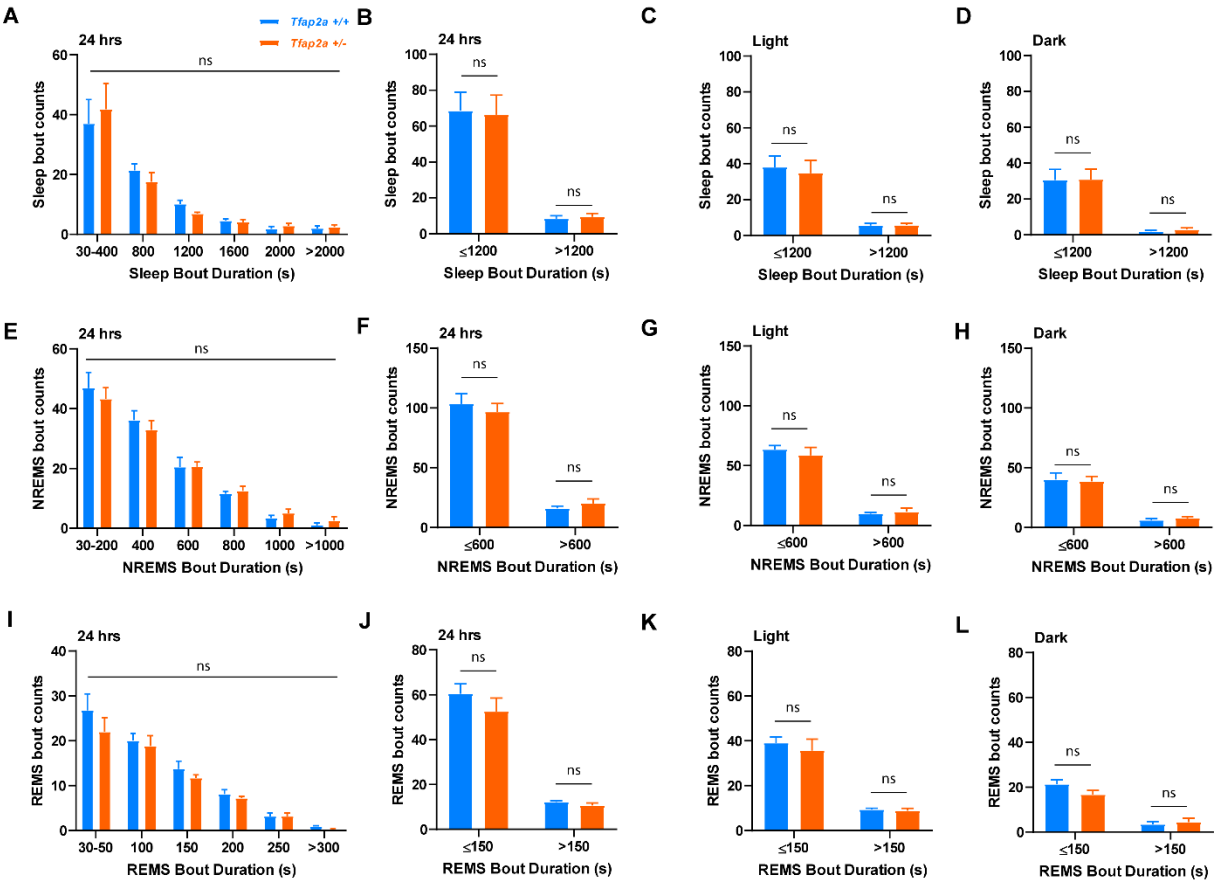

Fig.S2. Sleep bout distributions were normal in *Tfap2a*$^{+/-}$ mice.

(A) 24 h of sleep bout distribution: two-way ANOVA followed by Sidak's multiple comparisons test, the main effect of genotype, F (1, 60) = 0.210, p = 0.301.

(B) Accumulative counts of sleep bouts in 24 h: ≤ 1200-s, p = 0.570; > 1200-s, p = 0.935.

(C) Accumulative counts of sleep bouts in light phase: ≤ 1200-s, p = 0.935; > 1200-s, p = 0.459.

(D) Accumulative counts of sleep bouts in dark phase: ≤ 1200-s, p = 0.544; > 1200-s, p = 0.402.

(E) 24 h of NREMS bout distribution: two-way ANOVA followed by Sidak's multiple comparisons test, the main effect of genotype, F (1, 60) = 0.210, p = 0.648.

(F) Accumulative counts of NREMS bouts in 24h: ≤ 600-s, p = 0.544; > 600-s, p = 0.351.

(G) Accumulative counts of NREMS bouts in light phase: ≤ 600-s, p = 0.567; > 600-s, p = 0.574.

(H) Accumulative counts of NREMS bouts in dark phase: ≤ 600-s, p = 0.812; > 600-s, p = 0.442.

(I) 24 h of REMS bout distribution: two-way ANOVA followed by Sidak's multiple comparisons test, the main effect of genotype, $F(1, 50) = 4.031$, $p = 0.0501$.

(J) Accumulative counts of REMS bouts in 24h: ≤ 150-s, $p = 0.372$; > 150-s, $p = 0.416$.

(K) Accumulative counts of REMS bouts in light phase: ≤ 150-s, $p = 0.610$; > 150-s, $p = 0.715$.

(L) Accumulative counts of REMS bouts in dark phase: ≤ 150-s, $p = 0.108$; > 150-s, $p = 0.657$.

All data are shown as the mean ± SEM. n = 5 for *Tfap2a*$^{+/+}$, n = 7 for *Tfap2a*$^{+/-}$. To detect more subtle changes in the sleep architecture, we analyzed sleep bout distributions for total sleep, NREMS and REMS. Data were plotted on a scale of 400s per bin in sleep, 200s in NREMS and 50s in REMS using bout counts in 24 h. According to the distribution plots, cumulative counts were calculated by setting a cut-off at 1200s in sleep, 600s in NREMS sleep, and 150s in REMS and two-tailed unpaired *t* tests were used for accumulated effects.

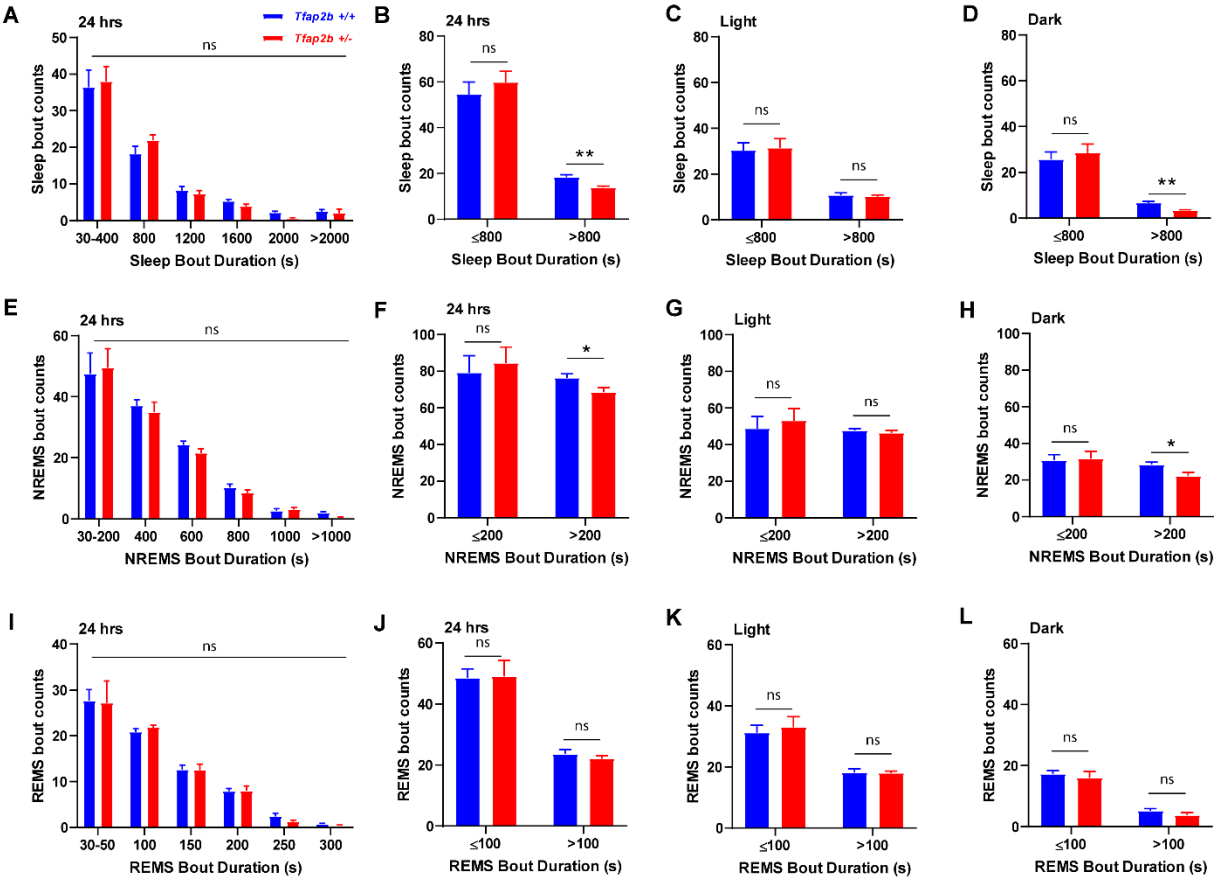

Fig.S3. Longer sleep bouts were reduced in *Tfap2b*$^{+/-}$ mice.

(A) 24 h of sleep bout distribution: two-way ANOVA followed by Sidak's multiple comparisons test, the main effect of genotype, $F(1, 66) = 0.011$, $p = 0.917$.

(B) Accumulative counts of sleep bouts in 24 h: ≤ 800-s, $p = 0.480$; > 800-s, $^{**}p = 0.007$.

(C) Accumulative counts of sleep bouts in light phase: ≤ 800-s, $p = 0.841$; > 800-s, $p = 0.631$.

(D) Accumulative counts of sleep bouts in dark phase: ≤ 800-s, $p = 0.586$; > 800-s, $^{**}p = 0.002$.

(E) 24 h of NREMS bout distribution: two-way ANOVA followed by Sidak's multiple comparisons test, the main effect of genotype, $F(1, 66) = 0.303$, $p = 0.584$.

(F) Accumulative counts of NREMS bouts in 24h: ≤ 200-s, $p = 0.691$; > 200-s, $^{*}p = 0.041$.

(G) Accumulative counts of NREMS bouts in light phase: ≤ 200-s, $p = 0.651$; > 200-s, $p = 0.412$.

(H) Accumulative counts of NREMS bouts in dark phase: ≤ 200-s, $p = 0.866$; > 200-s, $^{*}p = 0.019$.

(I) 24 h of REMS bout distribution: two-way ANOVA followed by Sidak's multiple comparisons test, the main effect of genotype, $F(1, 66) = 0.035$, $p = 0.852$.

(J) Accumulative counts of REMS bouts in 24h: ≤ 100-s, $p = 0.932$; > 100-s, $p = 0.933$.

(K) Accumulative counts of REMS bouts in light phase: ≤ 100-s, $p = 0.421$; > 100-s, $p = 0.927$.

(L) Accumulative counts of REMS bouts in dark phase: ≤ 100-s, $p = 0.588$; > 100-s, $p = 0.242$.

All data are shown as the mean ± SEM. n = 7 for *Tfap2b*$^{+/+}$, n = 6 for *Tfap2b*$^{+/-}$. Data were plotted on a scale of 400s per bin in sleep, 200s in NREMS and 50s in REMS using bout counts in 24 h. According to the distribution plots, accumulative counts were calculated by setting a cut-off at 800s in sleep, 200s in NREMS sleep, and 100s in REMS. Two-tailed unpaired *t* tests were used for accumulated effects.

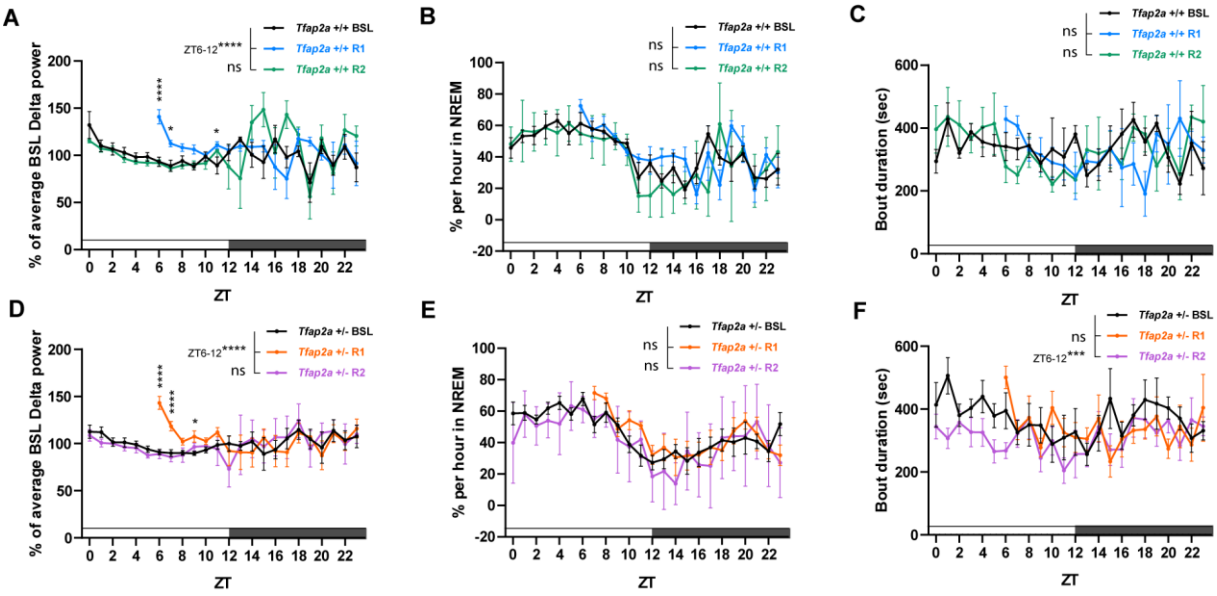

Fig. S4. NREMS sleep rebound of the sleep-deprived *Tfap2a*$^{+/-}$ mice.

Analysis of circadian delta power changes in control animals: BSL vs. R1 ZT6-12, the main effect of SD, F (1, 48) = 47.60, ****p < 0.0001, Sidak's multiple comparisons, *p < 0.05, ****p < 0.0001; BSL vs. R2, the main effect of SD, F (1, 192) = 0.8817, p = 0.3489.

NREMS time changes in control animals: BSL vs. R1 ZT6-12, the main effect of SD, F (1, 48) = 1.789, p = 0.187; BSL vs. R2, the main effect of SD, F (1, 192) = 1.647, p = 0.201.

NREMS bout changes in control animals: BSL vs. R1 ZT6-12, the main effect of SD, F (1, 48) = 0.294, p = 0.590; BSL vs. R2, the main effect of SD, F (1, 190) = 0.000158, p = 0.990.

Circadian delta power changes in *Tfap2a*$^{+/-}$ mutant animals: BSL vs. R1 ZT6-12, the main effect of SD, F (1, 72) = 80.34, ****p < 0.0001, Sidak's multiple comparisons, *p < 0.05, ****p < 0.0001; BSL vs. R2, the main effect of SD, F (1, 288) = 0.0651, p = 0.799.

NREMS time changes in *Tfap2a*$^{+/-}$ mutant animals: BSL vs. R1 ZT6-12, the main effect of SD, F (1, 72) = 2.108, p = 0.151; BSL vs. R2, the main effect of SD, F (1, 288) = 2.985, p = 0.085.

NREMS bout changes in *Tfap2a*$^{+/-}$ mutant animals: BSL vs. R1 ZT6-12, the main effect of SD, F (1, 72) = 1.156, p = 0.286; BSL vs. R2, the main effect of SD, F (1, 286) = 14.46, ***p = 0.0002.

All data were analyzed by two-way ANOVA followed by Sidak's multiple comparisons test and are shown as the mean ± SEM. *Tfap2a*$^{+/+}$ (n = 5) and *Tfap2a*$^{+/-}$ (n = 7).

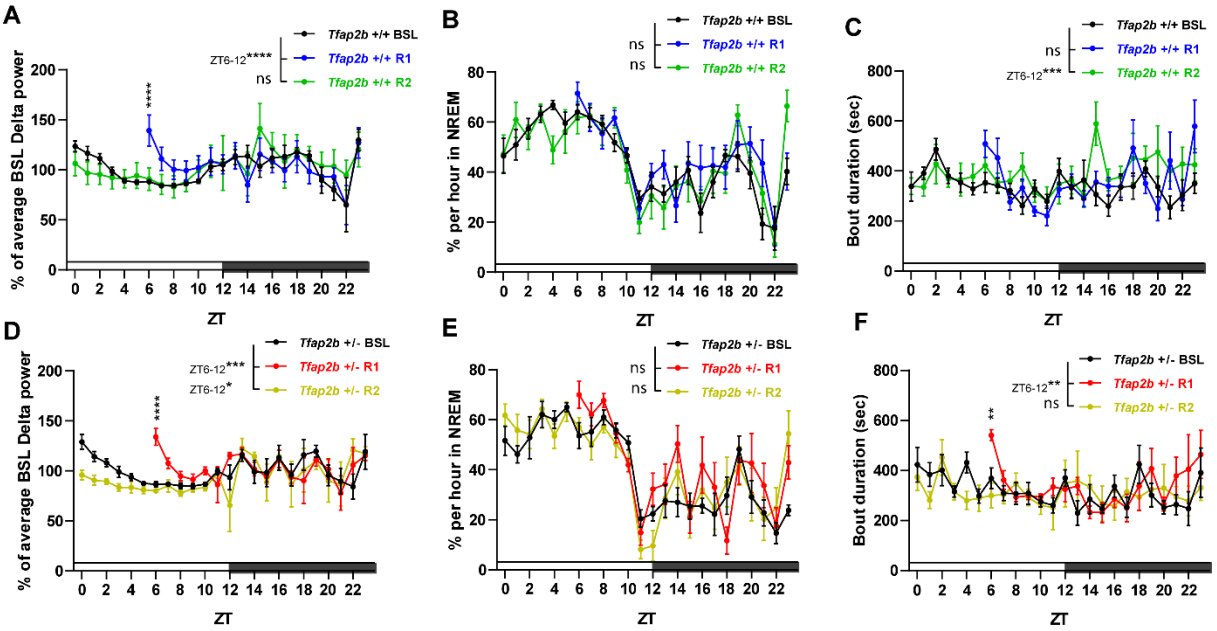

Fig. S5. NREMS sleep rebound of the sleep-deprived *Tfap2b*$^{+/-}$ mice.

(A) Analysis of circadian delta power changes in control animals: BSL vs. R1 ZT6-11, the main effect of SD, F (1, 71) = 18.08, ****p < 0.0001, Sidak's multiple comparisons, ****p < 0.0001; BSL vs. R2, the main effect of SD, F (1, 279) = 0.377, p = 0.540.

(B) NREMS time changes in control animals: BSL vs. R1 ZT6-11, the main effect of SD, F (1, 72) = 0.476, p = 0.492; BSL vs. R2, the main effect of SD, F (1, 288) = 0.167, p = 0.683.

(C) NREMS bout changes in control animals: BSL vs. R1 ZT6-11, the main effect of SD, F (1, 72) = 1.055, p = 0.308; BSL vs. R2, the main effect of SD, F (1, 288) = 10.33, ***p = 0.0015.

(D) Circadian delta power changes in *Tfap2b*$^{+/-}$ mutant animals: BSL vs. R1 ZT6-11, the main effect of SD, F (1, 60) = 13.68, ***p = 0.0005, Sidak's multiple comparisons, ****p < 0.0001; BSL vs. R2, the main effect of SD, F (1, 233) = 4.680, *p = 0.0315.

(E) NREMS time changes in *Tfap2b*$^{+/-}$ mutant animals: BSL vs. R1 ZT6-11, the main effect of SD, F (1, 60) = 1.026, p = 0.315; BSL vs. R2, the main effect of SD, F (1, 240) = 0.438, p = 0.509.

(F) NREMS bout changes in *Tfap2b*$^{+/-}$ mutant animals: BSL vs. R1 ZT6-11, the main effect of SD, F (1, 60) = 7.405, **p = 0.0085, Sidak's multiple comparisons, **p < 0.01; BSL vs. R2, the main effect of SD, F (1, 240) = 0.293, p = 0.589.

All data were analyzed by two-way ANOVA followed by Sidak's multiple comparisons test and are shown as the mean ± SEM. *Tfap2b*$^{+/+}$ (n = 7) and *Tfap2b*$^{+/-}$ (n = 6).

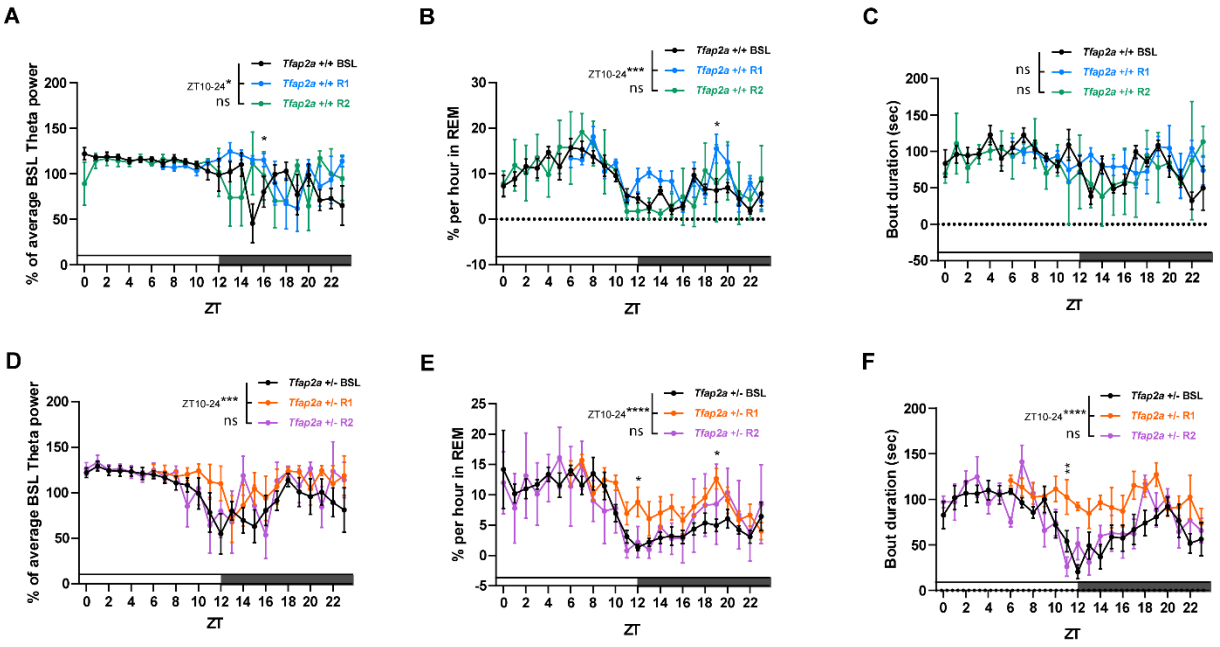

Fig. S6. REMS sleep rebound of the sleep-deprived *Tfap2a*$^{+/-}$ mice.

(A) Analysis of circadian theta power changes in control animals: BSL vs. R1 ZT10-24, the main effect of SD, F (1, 112) = 4.510, *p = 0.0359, Sidak's multiple comparisons, *p < 0.05; BSL vs. R2, the main effect of SD, F (1, 192) = 0.263, p = 0.609.

(B) REMS time changes in control animals: BSL vs. R1 ZT10-24, the main effect of SD, F (1, 112) = 13.78, ***p = 0.0003, Sidak's multiple comparisons, *p < 0.05; BSL vs. R2, the main effect of SD, F (1, 192) = 0.882, p = 0.349.

(C) REMS bout changes in control animals: BSL vs. R1 ZT10-24, the main effect of SD, F (1, 112) = 3.614, p = 0.060; BSL vs. R2, the main effect of SD, F (1, 192) = 0.740, p = 0.391.

(D) Circadian theta power changes in *Tfap2a*$^{+/-}$ mutant animals: BSL vs. R1 ZT10-24, the main effect of SD, F (1, 168) = 11.63, ***p = 0.0008; BSL vs. R2, the main effect of SD, F (1, 288) = 2.322, p = 0.129.

(E) REMS time changes in *Tfap2a*$^{+/-}$ mutant animals: BSL vs. R1 ZT10-24, the main effect of SD, F (1, 168) = 36.72, p < 0.0001, Sidak's multiple comparisons, *p < 0.05; BSL vs. R2, the main effect of SD, F (1, 288) = 0.514, p = 0.474.

(F) REMS bout changes in *Tfap2a*$^{+/-}$ mutant animals: BSL vs. R1 ZT10-24, the main effect of SD, F (1, 168) = 48.45, p < 0.0001, Sidak's multiple comparisons, **p < 0.05; BSL vs. R2, the main effect of SD, F (1, 288) = 1.607, p = 0.206.

All data were analyzed by two-way ANOVA followed by Sidak's multiple comparisons test and are shown as the mean ± SEM. *Tfap2a*$^{+/+}$ (n = 5) and *Tfap2a*$^{+/-}$ (n = 7).

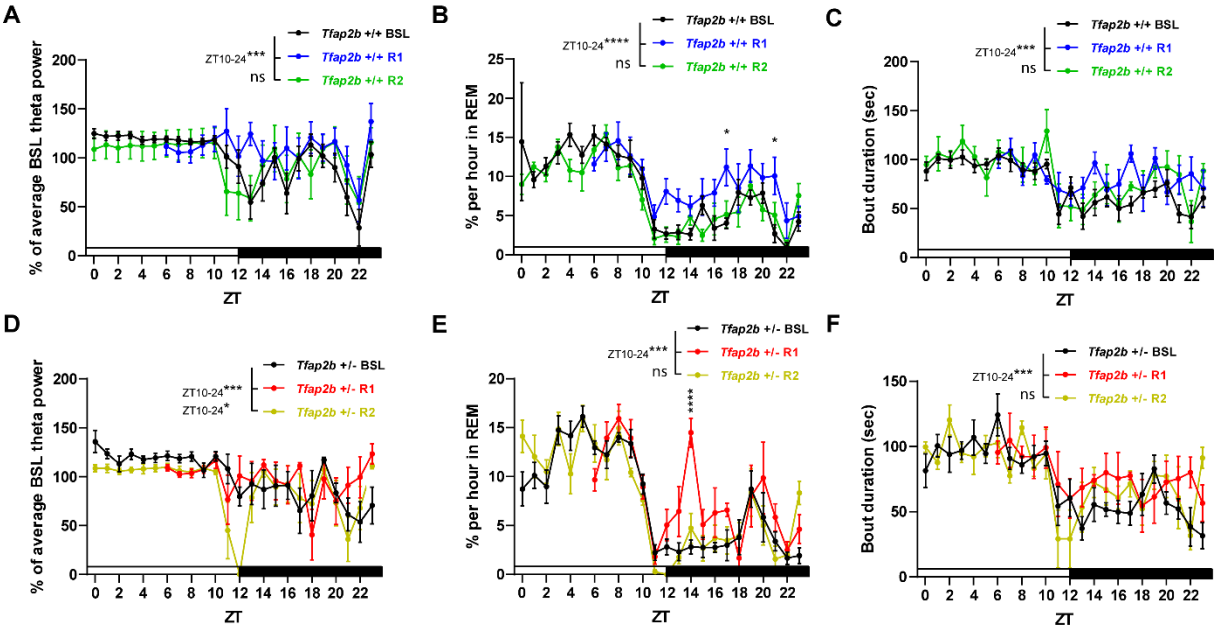

Fig. S7. REMS sleep rebound of the sleep-deprived *Tfap2b*$^{+/-}$ mice.

(A) Analysis of circadian theta power changes in control animals: BSL vs. R1 ZT10-24, the main effect of SD, F (1, 168) = 12.26, ***p = 0.0006; BSL vs. R2, the main effect of SD, F (1, 288) = 0.0788, p = 0.779.

(B) REMS time changes in control animals: BSL vs. R1 ZT10-24, the main effect of SD, F (1, 167) = 30.42, ****p < 0.0001, Sidak's multiple comparisons, *p < 0.05; BSL vs. R2, the main effect of SD, F (1, 288) = 1.667, p = 0.198.

(C) REMS bout changes in control animals: BSL vs. R1 ZT10-24, the main effect of SD, F (1, 216) = 15.85, ****p < 0.0001; BSL vs. R2, the main effect of SD, F (1, 192) = 0.740, p = 0.391.

(D) Circadian theta power changes in *Tfap2b*$^{+/-}$ mutant animals: BSL vs. R1 ZT10-24, the main effect of SD, F (1, 168) = 11.63, ***p = 0.0008; BSL vs. R2, the main effect of SD, F (1, 288) = 5.901, *p = 0.0157.

(E) REMS time changes in *Tfap2b*$^{+/-}$ mutant animals: BSL vs. R1 ZT10-24, the main effect of SD, F (1, 180) = 13.70, ***p = 0.0003, Sidak's multiple comparisons, ****p < 0.0001; BSL vs. R2, the main effect of SD, F (1, 240) = 0.938, p = 0.760.

(F) REMS bout changes in *Tfap2b*$^{+/-}$ mutant animals: BSL vs. R1 ZT10-24, the main effect of SD, F (1, 180) = 7.227, **p = 0.0079; BSL vs. R2, the main effect of SD, F (1, 240) = 1.304, p = 0.255.

All data were analyzed by two-way ANOVA followed by Sidak's multiple comparisons test and were shown as the mean ± SEM. *Tfap2b*$^{+/+}$ (n = 5) and *Tfap2b*$^{+/-}$ (n = 7).

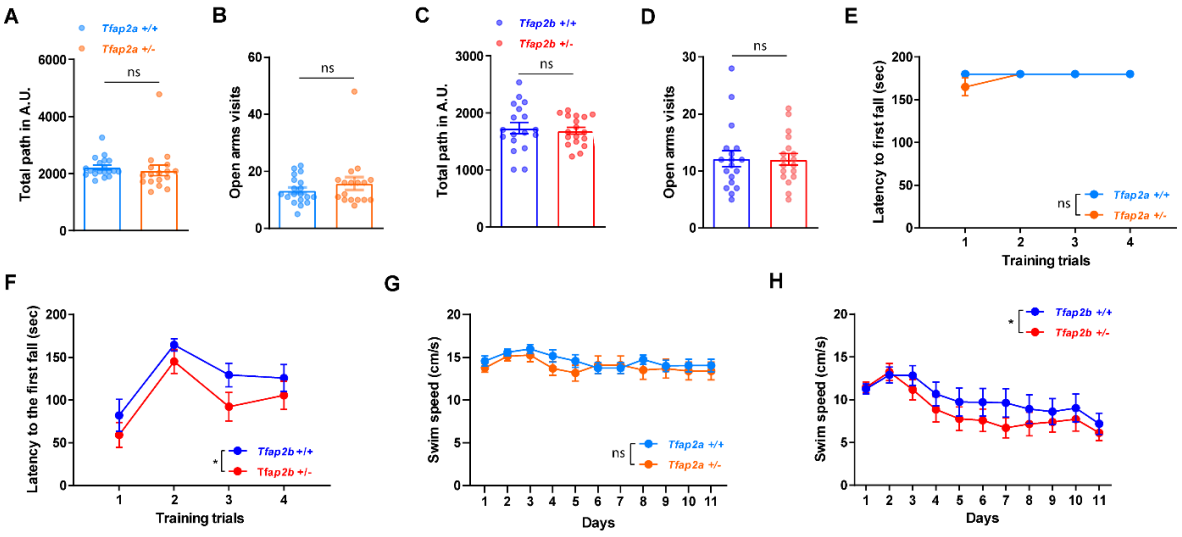

Fig. S8. Similar explorative behaviors or motor activities during EPM, rotarod, MWM tests between *Tfap2a/b* mutants and their controls.

(A) Total path of *Tfap2a* mice in EPM open arms. Mann-Whitney test, p = 0.107.

(B) Total visits of *Tfap2a* mice to EPM open arms. Mann-Whitney test, p = 0.654.

(C) Total path of *Tfap2b* mice in EPM open arms. Mann-Whitney test, p = 0.696.

(D) Total visits of *Tfap2b* mice to EPM open arms. Mann-Whitney test, p = 0.796.

(E) Latency to the first fall during the training section of Rotard in *Tfap2a* mice: two-way ANOVA followed by Sidak's multiple comparisons test, the main effect of genotype: F(1, 145) = 2.143, p = 0.146; the main effect of time: F(3, 145) = 2.135, p = 0.0983.

(F) Latency to the first fall during the training section of Rotard in *Tfap2b* mice: two-way ANOVA followed by Sidak's multiple comparisons test, the main effect of genotype: F(1, 126) = 6.965, **p = 0.0094; the main effect of time: F(3, 126) = 10.65, p < 0.0001.

(G) Swim speed in *Tfap2a* during MWM: two-way ANOVA followed by Sidak's multiple comparisons test, the main effect of genotype: F(1, 374) = 3.621, p = 0.058; the main effect of time: F(10, 374) = 1.403, p = 0.177.

(H) Swim speed in *Tfap2b* during MWM: two-way ANOVA followed by Sidak's multiple comparisons test, the main effect of genotype: F(1, 374) = 6.137, *p = 0.0137; the main effect of time: F(10, 374) = 4.528, p < 0.0001.

All data were shown as the mean ± SEM. n ≥ 10 for *Tfap2a*$^{+/+}$, *Tfap2a*$^{+/-}$, *Tfap2b*$^{+/+}$ or *Tfap2b*$^{+/-}$.

2.2 Part 2: *Tfap2b* regulated molecular changes in adult and developing mouse brain.

2.2.1 GABAergic gene expression was changed in *Tfap2b*$^{+/-}$ but not *Tfap2a*$^{+/-}$ adult mouse brain

GABAergic neurons are required for sleep initiation and regulation, especially NREMS. To investigate whether *Tfap2a* or *Tfap2b* regulates GABAergic related gene expression, mRNA was extracted from different brain areas of *Tfap2a* or *b* knockouts and their littermate controls. The expressions of GAD67, GAD65, Vgat were quantified using QPCR. As shown in **Fig. 4**, there was no significant changes in GAD67, GAD65, Vgat in all tested brain areas of *Tfap2a* mutants compared to their littermate controls. However, changes of expression were observed in *Tfap2b*$^{+/-}$ mice (**Fig. 5**). Specifically, an overall down regulation of all three genes was detected in CTX, BS, CB areas where the significant decrease for each gene was found in the CTX. Interestingly, an up-regulation of *Vgat* was observed in STR. These results suggest an indirect role of *Tfap2b* in regulating the expression of GABAergic system.

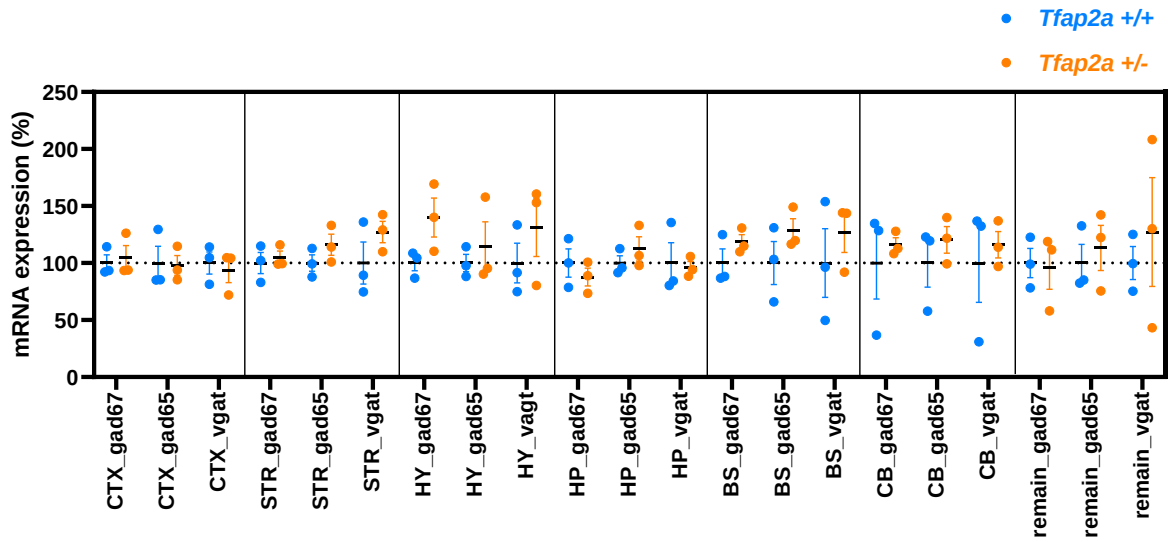

Figure 4. GAD67, GAD65 and Vgat gene expression was not changed in *Tfap2a*$^{+/-}$ adult mouse brain.

Data were analyzed by two-way ANOVA followed by Sidak's multiple comparisons test and were shown as the mean ± SEM. *Tfap2a*$^{+/+}$ (n = 3) and *Tfap2a*$^{+/-}$ (n = 3). CTX, cortex; HP, hippocampus; HY, hypothalamus; STR, striatum; BS, brainstem; CB, cerebellum.

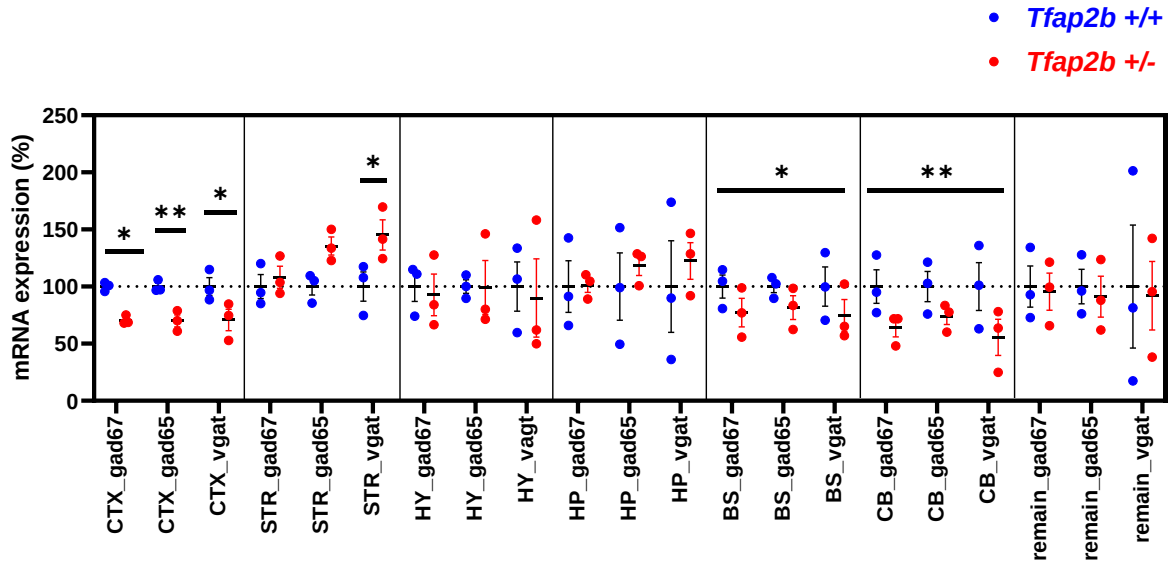

Figure 5. GAD67, GAD65 and Vgat gene expressions were altered in *Tfap2b*$^{+/-}$ adult mouse brain.

Data were analyzed by two-way ANOVA followed by Sidak's multiple comparisons test and were shown as the mean ± SEM, *p<0.05, **p<0.01. *Tfap2b*$^{+/+}$ (n = 3) and *Tfap2b*$^{+/-}$ (n = 3). CTX, cortex; HP, hippocampus; HY, hypothalamus; STR, striatum; BS, brainstem; CB, cerebellum.

2.2.2 GABAergic neurons expressing GAD67 was decreased in adult *Tfap2b*$^{+/-}$ mouse parafacial zone

Recent research has revealed an important sleep-promoting center in the mammalian lower brainstem, the medullary parafacial zone (PZ) [86]. Ablation of GABAergic neurons in PZ area reduces sleep whereas selective activation produces and maintains NREMS in mice [86, 89]. Therefore, I measured numbers of GAD67 expressing GABAergic neurons in the PZ of adult *Tfap2b* $^{+/-}$ mice using ISH. The ISH staining (**Fig. 6**) showed that GAD67 positive signals (**Fig. 6C**) was decreased in both counts and intensity in the PZ area of the adult *Tfap2b*$^{+/-}$ mice, indicating a decreased number of GABAergic neurons. Whereas the DAPI signals were similar between controls and mutants (**Fig. 6D**), suggesting same numbers of cells were included into GAD67 expression analysis. This is consistent with the qPCR result that showed a down-regulation GABAergic related genes in BS of the adult *Tfap2b*$^{+/-}$ mice (**Fig. 5**). Together, these results suggest that *Tfap2b* might be involved in the regulation of GABAergic neuronal population.

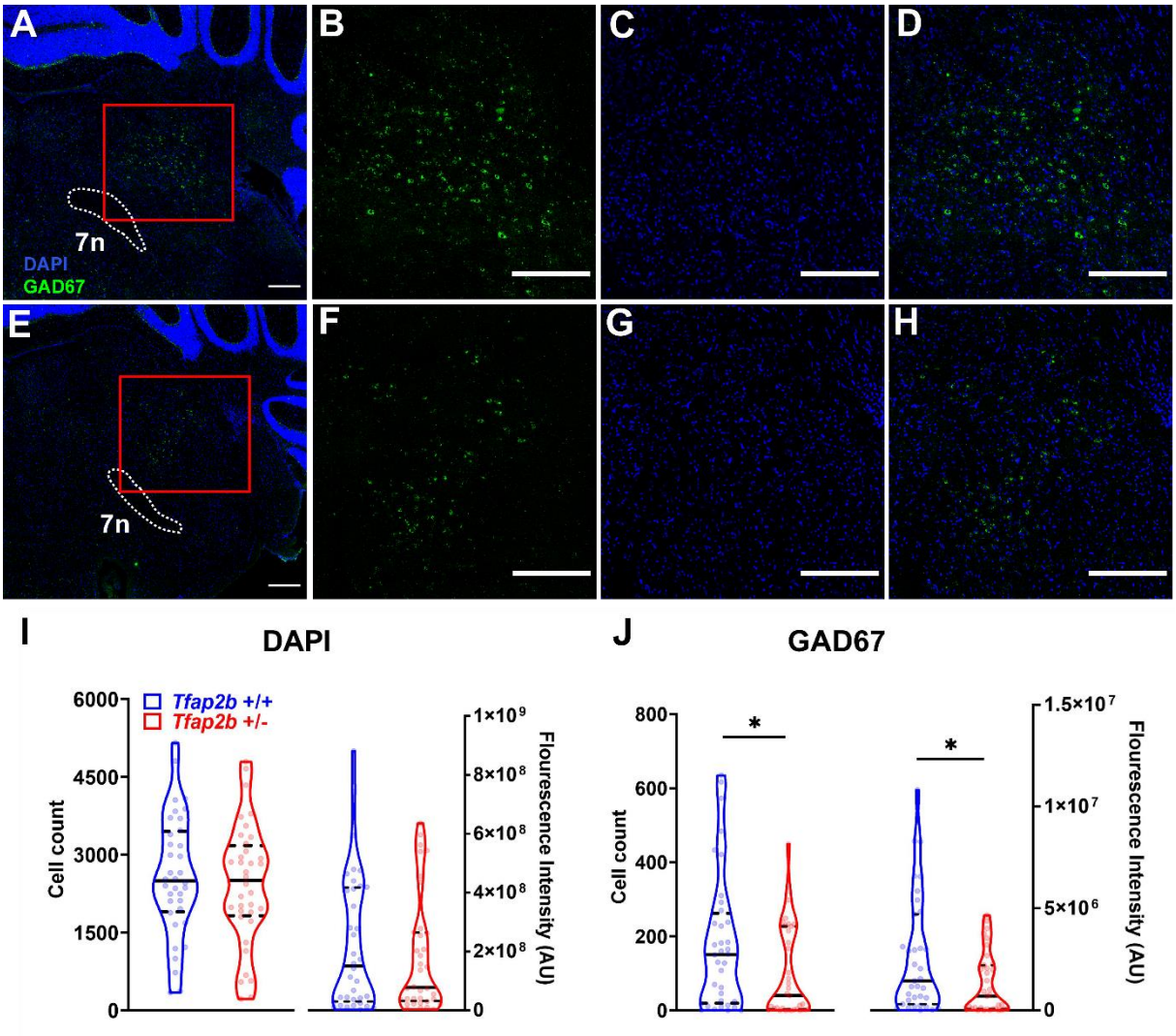

Figure 6. GAD67 expression was decreased in adult *Tfap2b*$^{+/-}$ mouse parafacial zone.

Representative GAD67 and DAPI positive signals in *Tfap2b*$^{+/+}$ (A) and *Tfap2b*$^{+/-}$ adult mouse medullary brainstem (B) were shown. The PZ area was selected in red rectangular above the 7th facial nerve marked in white dashed line. Scale bar = 1000 µm. Quantifications of DAPI (C) and GAD67 (D) signals in the PZ area were presented by cell count (left) and intensity (right). Outliers were identified by ROUT (Q = 0.2%) and removed from further analysis. Cleaned quantification data were analyzed by Mann-Whitney tests and were shown as the mean ± SEM, *p<0.05. *Tfap2b*$^{+/+}$ (n = 3) and *Tfap2b*$^{+/-}$ (n = 3); 12 brain sections per mouse at 10 µm thick.

2.2.3 Divergent gene expression changes in E14.5 *Tfap2b*$^{-/-}$ developing mouse brain

2.2.3a Scree plot analysis of principle components

Tfap2b expressed in very early embryo stages from E8 enriched in midbrain and hindbrain area [109, 118]. Although *Tfap2b* complete deletion is lethal at perinatal stages around P1-P2, *Tfap2b*$^{-/-}$ embryos of E14.5 were available for RNA-sequencing experiment. Therefore, I investigated how *Tfap2b* regulates the gene expression at developing stages. SP and DMH areas were dissected from female and male E14.5 embryos and comparisons were made between homozygotes and the wild-type littermate controls. Using principle component analysis (PCA), the overall genes expression pattern among samples and the correlations between samples were visualized. As shown in the scree plots, the first 2 PCs contributed to most of the variances (69% and 72.4%) in SP samples (**Fig. 7A, B**). More than 80% of total variances were explained by PC1 and PC2 in DMH samples (**Fig. 7C, D**).

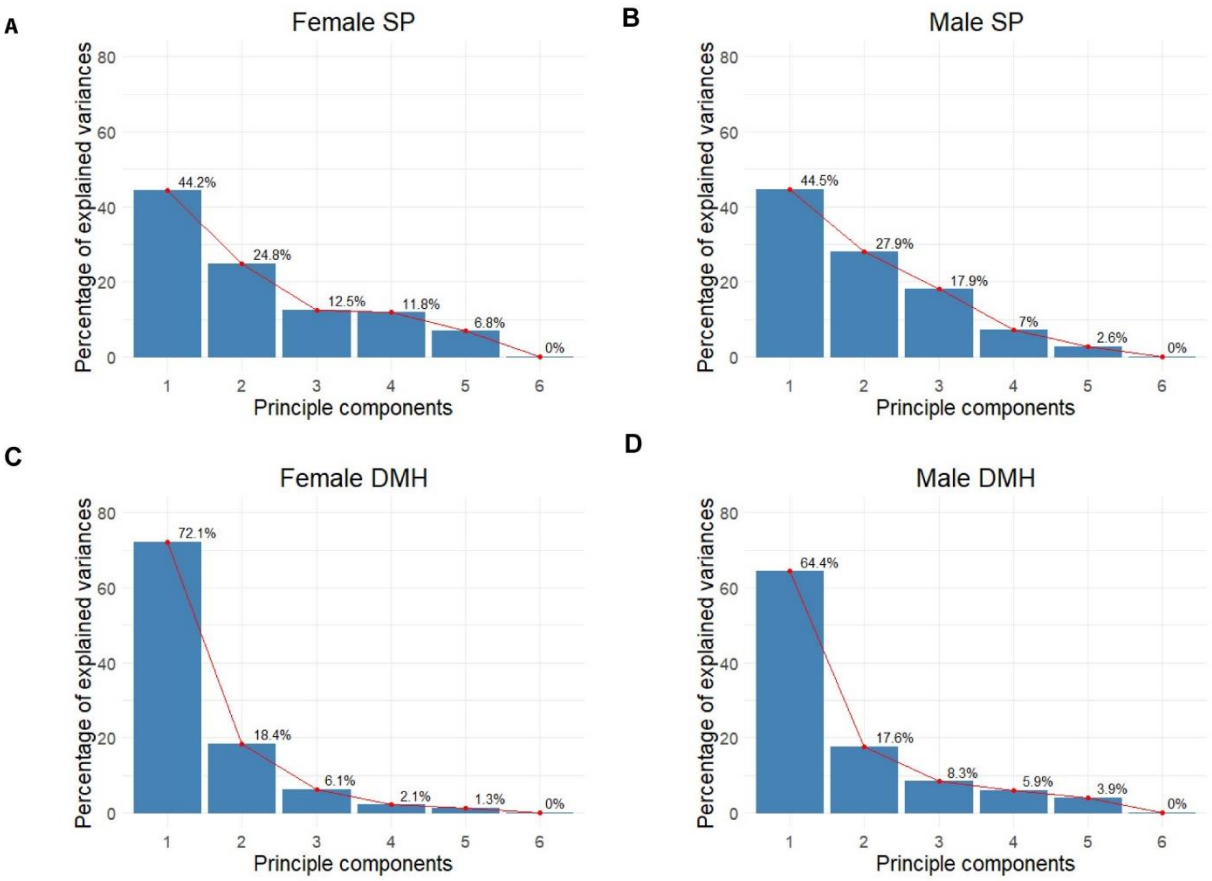

Figure 7. Proportion of variances explained by each principle component.

Scree plots showing the percentage of explained variances for all 6 principle components in the developing mouse brain samples female SP (A) male SP (B), female DMH (C), male DMH (D). Female E14.5 embryos *Tfap2b*$^{+/+}$, n=3; female E14.5 embryos *Tfap2b*$^{+/-}$, n=3; male E14.5 embryos *Tfap2b*$^{+/+}$, n=3; male E14.5 embryos *Tfap2b*$^{+/-}$, n=3; SP, secondary prosencephalon; DMH, diencephalon, midbrain and hindbrain.

2.2.3b Principle component analysis

PC1 vs PC2 was plotted for all samples (**Fig. 8**). In the female SP score plot (**Fig. 8A**), mut3_fdmh and ctrl2_fdmh were far away from each other and contributed the most to model PC1, while the other samples had only weak impacts. Along the PC2 axis, equal numbers of mutants and controls scattered in the positive or negative directions. In **Fig 8B**, mut3_fdmh scored particularly high (above 30), while the others scored negatively (or little, e.g. ctrl3_fdmh) in the PC1 direction. The three mutants and two controls (ctrl2_fdmh, ctrl3_fdmh) were on the opposite direction in the PC2 dimension, but ctrl1_fdmh was clustering with two of the mutants.

In male SP score plot (**Fig. 8C**), mut1_msp lied opposite from the others along PC1 axis away from origin. Mut3_msp was distant from ctrl1_msp and ctrl2_msp at PC2 direction, whereas the rest (mut1_msp, mut2_msp, ctrl3_msp) have minimum impact to the variance at PC2 dimension. Mut2_msp was close to ctrl3_msp and has no contribution to the clustering of the mutant samples. In male DMH score plot (**Fig. 8D**), one mutant (mut2_mdmh) and two controls (ctrl1_mdmh, ctrl2_mdmh) were away from the origin in opposite directions at PC1 axis. The other two mutants (mut1_mdmh, mut3_mdmh) and one control (ctrl3_mdmh) had little contribution to model the 64% of variance PC1. In the PC2 direction, ctrl1_mdmh and ctrl2_mdmh were distant from the two mutants of mut1_mdmh and mut3_mdmh, but ctrl3_mdmh was close to these mutants.

Overall, clusters of mutants and controls overlapped due to a larger variance from individual than that from groups. The overlaps between male mutant and control variables indicated that the embryonic brain with complete deletion of *tfap2b* shared some features with that of their wild-type littermates. Interestingly, in both female SP and DMH (**Fig. 8A, B**), mut3_fDMH was far away from all other variables. Therefore, only mut3_fDMH was removed from further analysis and all samples in male animals were kept for further analysis.

Figure 8. Principal components analysis of gene expression in E14.5 *Tfap2b* mutants brain.

Score plots of female embryonic SP (A) and DMH (B), male sp (C) and (D). The plots modeled above 70% of the total variance. The contributions of the first and second major components were shown along x and y axis, respectively. Female E14.5 embryos *Tfap2b*$^{+/+}$, n=3; female E14.5 embryos *Tfap2b*$^{+/-}$, n=3; male E14.5 embryos *Tfap2b*$^{+/+}$, n=3; male E14.5 embryos *Tfap2b*$^{+/-}$, n=3; SP, secondary prosencephalon; DMH, diencephalon, midbrain and hindbrain.

2.2.3c Differentially expressed genes in E14.5 Tfap2b homozygous knockouts

Next, qualified samples from PCA results were further analyzed using EdgeR to find differentially expressed (DE) genes. Overall, there were fewer DE genes in SP than in DMH samples, more downregulated genes than upregulated (**Fig. 9-10**). The most significantly regulated genes were labeled in the volcano plots (**Fig. 9**, FDR < 0.2; logFC > 0.5). Patterns of overlapped DE genes are plotted in Venn diagram and common genes were listed in the legend (**Fig. 10**). Among these highlighted genes, *Tfap2b* was significantly down regulated in both female and male DMH but not in SP (**Fig. 10**), this is consistent with the expression pattern of *in situ* analysis from *Zhao et al*. [109]. Gene expression of *Tfap2* family was further confirmed in E19 whole brain samples using qPCR. Consistent with the results from RNA-seq analysis, only AP-2β but not other AP-2 paralogs was down regulated in *Tfap2b*$^{+/-}$ as well as *Tfap2b*$^{-/-}$ developing mouse brains (**Fig. 11**).

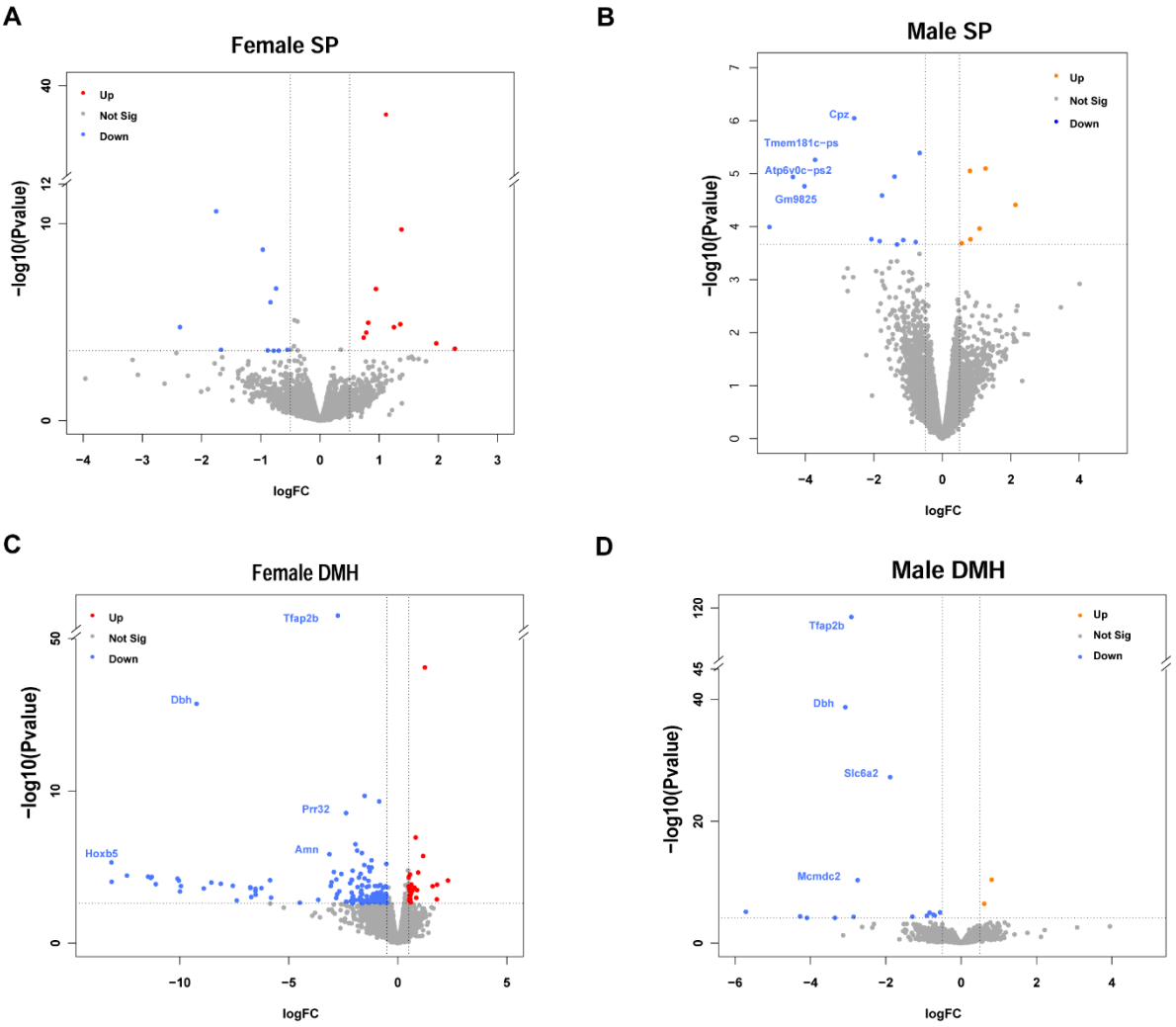

Figure 9. Differentially expressed genes in *Tfap2b* $^{-/-}$ developing mouse brains.

Volcano plots showing the significantly up-regulated (red) and down-regulated genes (blue) in female sp (A) and dmh (B). Up regulated genes are presented in orange for male (C) and dmh (D). Gene expressions were compared between homozygous mutant embryos (E14.5) and their wild-type littermates. Significantly changed genes (FDR < 0.2; logFC > 0.5) were highlighted and the most robustly regulated genes were labeled (FDR < 0.01; logFC > 2). Female E14.5 embryos tfap2b +/+, n=3; female E14.5 embryos tfap2b -/-, n=2 (based on PCA analysis, the sample named“mut3” was excluded from the DE genes analysis); male E14.5 embryos tfap2b +/+, n=3; male E14.5 embryos tfap2b +/+, n=3; SP, secondary prosencephalon; DMH, diencephalon, midbrain and hindbrain.

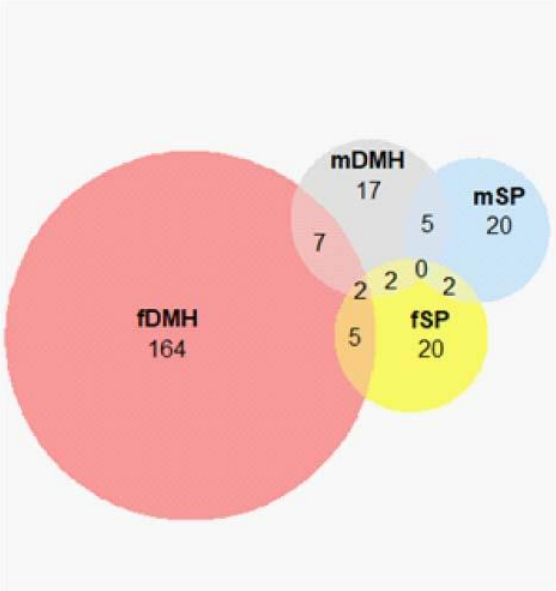

Legend

Intersected areas	Common DE genes	p Values
fDMH ∩ fSP	***Gm26809***, *Adhfe1*, ***Gm20186***, *Cdhr1*, *Snhg6*	4.29E-06
fDMH ∩ mDMH	*Tfap2b*, *Dbh*, ***Dmbx1***, *Adhfe1*, *Slc6a2*, *Hjurp*, *Snhg6*	2.90E-09
fSP ∩ mSP	*Gm37602*, *Gm21168*[#]	0.000371227
mDMH ∩ mSP	*Mcmdc2*, *Rps2-ps10*, *Atp6v0c-ps2*, *Tmem181c-ps*, *Gm9825*	1.23E-10

Genes that were up-regulated are in bold; down-regulated are underlined
#Gm37602 is down-regulated in fSP, but up-regulated in mSP

Figure 10. Overlapping DE genes in developing mouse brain.

Venn diagram showing the numbers of overlapping genes of each combination. In the legend, names of the common genes and p values were listed according to the corresponding intersection. The overlapping p values were calculated using Fischer's exact tests.

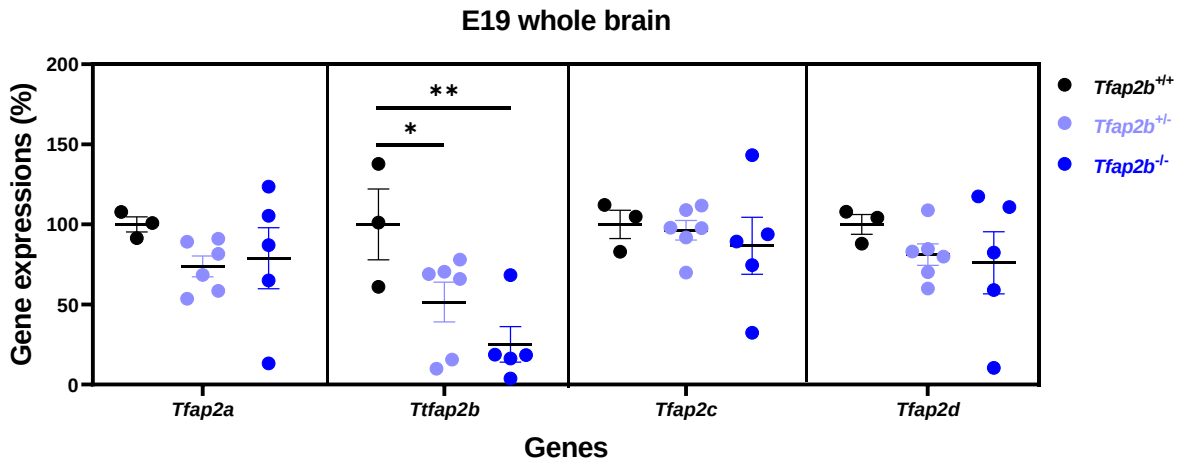

Figure 11. *Tfap2b* was downregulated in the mutant E19 brain.

Expression of *Tfap2a* to *d* in the E19 whole brain of heterozygous and homozygous *Tfap2b* knockouts was quantified using qPCR. Data were analyzed by two-way ANOVA followed by Sidak's multiple comparisons test and were shown as the mean ± SEM, *p<0.05, **p<0.01. E19 *Tfap2b*$^{+/+}$ (n = 3), *Tfap2b*$^{+/-}$ (n = 6), *Tfap2b*$^{+/-}$ (n = 5).

2.2.3d Network analysis of differentially expressed genes in E14.5 female DMH

The most DE genes (133 genes) were found in female DMH and were downregulated. These genes were grouped into two networks by embryonic development and neural activity (**Fig. 12**). All of the DE genes related to the embryonic brain development are from *Hox* gene family except for *Pax8*, which is from *Pax* family that can be recruited by AP-2 paralogs when activating a target gene [115]. The group of DE genes involved in the neurotransmission belongs to solute carrier (*Slc*) family, except for Aqp1. Upregulated genes (31 genes) were grouped into one network by neuronal generation and glial cell differentiation (**Fig. 13**). Six genes were found under the most significant GO terms.

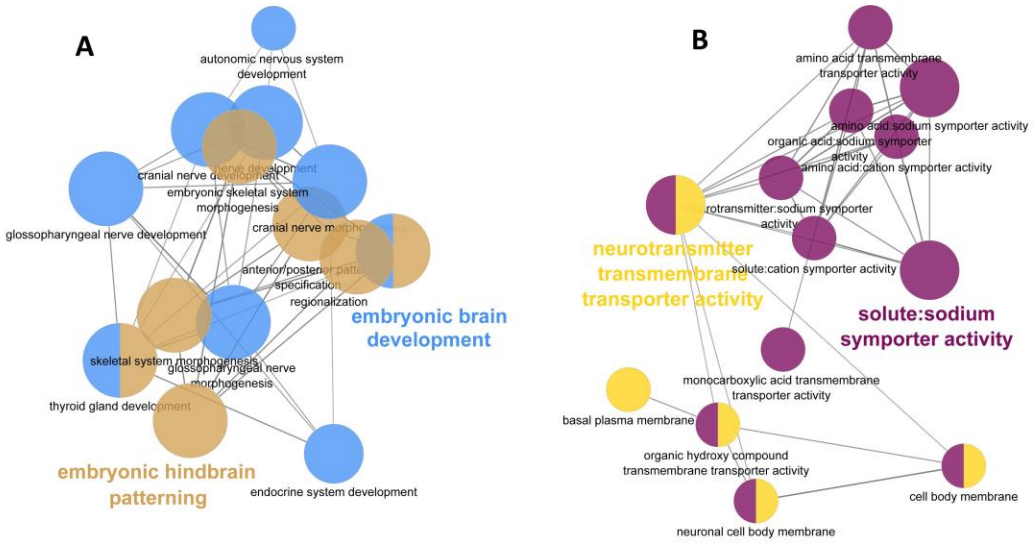

Legend

GO Term	Associated Genes Found
embryonic brain development	Hoxa3, Hoxa4, Hoxa5, Hoxa6, Hoxb2, Hoxb3, Hoxb4, Hoxb5, Hoxb6, Hoxb7, Hoxb8, Hoxc4, Hoxd3, Pax8
embryonic hindbrain patterning	Hoxa3, Hoxa4, Hoxa5, Hoxa6, Hoxb2, Hoxb3, Hoxb4, Hoxb5, Hoxb6, Hoxb7, Hoxb8, Hoxc4, Hoxc5, Hoxc6, Hoxd3
neurotransmitter transmembrane transporter activity	Aqp1, Slc18a3, Slc6a11, Slc6a15, Slc6a2
solute:sodium symporter activity	Slc4a10, Slc4a5, Slc6a11, Slc6a15, Slc6a2

Figure 12. ClueGO network analysis of the downregulated genes in female DMH.

Grouped networks of embryonic brain development (A) and neurotransmission (B) by biological function with GO terms as nodes where the most significant terms were highlighted, poorly grouped terms (< 10 nodes) are not shown. Legend showed the genes found under each GO term.

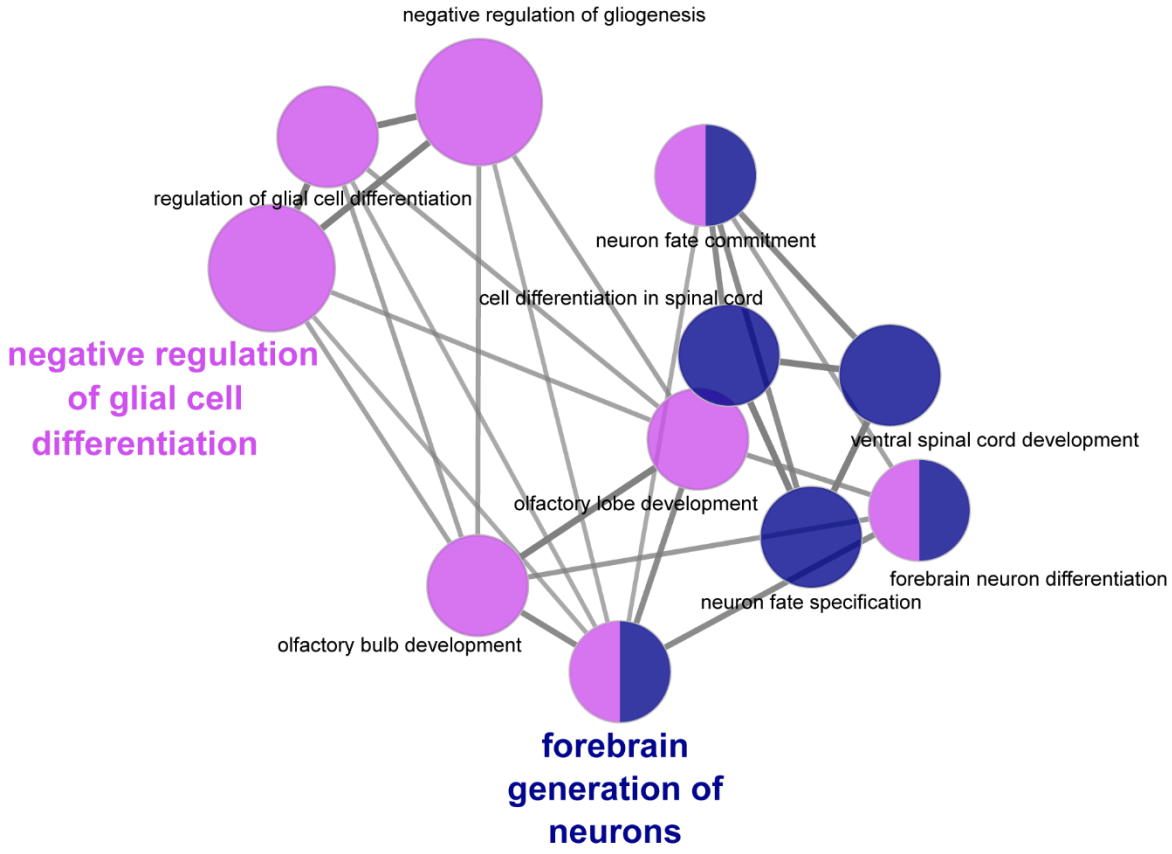

Legend

GO Term	Associated Genes Found
forebrain generation of neurons	Dlx2, Dlx5, Nr2e1, Sox1
negative regulation of glial cell differentiation	Dlx2, Hmga2, Nr2e1, Tmem98

Figure 13. ClueGO network analysis of the upregulated genes in female DMH.

Grouped networks of "negative regulation of glial cell differentiation" and "forebrain generation of neurons" by biological function with GO terms as nodes where the most significant terms were highlighted, poorly grouped terms (< 10 nodes) are not shown. Legend showed the genes found under each GO term.

2.3 Part 3: Shortened sleep in GABAergic specific Tfap2b knockouts.

All results from this section were included in the manuscript we are currently writing.

My previous results showed that heterozygous deletion of *Tfap2b* in all cells had resulted in a shortened sleep in mice [119]. In addition, this *Tfap2b* deletion downregulated the expression of GABAergic genes in brainstem of *Tfap2b* $^{+/-}$ mice. Therefore, to investigate the function of *Tfap2b* in GABAergic-regulated sleep in female and male mice, I characterized the sleep behavior in conditional knockouts of *Tfap2b* in GABAergic neurons. Firstly, I generated GABAergic specific knockouts (*Vgat-tfap2b* $^{-/-}$) by crossing *Tfap2b* $^{fl/fl}$ with *Vgat-cre* line, and measured sleep in both female and male animals by EEG/EMG recordings. Next, to examine how GABAergic deletion of *Tfap2b* affects sleep homeostasis, a 6-h sleep deprivation (SD) was applied to all groups of mice. Twenty-four hours of baseline (BSL) sleep and two consecutive days of recovery (R1 and R2) sleep after SD were recorded using EEG.

2.3.1 Shortened sleep and reduced sleep depth in female *Vgat-tfap2b* $^{-/-}$ mice

The EEG data from the female knockouts showed that total sleep amount was decreased ~120 min in 24-hour day (**Fig. 14A, B**). This decreased sleep quantity of NREMS and REMS was most obviously demonstrated within the first half of dark phase (**Fig. 14C-F**) over the 24-hour Zeitgeber Time (ZT) course, although not all pairwise comparisons for each time point were significant. In parallel with the shortened sleep quantity, the delpha and theta power during the 24-hour baseline was also lower in the female *Vgat-tfap2b* $^{-/-}$ mice (**Fig. 15A-D**). The trend of delta and theta power changes over the ZT course synchronized with the quantity changes, again, with the largest discrepancies observed during the first half of the dark phase (**Fig. 15B,D**). A small difference between two groups of controls were observed in the spectra power analysis of the wake state (**Fig. 15E, F**), where the EEG spectral power at slower frequency in *Vgat-tfap2b* $^{fl/fl}$ control was lower than that from *Vgat* control. Wake spectral power intensity of *Vgat-tfap2b*$^{-/-}$ knockouts fell in between of the controls. This intensity of wakefulness seems to change independently of the slow wave intensity in sleep. The sleep and wake bout lengths in the mutant group were not affected by the altered sleep or wake spectral power (**Fig. 16**). In summary, the female *Vgat-tfap2b*$^{-/-}$ mice suffered from sleep loss and reduced sleep depth.

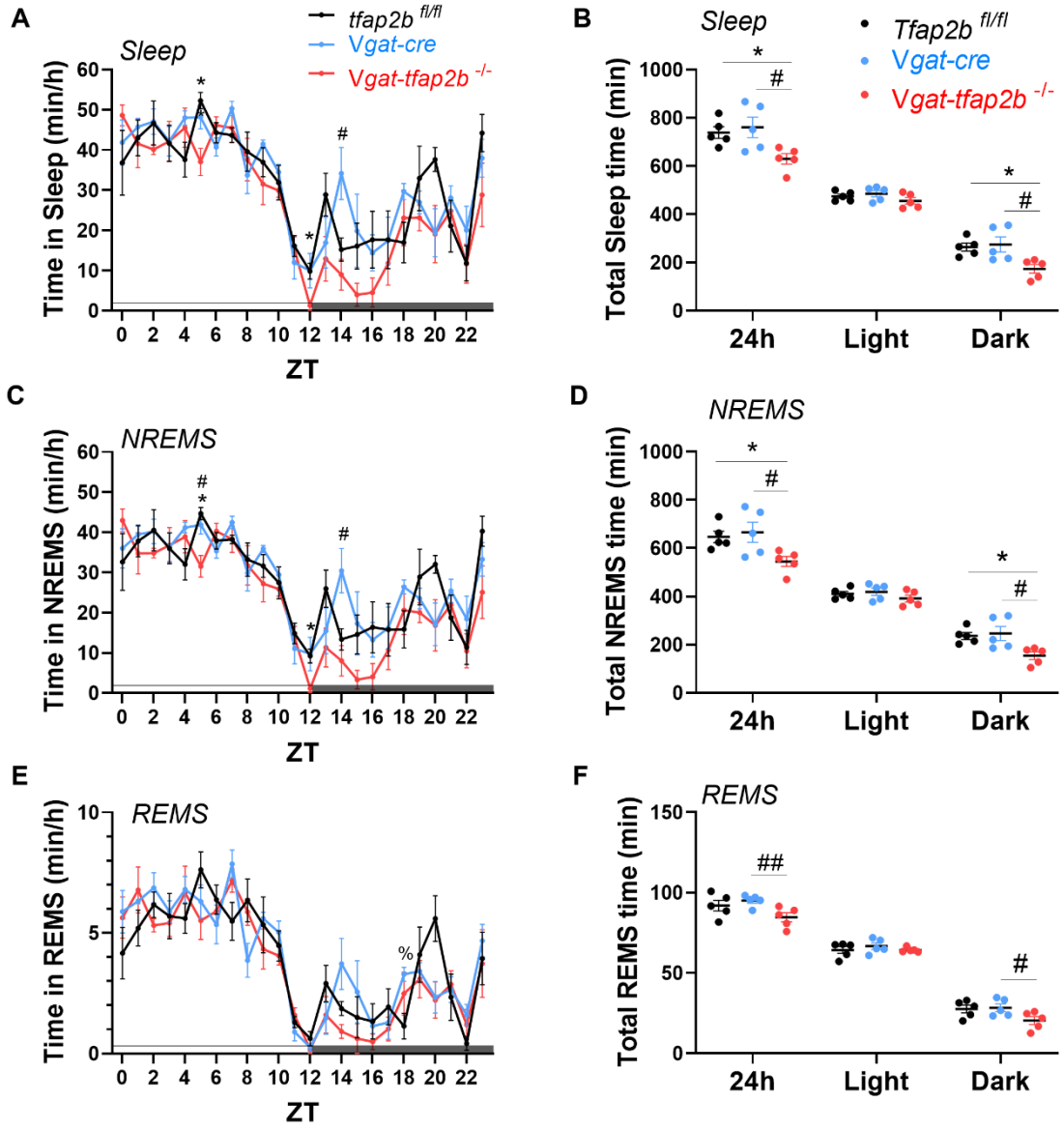

Figure 14. Sleep amount is shortened in female GABAergic specific *Tfap2b* homozygous knockouts in baseline recording.

(A) Sleep quantity changes in female *Tfap2b*$^{fl/fl}$, *Vgat-cre*, *Vgat-tfap2b* $^{-/-}$ mice over the Zeitgeber time (ZT) course. (B) Sleep quantity during 24h, light and dark phase. ZT course NREMS quantification (D) and total NREMS amount during 24h, light and dark phase. REMS quantification over the ZT course (E) and during 24h, light and dark phases (F). All data were analyzed by two-way ANOVA followed by Sidak's multiple comparisons test and were shown as the mean ± SEM. Significant pairwise comparisons of *Tfap2b*$^{fl/fl}$ vs. *Vgat-tfap2b* $^{-/-}$ were marked with $^{*}P < 0.05$, $^{**}P < 0.01$; *Vgat-cre* vs. *Vgat-tfap2b* $^{-/-}$, $^{\#}P < 0.05$, $^{\#\#}P < 0.01$; *Tfap2b* $^{fl/fl}$ vs. *Vgat-cre*, $^{\%}P < 0.05$. Female *Tfap2b* $^{fl/fl}$ (n = 5), *Vgat-cre* (n = 5), *Vgat-tfap2b* $^{-/-}$ (n = 5).

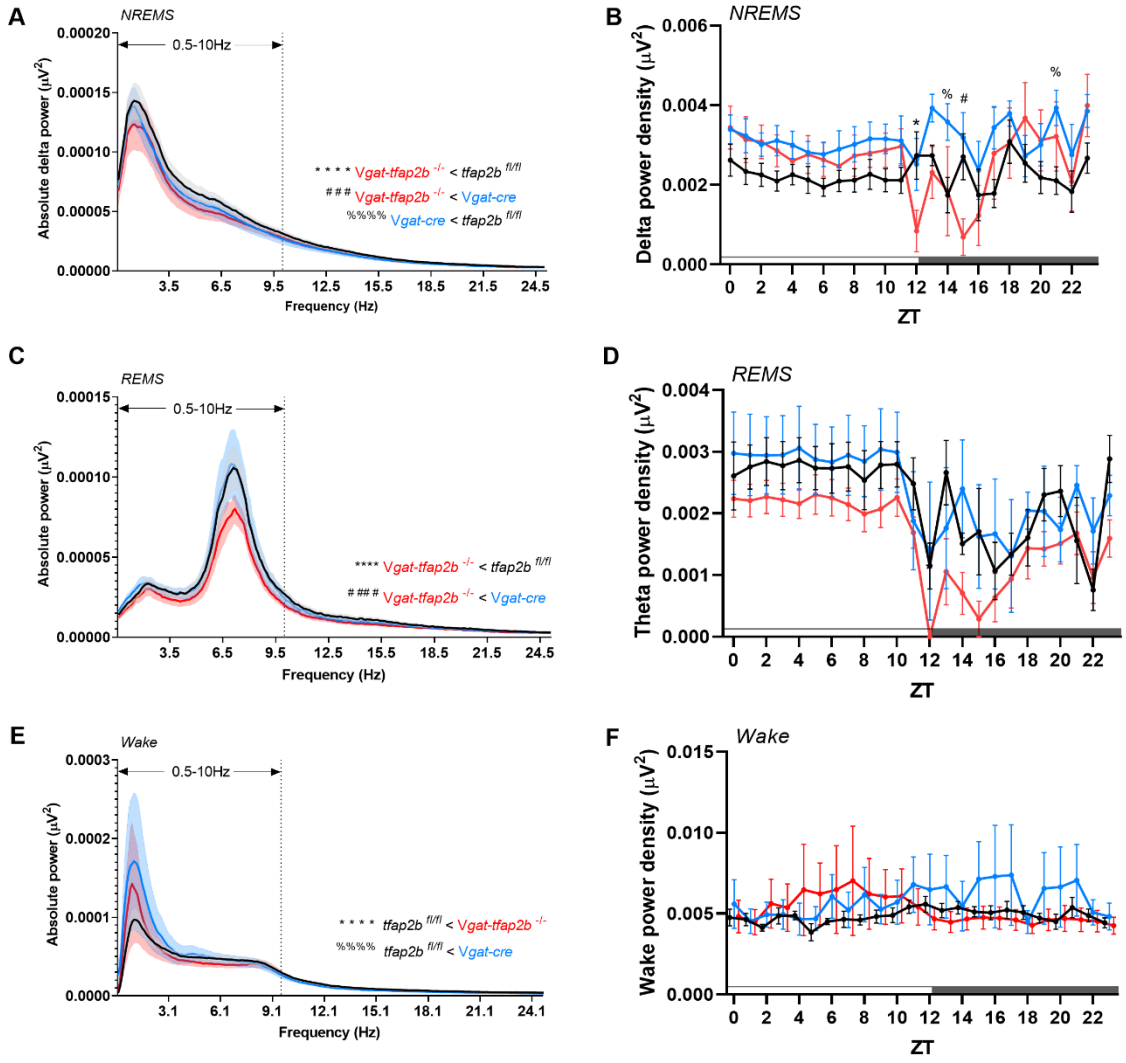

Figure 15. Weaker sleep drive in female *Vgat-tfap2b* $^{-/-}$ mice.

NREMS power spectra in 24h scale (A) and delta power (0.5 – 4.0 Hz) changes over ZT course (B). REMS power spectra in 24h scale (C) and theta power (5 – 10 Hz) changes over ZT course (D). Wake power spectra and 0.2- 10 Hz power changes over ZT course. Data in (A, C, E) were analyzed using Friedman test followed by Dunn's multiple comparisons test. Data in (B, D, F) were analyzed by two-way ANOVA followed by Sidak's multiple comparisons test and were shown as the mean ± SEM. Significant pairwise comparisons of *Tfap2b*$^{fl/fl}$ vs. *Vgat-tfap2b* $^{-/-}$ were marked with $^{*}P < 0.05$, $^{****}P < 0.0001$; *Vgat-cre* vs. *Vgat-tfap2b* $^{-/-}$, $^{\#}P < 0.05$, $^{\#\#\#}P < 0.001$, $^{\#\#\#\#}P < 0.0001$; *Tfap2b* $^{fl/fl}$ vs. *Vgat-cre*, $^{\%}P < 0.05$, $^{\%\%\%\%}P < 0.0001$. Female *Tfap2b* $^{fl/fl}$ (n = 5), *Vgat-cre* (n = 5), *Vgat-tfap2b* $^{-/-}$ (n = 5).

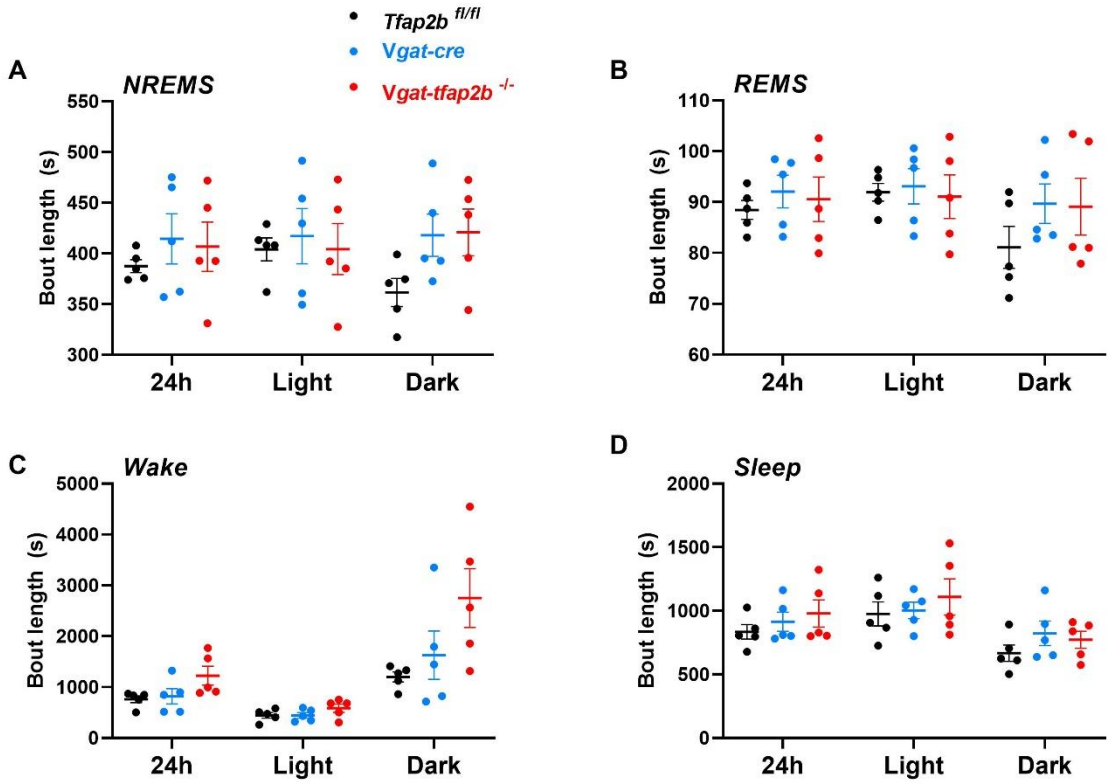

Figure 16. Sleep and wake bout lengths were not changed in female *Vgat-Tfap2b*$^{-/-}$ mice.

Bout analysis of female *Tfap2b*$^{fl/fl}$, *Vgat-cre*, *Vgat-Tfap2b*$^{-/-}$ mice during NREMS (A), REMS (B), wake (C) and sleep (D) state. Data were analyzed by two-way ANOVA followed by Sidak's multiple comparisons test and were shown as the mean ± SEM. Female *Tfap2b*$^{fl/fl}$ (n = 5), *Vgat-cre* (n = 5), *Vgat-tfap2b*$^{-/-}$ (n = 5).

2.3.2 Reduced homeostatic sleep response in female *Vgat-tfap2b* $^{-/-}$ mice

To determine if the sleep loss phenotype observed in BSL recording influence the homeostatic sleep response, mice were exposed to 6-h SD after BSL recording. After SD, a trend of sleep increase was observed during the first recovery day (R1) in both control and knockout groups with the main effect occurred in the dark phase following the SD (**Fig. 17**). The sleep schedule was restored in all groups within R2 as the NREMS and REMS architectures in the R2 were not significantly altered compared with BSL (**Fig. 18**). Spectral power was also analyzed after the 6 hours SD. During R1, the delta power was increased compared to the BSL sleep power within the equivalent ZT range in all groups tested. Subsequently, the delta power was recovered during R2. Although the theta power rebound was significant in female *Vgat-tfap2b* $^{-/-}$ mice REMS not in controls over the time course, the accumulative effect was therefore calculated to evaluate the strength of power rebound among all genotypes. The cumulative effect was calculated for NREMS and REMS. Results of both delta and theta oscillations showed that the recovery sleep in female *Vgat-tfap2b* $^{-/-}$ mice was slower and weaker than their wild-type littermates (**Fig. 19**). Taken together, the homeostatic sleep response was reduced in female *Vgat-tfap2b* $^{-/-}$ mice.

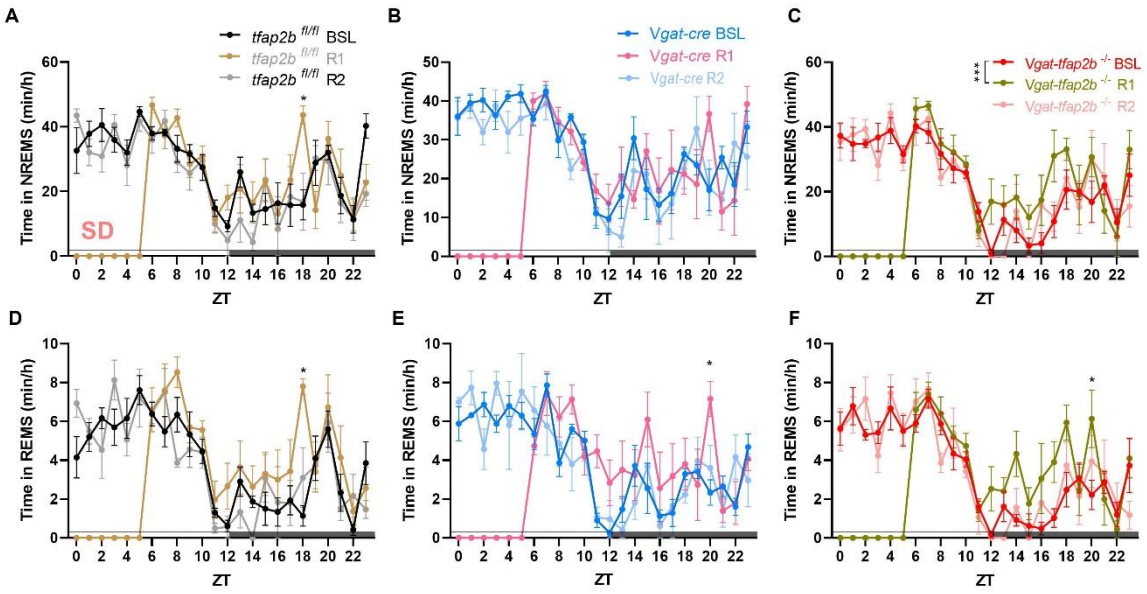

Figure 17. Sleep is increased after 6-hour sleep deprivation in all tested female mice.

NREMS quantity changes over ZT course during baseline (BSL), the first / second recovery day (R1/R2) in female *Tfap2b*$^{fl/fl}$ (A), *Vgat-cre* (B), *Vgat-tfap2b* $^{-/-}$ mice (C). REMS quantity changes over ZT course during BSL, R1, R2 in female *Tfap2b*$^{fl/fl}$ (D), *Vgat-cre* (E), *Vgat-tfap2b* $^{-/-}$ mice (F). All data were analyzed by two-way ANOVA followed by Sidak's multiple comparisons test and were shown as the mean ± SEM. Significant pairwise comparisons of BSL vs. R1 were marked with *$P < 0.05$. Female *Tfap2b* $^{fl/fl}$ (n = 5), *Vgat-cre* (n = 5), *Vgat-tfap2b* $^{-/-}$ (n = 5).

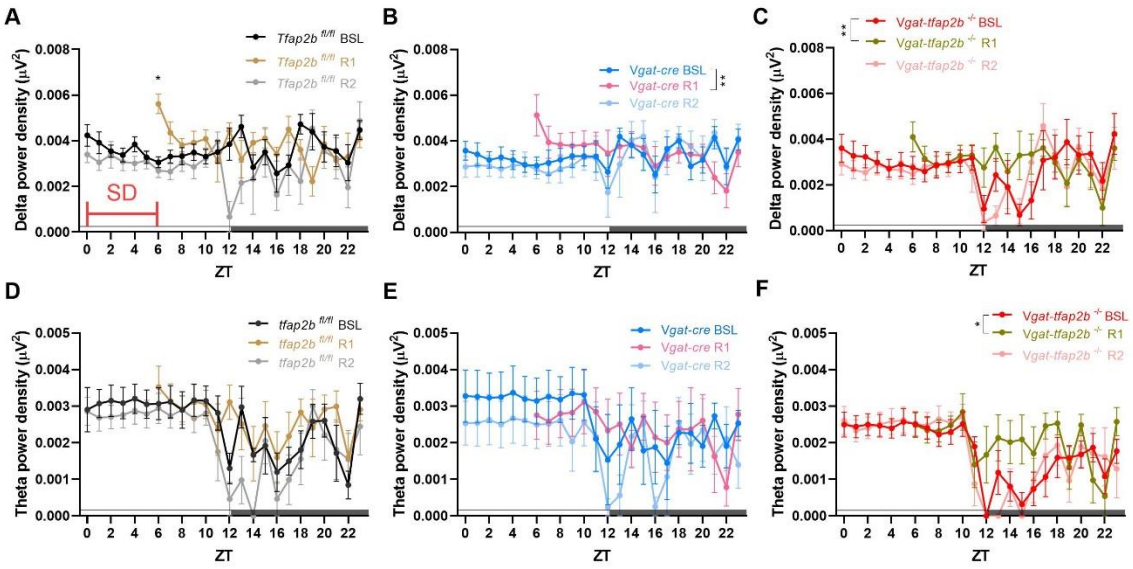

Figure 18. Weaker sleep power rebound in female *Vgat-tfap2b* $^{-/-}$ mice after 6-hour sleep deprivation.

Delta power changes over ZT course during BSL, R1, R2 in female *Tfap2b*$^{fl/fl}$ (A), *Vgat-cre* (B), *Vgat-tfap2b* $^{-/-}$ mice (C). Theta power changes over ZT course during BSL, R1, R2 in female *Tfap2b*$^{fl/fl}$ (D), *Vgat-cre* (E), *Vgat-tfap2b* $^{-/-}$ mice (F). All data were analyzed by two-way ANOVA followed by Sidak's multiple comparisons test and were shown as the mean ± SEM. Significant Time x Sleep deprivation interactive variations were specified between groups and marked with $*P < 0.05$, $**P < 0.01$; pairwise comparisons of BSL vs. R1 were marked with $*P < 0.05$. Female *Tfap2b* $^{fl/fl}$ (n = 5), *Vgat-cre* (n = 5), *Vgat-tfap2b* $^{-/-}$ (n = 5).

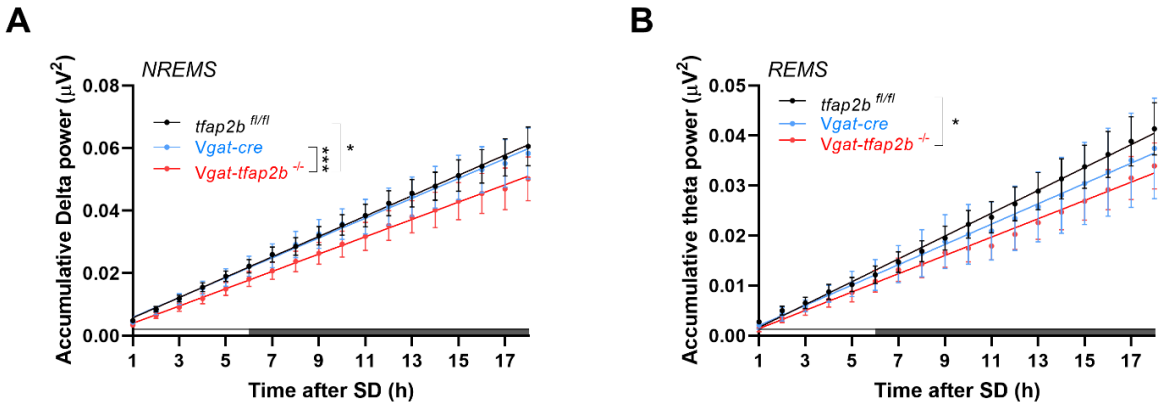

Figure 19. Sleep rebound power is weaker in female *Vgat-tfap2b* $^{-/-}$ mice after 6-hour sleep deprivation.

Linear regression plots of accumulative delta (A) and theta power (B) after SD. Equality of slopes or intercepts was tested by simple linear regression analysis. Significantly differences were specified between groups and marked with $*P < 0.05$, $***P < 0.001$. Female *Tfap2b* $^{fl/fl}$ (n = 5), *Vgat-cre* (n = 5), *Vgat-tfap2b* $^{-/-}$ (n = 5).

2.3.3 Sleep patterns differ within controls as well as the mutant in male *Vgat-tfap2b*$^{-/-}$ mice

Next, I tested the sleep behavior in male animals. In sleep quantity analysis, a similar phenotype to female mutants was observed. The total sleep / NREMS amount was decreased in male *Vgat-tfap2b*$^{-/-}$ mutants during the dark phase compared with the *Tfap2b*$^{fl/fl}$ control, although significance failed to occur when compared with *Vgat-cre* controls (**Fig. 20A-D**). The main effect of the sleep loss also occurred during the first 6 hours after lights-off (**Fig. 20A, C**). Different from their female mutants, the REMS quantity in male *Vgat-tfap2b*$^{-/-}$ mice was not altered (**Fig. 20E, F**). However, despite the sleep loss, the EEG power analysis revealed a conflictingly higher sleep pressure in male knockouts compared with female mutants, which exhibit a decreased sleep drive. The *Vgat-tfap2b*$^{-/-}$ mice displayed a higher NREMS/REMS power intensity than the floxed control while similar to *Vgat-cre* controls (**Fig. 21A-D**). Surprisingly, this increase of NREMS/REMS power intensity already existed in the control carrying *Vgat-cre*, compared with the floxed control. Similar to female analysis, spectral power during wakefulness seems to behave independently and irrelevantly of the sleep intensity. Although not significant, the power intensity of the major peak (0.2–5Hz) was the highest in the *Tfap2b*$^{fl/fl}$ control, but the weakest in *Vgat-tfap2b*$^{-/-}$ mice, while the order was completely the opposite as for the second peak (5-10Hz) (**Fig. 21E, F**). Overall sleep and wake bout lengths of *Vgat-tfap2b* knockouts were not changed, only that the average wake bout was longer in the active phase (**Fig. 22**). In summary, the sleep quantity reduction from male mice agrees with the female phenotype, whereas the EEG power analysis disagrees. This disagreement might come from a CRE effect to the sleep intensity in male knockouts.

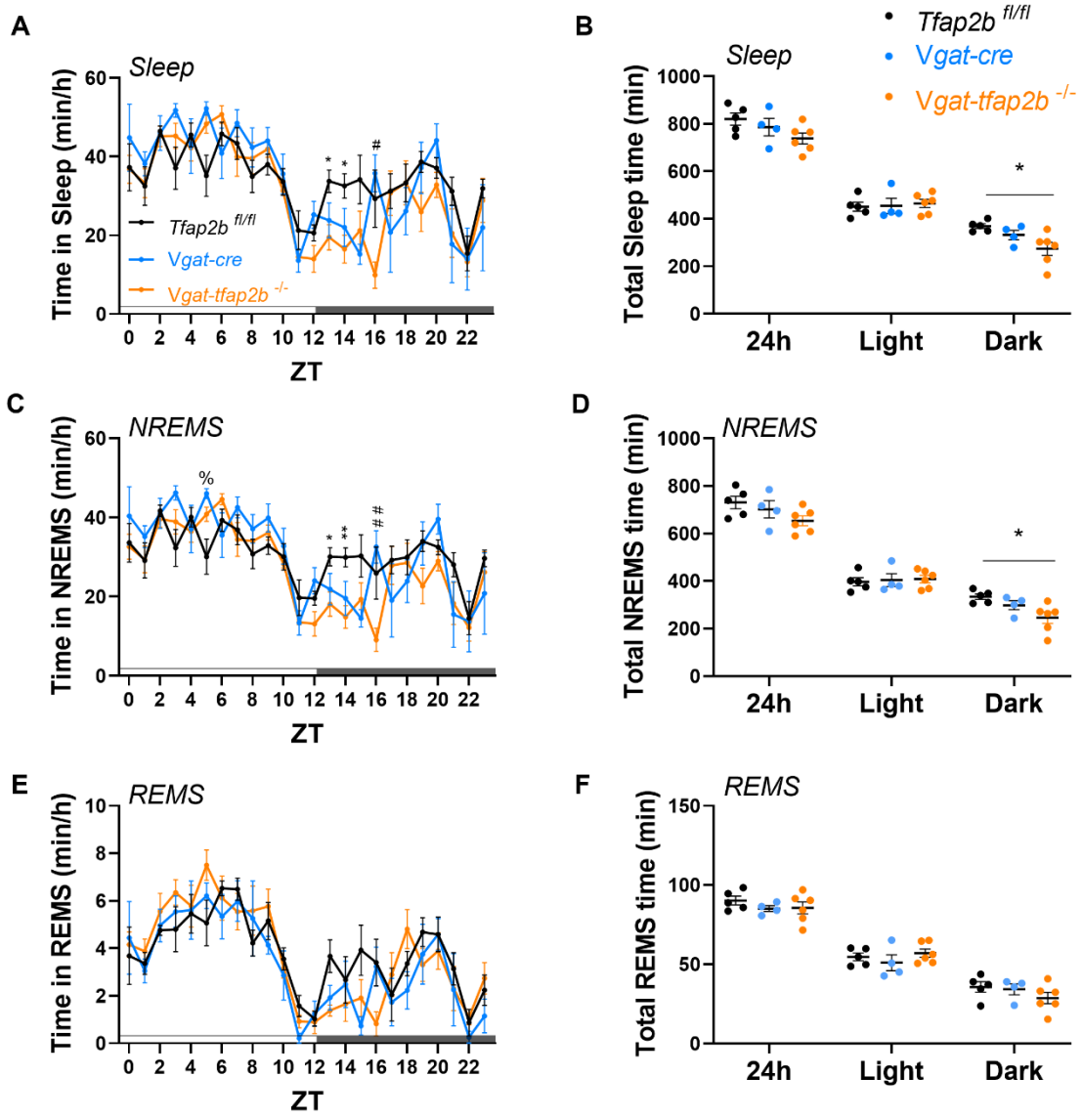

Figure 20. Sleep amount is shortened in male GABAergic specific *Tfap2b* homozygous knockouts in baseline recording.

(A) Sleep quantity changes in male *Tfap2b*$^{fl/fl}$, *Vgat-cre*, *Vgat-tfap2b* $^{-/-}$ mice over the Zeitgeber time (ZT) course. (B) Sleep quantity during 24h, light and dark phase. ZT course NREMS quantification (D) and total NREMS amount during 24h, light and dark phase. REMS quantification over the ZT course (E) and during 24h, light and dark phases (F). All data were analyzed by two-way ANOVA followed by Sidak's multiple comparisons test and were shown as the mean ± SEM. Significant pairwise comparisons of *Tfap2b*$^{fl/fl}$ vs. *Vgat-tfap2b* $^{-/-}$ were marked with **P* < 0.05, ***P* <0.01; *Vgat-cre* vs. *Vgat-tfap2b* $^{-/-}$, $^{\#}$*P* < 0.05, $^{\#\#}$*P* <0.01; *Tfap2b* $^{fl/fl}$ vs. *Vgat-cre*, $^{\%}$*P* < 0.05. Male *Tfap2b* $^{fl/fl}$ (n = 5), *Vgat-cre* (n = 4), *Vgat-tfap2b* $^{-/-}$ (n = 6).

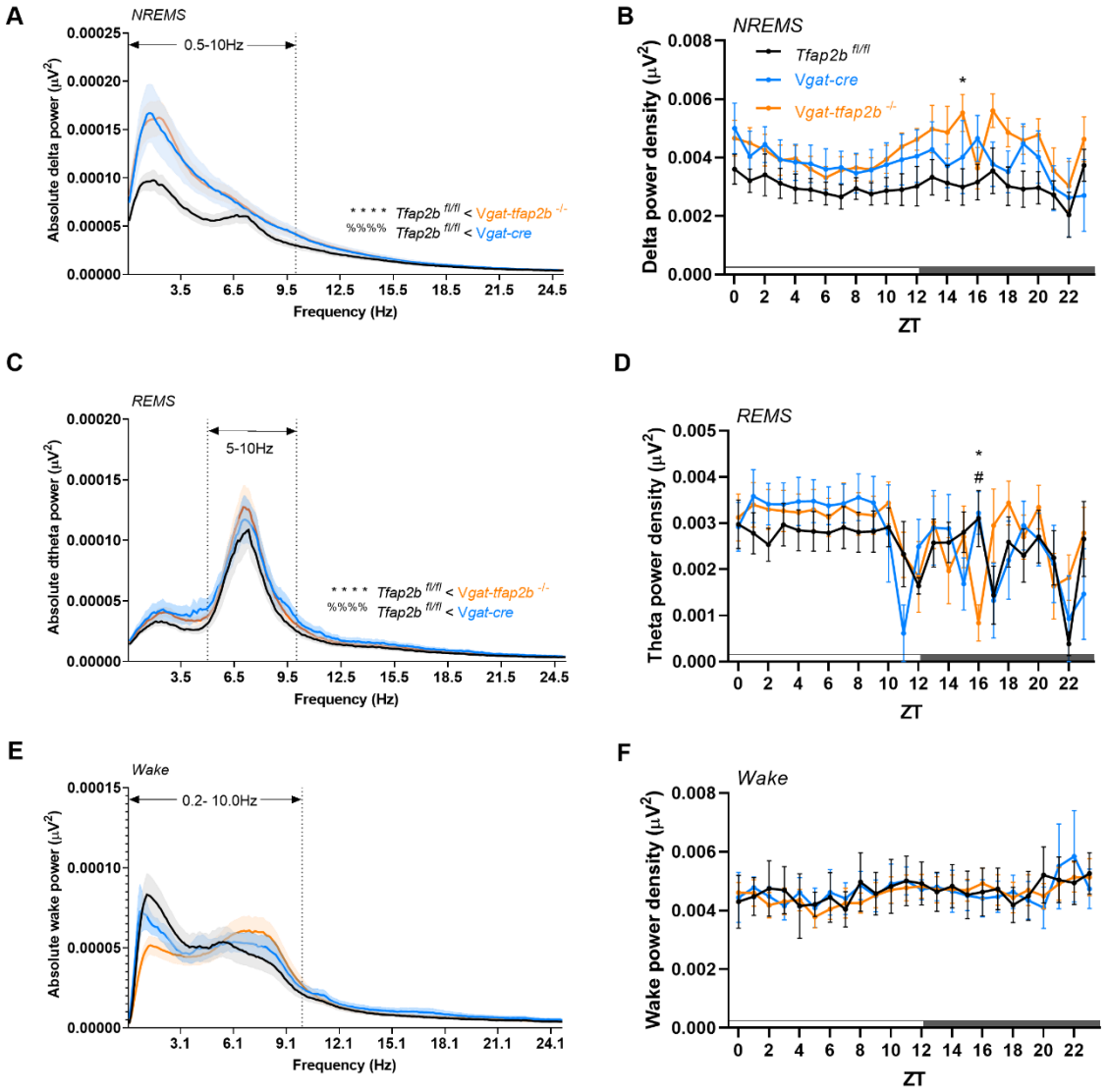

Figure 21. Sleep powers are stronger in male *Vgat-tfap2b* $^{-/-}$ mutants and the *Vgat-cre* control.

NREMS power spectra in 24h scale (A) and delta power (0.5 – 4.0 Hz) changes over ZT course (B). REMS power spectra in 24h scale (C) and theta power (5 – 10 Hz) changes over ZT course (D). Wake power spectra and 0.2- 10 Hz power changes over ZT course. Data in (A, C, E) were analyzed using Friedman test followed by Dunn's multiple comparisons test. Data in (B, D, F) were analyzed by two-way ANOVA followed by Sidak's multiple comparisons test and were shown as the mean ± SEM. Significant pairwise comparisons of *Tfap2b*$^{fl/fl}$ vs. *Vgat-tfap2b* $^{-/-}$ were marked with *$P < 0.05$, ****$P < 0.0001$; *Vgat-cre* vs. *Vgat-tfap2b* $^{-/-}$, $^{\#}P < 0.05$; *Tfap2b*$^{fl/fl}$ vs. *Vgat-cre*, $^{\%\%\%\%}$ $P < 0.0001$. Male *Tfap2b*$^{fl/fl}$ (n = 5), *Vgat-cre* (n = 4), *Vgat-tfap2b* $^{-/-}$ (n = 6).

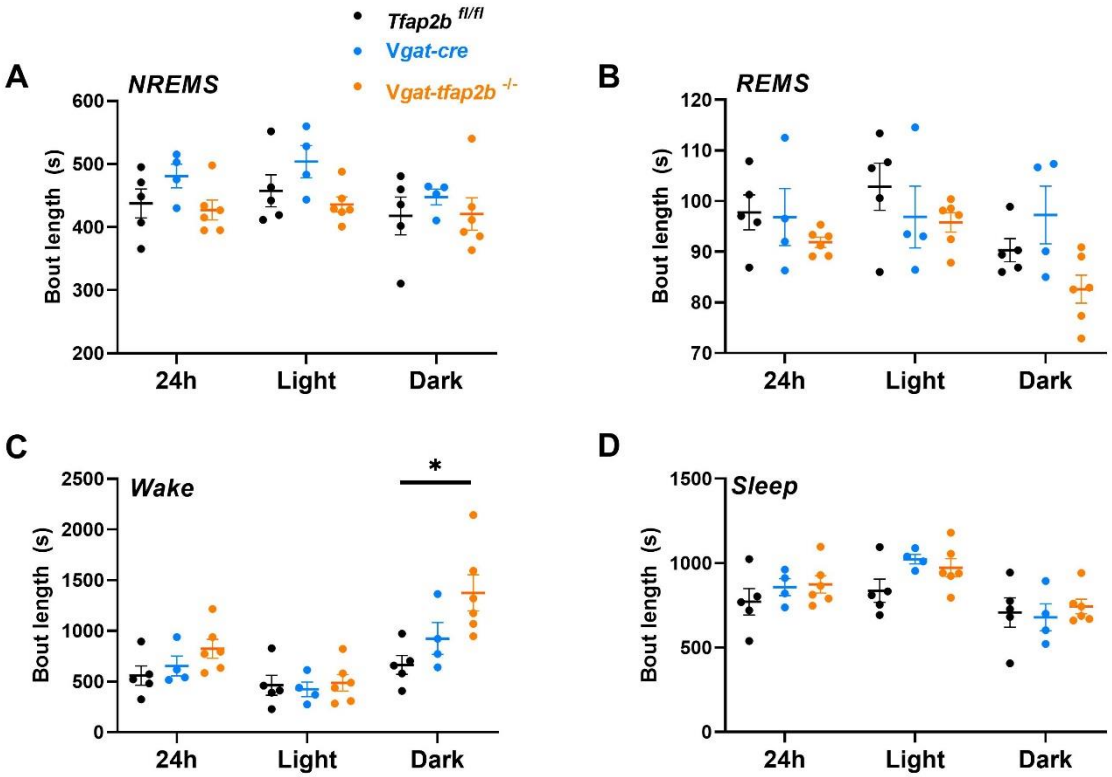

Figure 22. Sleep and wake bout lengths were not changed in the male *Vgat-fap2b*$^{-/-}$ mice.

Bout analysis of male *Tfap2b*$^{fl/fl}$, *Vgat-cre*, *Vgat-Tfap2b*$^{-/-}$ mice during NREMS (A), REMS (B), wake (C) and sleep (D) state. Data were analyzed by two-way ANOVA followed by Sidak's multiple comparisons test and were shown as the mean ± SEM. Male *Tfap2b*$^{fl/fl}$ (n = 5), *Vgat-cre* (n = 4), *Vgat-tfap2b*$^{-/-}$ (n = 6).

2.3.4 Altered sleep rebound within controls as well as knockouts in male mice

Homeostatic sleep response was also investigated in male mice. NREMS quantity after 6 hours SD (**Fig. 23A-D**) was not significantly changed in R1, but REMS was significantly increased in all groups (**Fig.23 E, F**). The major variances in REMS amount occurred in the first 6 hours from the lights-off. During R2, the recovery sleep was significantly different from BSL over the ZT course in the male *Vgat-tfap2b* $^{-/-}$ mutants, indicating that the sleep was not fully restored to the baseline level. Homeostatic sleep rebound was characterized by the increased delta power during R1 in all tested genotypes (**Fig. 24A-D**). The rebound changes between genotypes were consistent with the analysis of sleep power intensity during BSL recording. The theta power rebound was only found to be significant in the *Vgat-tfap2b*$^{-/-}$ mice, but the trend of a later rebound was observed in both controls (**Fig. 24E, F**).I next analyzed rebound power across all genotypes in male animals. In line with a stronger BSL sleep power, male knockouts also exhibited a faster rebound in both NREMS and REMS power (Fig. 25). As NREMS power intensity is the marker of sleep homeostasis, the rebound power in the *Vgat-tfap2b*$^{-/-}$ mice seems to be similarly affected by the introduction of *Vgat-cre* gene.

Taken together, the deletion of *Tfap2b* in GABAergic neurons have reduced approximately 2h of sleep in female mice. This sleep loss is more likely a main effect of the homeostatic regulation rather than circadian, because: (1) the timing and bout lengths of sleep are not changed; (2) conditional deletion of *Tfap2b* in GABAergic neurons reduced the sleep power, the maker of sleep homeostasis; (3) the quantity changes of sleep over the time course coincide with the pattern of power intensity. Surprisingly, two controls in the male colony behaved differently in sleep as the *Vgat-cre* control has an increased sleep pressure compared with the *Vgat-tfap2b* $^{fl/fl}$ control. Sleep intensity observed in male conditional knockouts resembled that from the *Vgat-cre* control while differed from the *floxed* control mice. Therefore, it is very likely that the contradictory phenotype of high sleep pressure but low sleep amount in *Vgat-tfap2b* $^{-/-}$ comes from the combination effect of the *Vgat-cre* gene as well as the GABAergic *Tfap2b* deletion.

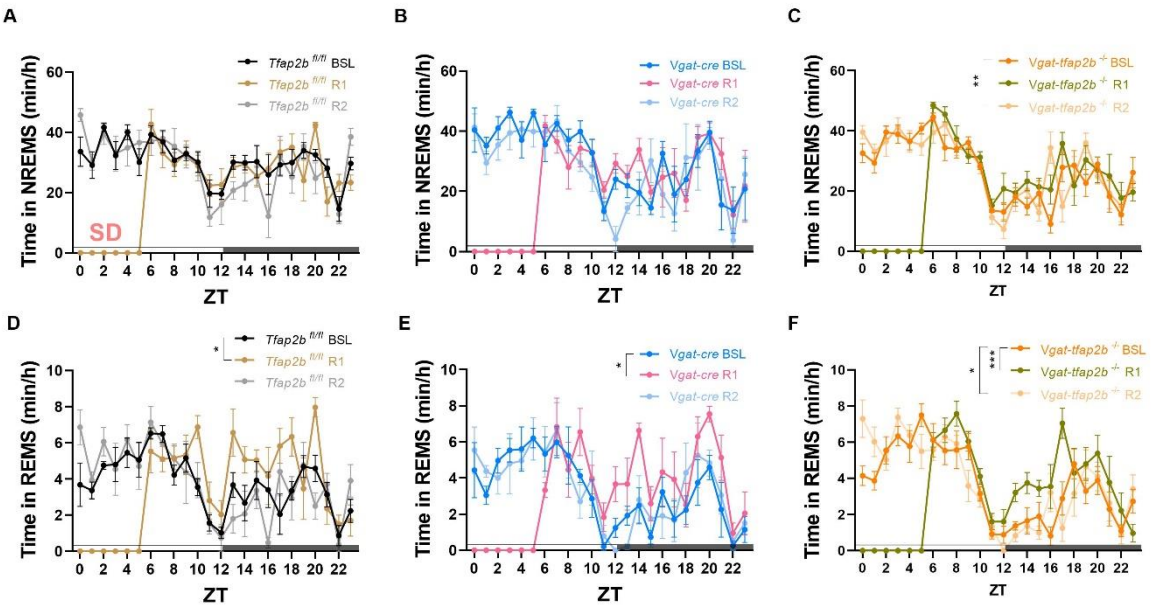

Figure 23. Sleep is increased after 6-hour sleep deprivation in the male *Vgat-tfap2b* $^{-/-}$ mutant and the *Vgat-cre* control.

NREMS quantity changes over ZT course during baseline (BSL), the first / second recovery day (R1/R2) in female *Tfap2b*$^{fl/fl}$ (A), *Vgat-cre* (B), *Vgat-tfap2b* $^{-/-}$ mice (C). REMS quantity changes over ZT course during BSL, R1, R2 in female *Tfap2b*$^{fl/fl}$ (D), *Vgat-cre* (E), *Vgat-tfap2b* $^{-/-}$ mice (F). All data were analyzed by two-way ANOVA followed by Sidak's multiple comparisons test and were shown as the mean ± SEM. Significant Time x Sleep deprivation interactive variations were specified between groups and marked with *P < 0.05, **P < 0.01, ***P < 0.001. Male *Tfap2b*$^{fl/fl}$ (n = 5), *Vgat-cre* (n = 4), *Vgat-tfap2b* $^{-/-}$ (n = 6).

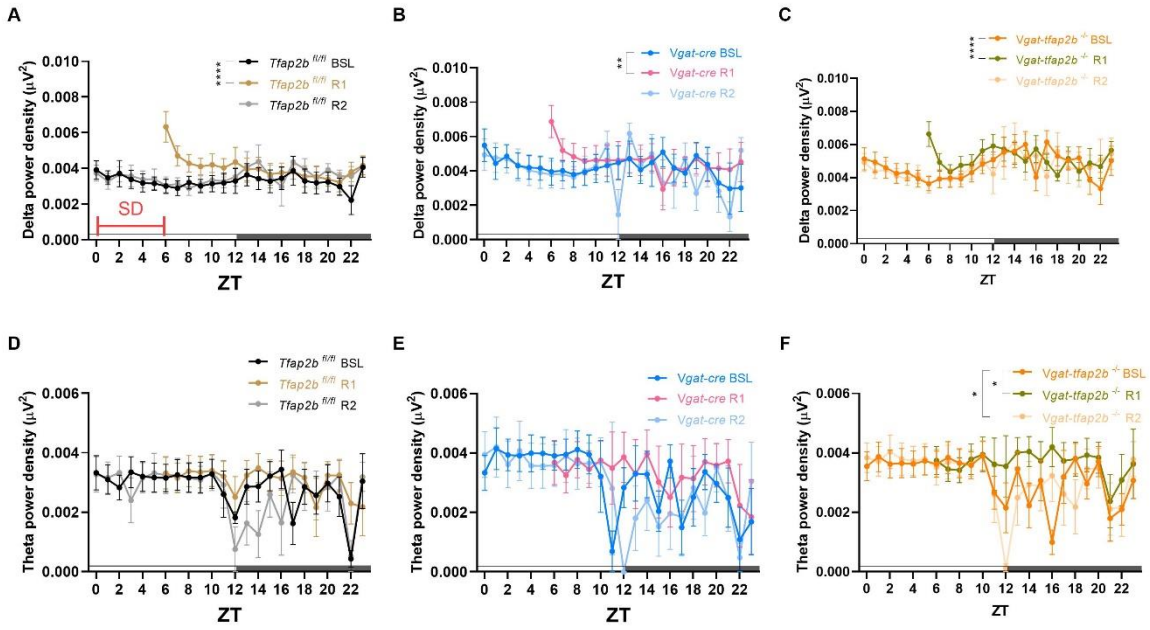

Figure 24. Sleep power rebound in both control and mutant mice after 6-hour sleep deprivation.

Delta power changes over ZT course during BSL, R1, R2 in female *Tfap2b*$^{fl/fl}$ (A), *Vgat-cre* (B), *Vgat-tfap2b* $^{-/-}$ mice (C). Theta power changes over ZT course during BSL, R1, R2 in female *Tfap2b*$^{fl/fl}$ (D), *Vgat-cre* (E), *Vgat-tfap2b* $^{-/-}$ mice (F). All data were analyzed by two-way ANOVA followed by Sidak's multiple comparisons test and were shown as the mean ± SEM. Significant Time x Sleep deprivation interactive variations were specified between groups and marked with * $P < 0.05$, ** $P < 0.01$, **** $P < 0.0001$. Male *Tfap2b*$^{fl/fl}$ (n = 5), *Vgat-cre* (n = 4), *Vgat-tfap2b* $^{-/-}$ (n = 6).

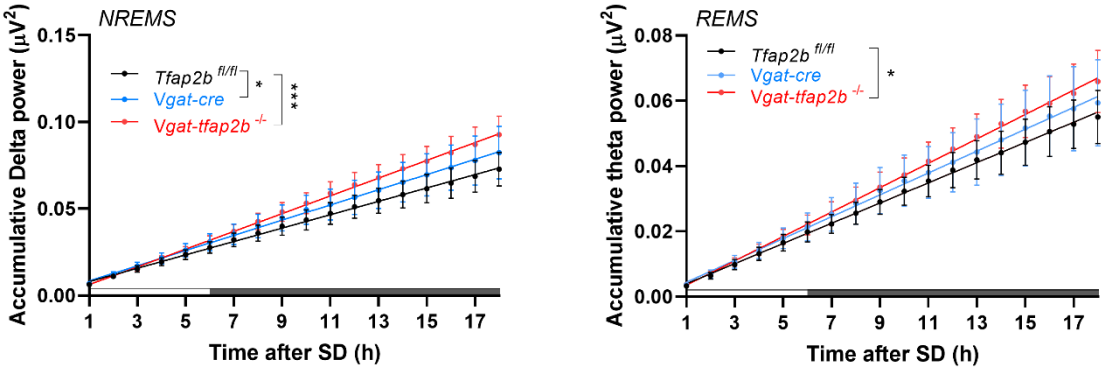

Figure 25. Sleep rebound power is stronger in the male *Vgat-tfap2b* $^{-/-}$ mutant and *Vgat-cre* control after 6-hour sleep deprivation.

Linear regression plots of accumulative delta (A) and theta power (B) after SD. Equality of slopes or intercepts was tested by simple linear regression analysis. Significantly differences were specified between groups and marked with **P* < 0.05, ****P* < 0.001, *****P* < 0.0001. Male *Tfap2b* $^{fl/fl}$ (n = 5), *Vgat-cre* (n = 4), *Vgat-tfap2b* $^{-/-}$ (n = 6).

3. Discussion

3.1 *Tfap2b* regulated GABAergic gene expression

Our previous study shows that *APTF-1* is required for the GABAergic interneuron RIS to induce sleep in *C. elegans* [6]. In mammals, GABAergic neurons in the central nervous system play a key role promoting sleep. Sleep inducing GABAergic neurons have been confirmed in multiple brain areas [77, 86, 94, 99]. In this study, GABAergic gene expression was affected by *Tfap2b* half deletion but not *Tfap2a*. AP-2β transcativates target gene expression in homodimeric or heterodimeric association with AP-2α/β/γ [104]. However, the expression of *Tfap2a*, *c*, *d* is not changed in *Tfap2b*-deleted embryonic brain. Therefore, *Tfap2b* is indispensable in the combination of dimers involved in the regulation of GABAergic genes.

At early developmental stage, the GABAergic cell fate is determined by a concert of transcription factors, such as *Ascl1*, *Dlx1/Dlx2*, *bHLH-Rbpj* [120-122]. These transcription factors act in pairs as heterodimers to transactivate the differentiation or specification of GABAergic neurons. In this study, I found that *Tfap2b* regulated the expression of *Gad65*, *Gad67*, *Vagt* in a heterogeneous way depends on different brain areas. This implied that *Tfap2b* might not directly control the development of GABAergic system, but could possibly targeting other transcription factors or enhancers that directly activate GABAergic expression.

Tfap2b is highly expressed in the midbrain/hindbrain area in embryonic mouse. Therefore, I examined the brainstem area in more a detailed way using ISH. PZ contains a delimited node of neurons in a rather small-sized area which allows a more precise quantification [86]. The ISH results showed the number of GABAergic neurons were decreased in PZ. This is consistent with the results from qPCR that showed a down-regulation of GABAergic genes in the brainstem where the PZ locates. Another study has also revealed a role of *Tfap2b* in GABAergic neuron differentiation [123]. These results indicate an important but complex role of *Tfap2b* in the expression of GABAergic system.

3.2 Genes regulated by *Tfap2b* in E14.5 mouse brains

It was revealed by this experiment that the DE gene patterns resulted from tfap2b deletion were not uniform across different brain areas, since the *Tfap2b* is restrictedly expressed in midbrain and hindbrain areas in a developing mouse [109]. Interestingly, the expression pattern also differed between female and males. Literature analysis of the differentially regulated genes in the network analysis (**Fig. 12, 13**) and related to sleep is discussed in the following sections.

3.2.2 Literature analysis of down-regulated genes

***Hox* genes**

Hox genes belong to the homeobox gene superfamily. Many genes in the *Hox* gene family implicate in brain development of both invertebrates and vertebrates [124, 125]. More importantly, *Hox* genes play an important role in the segmentation of the vertebrate hindbrain at early embryonic stages [126]. They are also important for neuronal patterning at later stages, including neuronal migration and axon guidance [127]. Consistent with my finding, downregulated *Hox* genes were found in the developing posterior brain. *Hox* genes encode transcription factors that structure the neural tube along anteroposterior (AP) direction [128]. Similarly, most of the downregulated genes (a3 to 6; b2 to b8; c4; d3) found are expressed in the anterior to middle structure of central nervous system where major classes of neurons are generated [129]. Changes of the *Hox* gene expression found in DMH implied that the neuronal patterning in the hindbrain might be altered.

Solute carrier genes

Most of the down-regulations occurred in solute carrier 6 (Slc6) gene family which includes NE, GABA and sodium-dependent branched-chain amino acid transporters [130]. Norepinephrine transporter (NET), encoded by *Scl6a2*, regulates the noradrenergic neurotransmission by mediating reuptake of NE [131]. Allelic mutation represses *SLC6A2* transcription [132] and confers to ADHD (attention-deficit hyperactivity disorder) [133]. *Slc6a11* encodes GABA transporter 3, polymorphism of the gene increased the susceptibility to the tardive dyskinesia, an involuntary neurological movement disorder

[134]. *Slc6a15* functions as a brain transporter that facilitate the uptake of proline and leucine [135, 136]. Mutation in *SLC6A15* is correlated with major depression and risk allele carrier has a reduced expression in hippocampus [137], which might relate to its involvement of glutamatergic signaling [138] (tend to stay longer on Rotarods). All of these genes are correlated with motor functions and tend to induce hyperactivity symptoms that could potentially disturb sleep.

Slc4 gene family has also two members down-regulated in female DMH. *Slc4a5* encodes NBCe2 that transports sodium bicarbonate (and/or carbonate) in peripheral organs [139]. Mutations in this gene is related with hypertension or renal metabolic acidosis [140]. This could probably explain the renal failure induced perinatal-lethality reported in *Tfap2b* homozygous deletion [112]. Brain specific *Slc4a10* encoded NBCn2 transports sodium bicarbonate and disruption of the gene increases neuronal excitability [141, 142]. Interestingly, from our previous study, we observed a reduced sleep but increased wakefulness during active phase in *Tfap2b* $^{+/-}$ mice [119]. The molecular analysis of the down-regulated of *Slc* genes in MDH, again, seem to support a hyperactive phenotype with a more excited brain.

Noradrenergic/dopaminergic neurotransmission related genes

Dbh, dopamine beta-hydroxylase, converts dopamine to noradrenaline. Impaired beta-hydroxylation of dopamine results in a complete absence of noradrenaline (NA) and adrenaline in plasma (orthostatic hypertension), consequently the dopamine is elevated [143]. Patients with DBH deficiency is mainly characterized by cardiovascular disorders [144]. *Dbh* $^{-/-}$ mice exhibit longer NREMS [62] and shorter sleep latency after mild stress [145] compare with their heterozygous littermates which has normal level of NE. Further, optogenetic disruption of *Dbh* gene abolished the awakening effect of LC (Locus coeruleus) stimulation [146]. Importantly, both dopamine [147] and noradrenaline [148] are important neurotransmitters in wake-promoting circuitry. In our study, both *Dbh* and *Slc6a2* (discussed in section 3.3.2) were down regulated in female and male DMH (Table 2.3). However, while *Dbh* deletion deprives the body of NE, *Slc6a2* mediates reuptake of NE and dopamine [149], it would be difficult to predict how the dopamine/NE ratio would be in the tested brain area. However, it would be interesting to measure how the dopamine and NE concentration within sleep centers and therefore to shed some light upon their roles in sleep regulation.

3.2.3 Literature analysis of up-regulated genes

Dmbx1

Dmbx1, diencephalon/mesencephalon-expressed brain homeobox gene 1, is a novel evolutionarily conserved (zebrafish and human) paired-like homeobox gene whose expression was detected at E8.5 in the midbrain region [150, 151]. *Dmbx1* gene functions predominantly in midbrain that paralogs knockout of its paralogs result in reduced growth of the midbrain [152]. Mice deficient in *Dmbx1* exhibit severe leanness associated with hyperactivity. Further, a *Dmbx1* $^{-/-}$ mouse being isolated from its cohabitants sometimes starves itself to death [153]. However, in this study, Dmbx1 was up-regulated in female/male DMH and it is not clear how the *Dmbx1* gain-of-function mice behave. Further, there was no differences in body weights from the tested heterozygous colony between genotypes. Yet, up-regulation might potentially contribute to the depression-like behavior observed in the *Tfap2b* $^{+/-}$ mutants.

***Dlx* homeobox transcription factors**

Dlx homeobox transcription factors are functionally highly redundant. *Dlx1* and *Dlx2* play a central role determining neuron-glial cell fate [154, 155], differentiation [156] and migration [157] of GABAergic interneurons in developmental forebrain. The *Dlx5* and *Dlx6* are critical for craniofacial, limb, A-P axial development [158]. *Dlx2* and *dlx5* are both involved in the MAGE-D1 mediated GABAergic neuron differentiation [159]. The upregulation of *Dlx2* and *Dlx5* in posterior embryonic brain implied an alternation in GABAergic neuronal development due to *Tfap2b* deletion. In addition, qPCR and ISH data showed a decreased in GABAergic expression in the adult brainstem. Therefore, it is very tempting to speculate that some of these GABAergic neurons are sleep-promoting.

3.3.4 Summary

Tfap2b deletion induced a major change in homeobox genes, *Slc* genes and neurotransmission related genes. Taken together, the expression changes of these genes may pattern the model of flip-flop switch in sleep-wakefulness regulation in a way that the up regulated genes favor the sleep loss side meanwhile the down-regulated genes support a more active wakefulness phenotype. Further, these DE genes might act cooperatively to determine the development of sleep neurons.

3.3 GABAergic neurons expressing *Tfap2b* control sleep in mice

Many genes are related to sleep behavior (as summarized in introduction), but the pathways between target gene and behavior remain elusive. In this study, I observed a gene-brain-behavior control in sleeping mice.

Homologs of *Tfap2b* and their functional importance have been revealed in sleep behaviors of *C. elegans* and drosophila [6, 117]. Severe morphological and pathological changes have been reported in *Tfap2b* deleted mouse pups [112]. However, the neural targets of *Tfap2b* remain unclear. The previous results from qPCR, ISH, RNA-seq suggest a role of *Tfap2b* in regulating GABAergic gene expression. Therefore, it was hypothesized that *Tfap2b* regulates the GABAergic neuronal function in sleep. In addition, both the RNA-seq analysis and the research from Nakai *et al.* using *Tfap2b*-mutated mouse strain [160] suggest a gender difference in manifestation of the *Tfap2b* deletion/mutation. Therefore, to test the hypothesis, I used both female and male mice with GABAergic specific *Tfap2b* knockouts. The EEG recordings analysis suggest that GABAergic neurons expressing *Tfap2b* control sleep in mice, at least in female.

DNA binding site of AP-2β protein is highly conserved [105]. Its function diversifies as organism evolve to have more complex nervous system. However, some basic component of its function, such as sleep control, are still reserved though expressed in a more complicated way [119, 160, 161]. Interestingly, such common feature in function is also observed in between less conserved analogs. TF *LIM-6*, which controls the expression of the sleep-promoting neuropeptide FLP-11 in *C. elegans* [162]. Deletion of *Lhx6*, member of LIM-homeobox from *M. musculus*, in ZI (sleep-promoting brain area) resulted in decreased sleep [99].

Sleep homeostasis and the use of behavioral criteria has bridged the sleep research of vertebrates with invertebrates [163]. Conserved genes and neural system are valuable keys for exploring the evolutionary origin of sleep. In *C. elegans*, the *APTF-1* expressing GABAergic interneuron RIS controls its sleep [6]. In mice, we found that GABAergic neurons expressing *Tfap2b* regulates the homeostatic sleep. In my study, *Tfap2b*-GABAergic control of sleep homeostasis seems to be a conserved function.

3.4 Conclusion

The first part of results has revealed the divergent roles of *Tfap2a* and *Tfap2b* played in sleep control. In addition, the function of these transcription factors extend to behaviors beyond sleep. The results from the second part have confirmed that *Tfap2b* affects GABAergic system at molecular level. Further, the bidirectional expression pattern of GABAergic genes within different brain areas implied a complex mechanism underlying this regulation. Moreover, many interesting gene targets were discovered as a result from RNA-seq gene expression analysis in developing brain. For example, genes from the homeobo*x* family that are closely related to neural development. Finally, in the third part of the results, gene-brain to function relationship was verified in murine sleep behavior that GABAergic neurons expressing *Tfap2b* control sleep. One of the most challenging part of studying a gene's function is that there is a long way from a single gene end to the behavioral end, where there have been multiple behaviors waiting, perhaps, since millions of years ago. Therefore, I find it very exciting meeting GABAergic system on the way. It was astonishing that, in the circadian field, such a gene-to-behavior dream has been realized. However, our sleep is still full of mysterious dreams.

3.5 Outlook

The previous results have raised more questions than answers. The most urgent one is: which GABAergic neurons were affected by the *Vgat-tfap2b* deletion? In another word, the strength of this deletion has to be tested. For example, the proportion and distribution of the GABAergic neurons in the wild types and knockouts need to be measured. Comparisons between genotypes are necessary to know the ratio of GABAergic neurons that could be down or up regulated in a specific brain area or overall brain. *Tfap2b* expresses early in the developing stages. Its expression dissipates as the animal grows older and minimize in adult brain. Therefore, embryos should be included in the test.

Except for GAD67, GAD65, Vgat, expression of genes that are involved in GABAergic development also need to be characterized: (1) Transcription factors *Dlx1* and *Dlx2* from *Distal-less* homeobox, which is important for GABAergic cell maturation [164]; (2) *Dlx5*, which is critical for AP axial development, together with *Dlx2,* they influence the neuronal differentiation [158, 159] and they were upregulated in Tfap2b$^{-/-}$ embryonic brain; (3) Lhx6, which is recruited for interneuron migration and a role in GABA has already been proved [99, 164]; (4) Nkx2.1 from NK2 homeobox transcription factors, which decide cell fate [164].

The above goals can be achieved by qPCR, ISH or RNA-sequencing. The results shall pave the way for function analysis under genetic ablation or activation conditions.

4. Methods

4.1 Generation of V*gat-tfap2b* $^{-/-}$ mouse line

We purchased *tfap2b*^{tm1a} strain with the knock-out first (tm1a) allele of from EMMA. V*gat- cre* mouse (#028862, Jackson laboratory) was a gift from Professor Nils Brose from Max Planck Institute of Experimental Medicine. We first crossed *tfap2b*^{tm1a} mouse with the FLP deleter strain (#003946, Jackson laboratory). This removed the trapping cassette from *tfap2b*^{tm1a} line, therefore converted the tm1a strain to the conditional (floxed) strain (*tfap2b* $^{fl/+}$). We further crossed *tfap2b* $^{fl/+}$ mouse with V*gat-cre* mouse to delete *tfap2b* from GABAergic neurons expressing vGAT and produced V*gat-tfap2b* $^{-/+}$ mouse. V*gat-tfap2* $^{+/-}$ mice were bred to *tfap2b* $^{fl/+}$ line to generate homozygous knockouts (V*gat-tfap2b*$^{-/-}$) and littermate controls. We chose the *tfap2b* $^{fl/fl}$ and heterozygous V*gat-cre* mice as the control groups in this experiment due to potential behavioral differences caused by the expression of Cre recombinase and loxP site. Both male and female mouse were used in this experiment.

4.2 Genotyping

Ear biopsies of mice were collected and genomic DNA was extracted as described previously [119] with minor modifications. Briefly, samples were lysed in 50 µl of PBND buffer (50mM KCl, 10mM Tris HCl pH 8.3, 0.1mg/mL $MgCl_2 \cdot 6H_2O$, 0.1mg/mL Gelatin, 0.45% NP-40, 0.45% Tween20) with 2.5 µl proteinase K (#P8107S, New England BioLabs) freshly added. Incubate the samples in the thermomixer at 55°C overnight until samples are completely lysed. Deactivate the proteinase K in the samples by incubating at 85°C for 45 min. Centrifuge the lysate at 6000 x g and use the supernatant for PCR. Primers used for genotyping and PCR conditions are listed in **Table 1**.

Table 1. Genotyping primers and protocols

Gene	Primer names	Primer sequence 5' - 3'	PCR conditions	Products
[1]*Vgat-cre*	Common-F (12785)	CTTCGTCATCGGCGGCATCTG	10s at 95°, 10s at 65°(0.5°C per cycle decrease), 10s at 68° for 10 cycles;	*Vgat-cre* allele 200bp; wild-type allele 323bp
	Wildtype-R (12786)	CAGGGCGATGTGGAATAGAAA		
	Mutant-R (oIMR8292)	CCAAAAGACGGCAATATGGT	10s at 95°C, 10s at 60°C, 10s at 72°C for 28 cycles	
Tfap2b^{tm1a}	Tfap2 5'arm	GACATCCTACAATGCACAGCT	30s at 95°, 45s at 65°, 45s at 72° for 39 cycles	*Tm1a* allele 529bp (5'arm + LAR3); wild-type allele 381bp (3'arm + 5'arm)
	Tfap2 3'arm	TTGCTGTGAGCTAAGAGCTTC		
	LAR3	CAACGGGTTCTTCTGTTAGTCC		
Tfap2b^{floxed}	Tfap2 5'arm	GACATCCTACAATGCACAGCT	30s at 95°, 45s at 65°, 45s at 72° for 39 cycles	floxed allele 497bp; wild-type allele 381bp
	Tfap2 3'arm	TTGCTGTGAGCTAAGAGCTTC		

[1]The high speed Taq DNA polymerase (KAPA2G Fast HotStart PCR-kit, KK5503) was used for the corresponding PCR condition.

4.3 RNA extraction.

The user guide protocol of TRIzol was adapted to the brain tissue RNA extraction.

Brian tissue were lysed in TRIzol reagent (1mL to 50-100mg of tissue) and homogenized using Omni bead ruptor. Centrifuge the lysate for 5min at 12,000 x g at 4 ℃, then transfer the supernatant to a new tube. Incubate for 5 min at RT. Add 0.2mL of chloroform per 1mL TRIzol reagent and close the lids. Mix the samples gently by turning up and down for ~ 10 rounds. Incubate for 3 min at RT. Then, centrifuge the sample for 15min at 12,000 x g at 4 ℃. Pipette the clear supernatant containing RNA to a new tube without disturbing the interphase and add 0.5mL of isopropanol per 1mL TRIzol used. Incubate 10 min at RT, then centrifuge for 10min at 12,000 x g at 4 ℃. RNA shall precipitate and form a white pellet at the bottom of the tube. Discard the supernatant. Wash the RNA pellet in 1mL of 75% ethanol per 1mL used by tapping till the pellet is floating. Centrifuge the sample for 5min at 7,600 x g at 4 ℃. Discard the supernatant and air dry the sample for ~ 10 min at RT. All processes shall be performed in the clean hood.

4.3 Reverse transcription

Measure the quality and quantity of RNA samples using NANO drop. Adjust the concentration of RNA samples according to need for the qPCR. Usually a total amount of up to 1ug in 10ul of RNA per 20 µl reverse transcription reaction is proper for later qPCR. All samples shall have the same concentration. High-Capacity cDNA Reverse Transcription Kit (Cat. 4368814) was used for reverse transcription. Master mix of 10 µl was prepared (2 µl of 10 x reverse transcription buffer; 0.8 µl of 25x dNTP Mix; 1 µl of 10 x random primers; 1 µl of reverser transcriptase; 1 µl of RNase inhibitor; 3.2 µl of Nuclease-free H_2O). Finally, a total of 20ul per reaction (10 µl master mix + 10ul RNA sample) was prepared for each sample. Reverse transcription was performed at 25℃ for 10 min, 37℃ for 120 min, 85℃ for 5 min and samples shall be kept in 4℃ or -20℃ until use.

4.4 qPCR

Primers used and qPCR conditions are listed in **Table 2**.

Table 2. Primers and protocols used in qPCR

Gene	Forward	Reverse	qPCR conditions
eef1a1	TGCCCCAGGACACAGAGACTTCA	AATTCACCAACACCAGCAGCAA	
Tfap2a	AGCAGGGAGACGTAAAGCTG	GGGATCGGAATGTTGTCGGT	
Tfap2b	CCTCAATGCATCTCTCCTGGG	CCAGTGAGGTGAGTAACGTGA	
Tfap2c	CGTCACTCTCCTCACGTCTC	GTGGCCATCTCATTCCGTC	1 min at 94°C, 30s at 62°C, 1min at 72°C for 40 cycles
Tfap2d	TCTGATCCGGGCAAAACCAT	GCTTACGATGCAATTTCCCCC	
Gad65	TCCGGCTTTTGGTCCTTCG	ATGCCGCCCGTGAACTTTT	
Gad67	TCCAGTGCTCTGCCATTCTG	CATAGGAGACGTCATACTGCTTGTC	
Vgat	ACCTCCGTGTCCAACAAGTC	CAAAGTCGAGATCGTCGCAGT	

4.5 EEG Surgery procedure

A brief version of the EEG surgery procedure was published here [119], same protocol with more details were provided in the following manual.

4.5.1 Materials and devices

4.5.1a Surgical maintenance

(1) Isoflurane anesthesia system (InterMed, Pelon sigma delta)
(2) Ophthalmic gel (eye protection during surgery)
(3) 0.9% (w/v) NaCl
(4) Disinfectant (70% ethanol)
(5) Sterile cotton swabs
(6) High-intensity light source (Operation light source)
(7) Analgesic (Buprenovet, Multidose, Bayer, 0.3 mg/ml)
(8) Adhesive Resin Cement and dental cement
(9) Heating pad

4.5.1b Surgical instruments

(1) Stereotaxic frame with marker pen
KOPF stereotaxic alignment system Model 1900 with the respective drilling unit (Model 1911), cannula (Model 1974) and syringe holders (Model 1972) as well as a small microscope (model 1915 centering scope 40x) to attach it to the z-arm and calibrating indicators.

(2) Sterilized surgical instrument kit including scissors, forceps and clamps
(3) Micro drill
(4) EEG electrodes: Miniature screw electrodes (The head diameter is 2.16mm and the shaft is 1.6mm, Bilaney Consultants GmbH) with 5mm wire attached**,** EMG pad - subcutaneous electrode (12mm, Bilaney Consultants GmbH).
(5) Wires assembler: plastic pedestal (MS363, PlasticsOne, Bilaney Consultants GmbH)
All instruments should be disinfected before starting and, if necessary, again during the operation (e.g., autoclave, 95% ethanol).

4.5.2 Analgesic reagent preparation

Dilute the Buprenorphine using saline solution to 1:10. Prepare the syringe with the dilution and remove the bubbles. Administer at rate of 0.1ml / 30 gm (or 0.15ml / 45 gm), then a dosage of around 0.1 mg/kg is delivered.

4.5.2 Animal preparation and pre-surgical preparation

Age and body weight are two vital factors affecting the size of the skull. For sleep phenotyping, we start the operation using adult mice around 12 weeks of age with a body weight of 25 to 35g. According to our previous experiments, age has an effect on sleep behavior that implantations with adolescent mice (younger than 9 weeks) or under 20g had caused problems (which was mainly lack of delta power rebound). The adolescent mice (around 2 months old) were reported to have different homeostatic regulation of sleep [citation] compared with adult mice (3 to 9 months old). Male and female mice were recorded separately to avoid the influence of sexual excitation on the sleep pattern.

Check the general health condition according to the criteria in table.1 and transfer them to the recording room if no severe abnormality observed. Allow the mice to habituate to the single house condition and introduce them in the experiment room at least 1 week before surgery.

4.5.3 EEG surgical procedures

(1) Put or lead the mouse in the anesthesia chamber, then fill the chamber with 5% isoflurane. Observe carefully as the mouse becomes unconscious. Important behavior signs can be observed during the process. First there's a reduction of motor movements until it stops. Then, observe the frequency of breathing from the fluctuation of the abdomen. Disconnect the tube and reconnect it to the tube holder on the stereotaxic frame when the frequency decreases to around 2 to 3 times per second. Take out the mouse and hook its teeth to the tooth holder. Place the tongue out of the mouth to avoid suffocation and fix the nose mask. Cover the complete nose including whisker part with the mask and decrease the isoflurane to 1%-2% according to breathing frequency.

IMPORTANT NOTE If the mouse starts to choke inside the anesthesia chamber, take it out immediately or connect it to 100% O_2 when necessary. On the contrary, if the mouse start to move immediately after taking out of the chamber, do not force it to the nose mask, but put it back to the chamber to reinforce the anesthesia process.

(2) Place the anesthetized mouse into a stereotaxic frame to fix its head in. Check the anterior-posterior, dorsal-lateral and horizontal position (Fig. 1A) and keep them in parallel with the XYZ axes with the stereotaxic frame. Use the ear bars when adjust the head at horizontal and vertical level, so it's not tilted in any of the direction. Fix the head by the ear bars inserted into the auditory canal. However, be very careful when using the ear bars, because when inserted too deeply they can severely damage the ear and this could lead to death. Put some surgical tissue beneath the body to keep the head at a bit higher level than the body. This head-higher position should help reduce possible bleeding during surgery.

(3) Moisturize the hairs on the scalp with 70% alcohol and shave them with bended scissors (avoid to cut the skin), so that the hair will not enter the wound or stick to the cement afterwards. Apply protective gel to the mouse's eyes to prevent them from drying out.

(4) Illuminate the surgical area with an intensive operational light source. After removing the hairs, make a longitudinal incision with a scalpel or a scissor along the midline, starting between the end of the eyes and measuring ~1 cm backwards (Fig. 1). Produce a broad window by placing some clamps on the edge of the cut skin, on both sides of the opening, to best expose the target area. Carefully remove the skull periosteum, clean thoroughly with saline and remove any blood or fluids by cotton swabs, and allow the bone to dry.

Drilling holes in preparation for implantation of EEG electrodes and screws

(5) Mark the hole position with the stereotactic frame (Fig.1B). Cautiously drill five holes into the cranium. Apply enough counter-pressure to keep the drill bit from engaging into the dura mater when it passes through the skull. Two holes are drilled over the right and left frontal cortex (anteroposterior, AP, +1.5mm from bregma; mediolateral, ML, 1.7mm). One is over the right parietal (AP +1.5mm from lambda, ML, 1.7mm) cortex. Two are bilaterally over the cerebellum (AP -1.5mm from lambda, ML, 1.7mm) as reference (left) and ground signal (right). The electrode positions are chosen to reconcile the heterogeneity between the frontal and parietal signals within same vigilance state and ensure the optimal differentiation among all

states. The rostral electrode placed over the frontal cerebral cortex captures EEG delta waves of NREM sleep (NREMS), the caudal electrode placed above the hippocampal structures captures the thaw-tooth like theta oscillation of REM sleep (REMS). Although the use of a neutral reference electrode allows recording from a monopolar derivation, we put one more electrode that makes it bipolar for frontal lobe. This helps increase the chance of capturing signals from the frontal cortex where, to our previous experiences, premature disconnection occurs the most. More importantly, the delta wave intensity of NREM is the major marker of homeostatic sleep.

CAUTION: If the dura mater is penetrated, cerebrospinal fluid (CSF) and/or blood will emerge from the hole. In this case, wet the cotton swab with saline water and, if necessary, apply some force to the bleeding point, remove the swab until no more fluid is emerging; the operation can be continued, but there is a risk of signal disturbance. Keep this noted in the lab record and check the quality of signal after connection to the cables. Make sure the skull is dry and clean before the implantation of screws.

(6) Place the screws into the holes using a hemostatic forceps as the screwdriver. To avoid puncturing the complete screw, around half of each screw should be kept above the surface of the cortex (with our screws this corresponds usually to two to three turns, if there's no invalid turns that the screw does not actually engage in depth). One subcutaneous pad is placed in the nuchal muscle for the electromyogram (EMG) recording. Remove the clamps.

(7) Prepare the dental cement mixture on aluminium foil. Next, cement the screw without covering the top of wires. Let the cement flow to cover all of the open wound area and ensure the cement meets and covers the margins of the wounded skin. Do not let the cement run into the sheath attached to the electrodes. Keep the unfixed EMG wire temporarily immobile by leaning it on one of the closest EEG electrodes. Quickly assemble the wires into the plastic pedestal before the cement dries out. Prepare another dental cement (flowing slower than the previous preparation) to cover all the contacts to fix the structure in place.

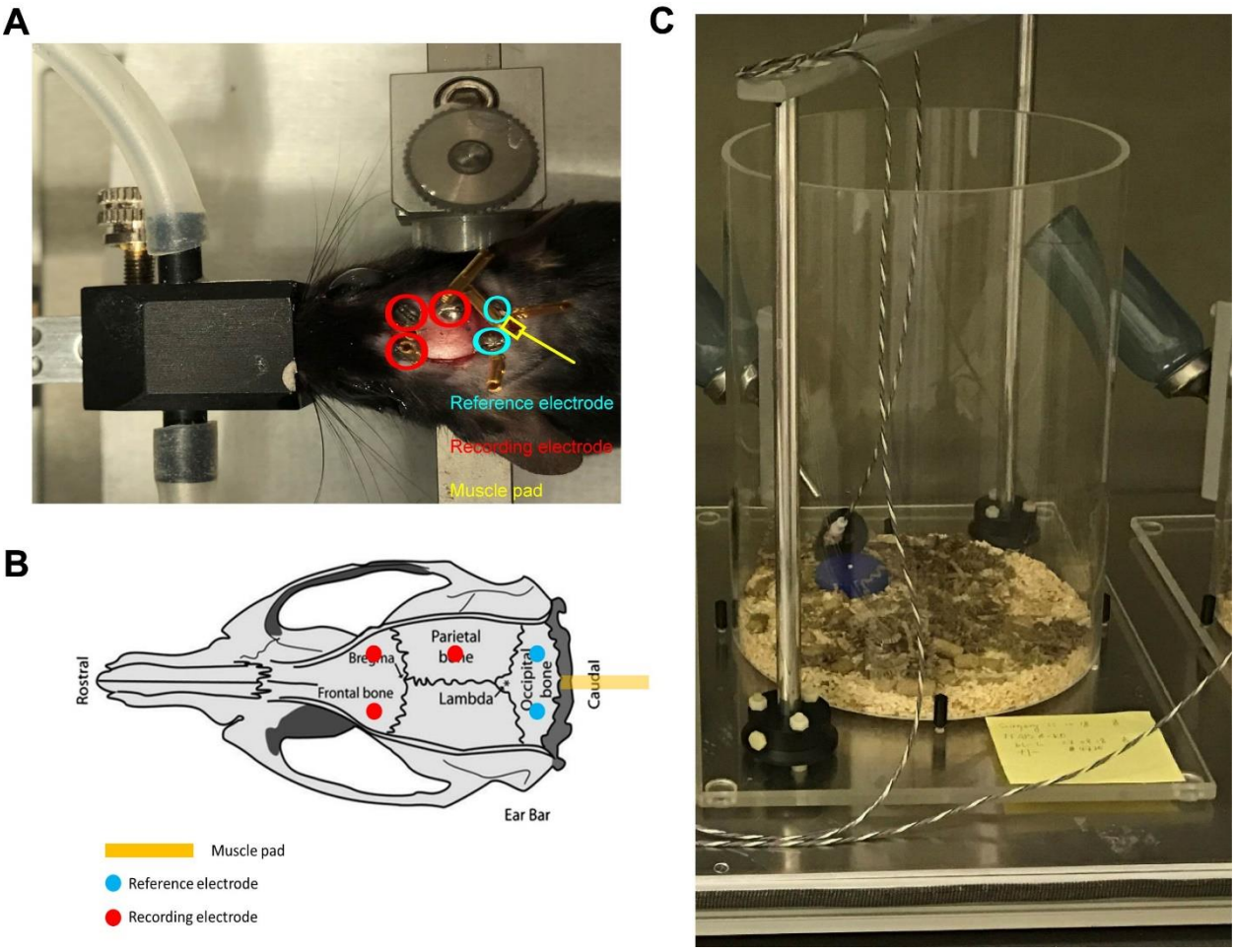

Figure 26. EEG surgery instruction and recording envioronment.

Surgical view with EEG/EMG elecotrodes implantations indicated (A). Schematic description of the brain areas where the EEG/EMG electrodes locate (B). Example view of the recording cylinder (d = 26 cm; h = 35 cm) envioronment for individual mouse.

4.5.4 Post-surgical considerations

(1) Cut a small piece of adhesive tape and cover the connector to keep the contacts clean and free of dust. Shape the tape to fit the size of the plastic pedestal to avoid removal by the animal.

(2) Weigh the animal. Put it back into a cage with heating pad and monitor constantly until anesthesia wears off and the mouse starts moving. Put it back to its home cage for recovery.

(3) After the surgery, allow the mouse to recover at least 10 days prior to cable connection under standard housing conditions, and check the health status (Mouse Grimace Scale, MGS) of the animal during the first 3 days of recovery. Analgesic shall be injected under anesthesia in case of moderate pain. Weigh the mouse again before connecting it to the recording cables. Allows the mouse at least 2 days to habituate to the cable and cylinder cage ((**Fig. 25C**).

4.6 EEG setup and recording schedule

4.6.1a EEG recording system devices

(1) Preamplifier with plug-in wires (**Fig. 26B**, Micro Preamplifier µPA16)

(2) Signal Collector (**Fig. 26C**, µPA32)

(3) Programmable Amplifier (**Fig. 26D**, PGA)

(4) Aata Acquisition Station (**Fig. 26E**)

(5) Recording cylinder: provided with beddings, water, nesting material, food (**Fig. 25C**)

All devices were purchased from Multi Channel Systems (Germany).

4.6.1b EEG recording schedule

(1) Place the animal into cylinder housing cage with free access to food and water. Connect it to the recording cable under anesthesia (**Fig. 25C**). The hardware setup of recording system is described in **Fig. 26**.

(2) When connecting the animal to the cable, hold the basic cement of the connector on the animal's head when inserting the cable plugged into the head connector. This is to avoid applying too much pressure on the mouse's head.

(3) The recording boxes are placed into a Faraday cage to avoid contamination of the signal from environmental electromagnetic field. Allow the mouse to habituate to the cable and the experimental cage for at least 2 days.

(4) After sufficient habituation, record for 2 consecutive days as baseline (BSL), without any disturbance. This allows determining day–to-day stability of the sleep and EEG variables being assessed.

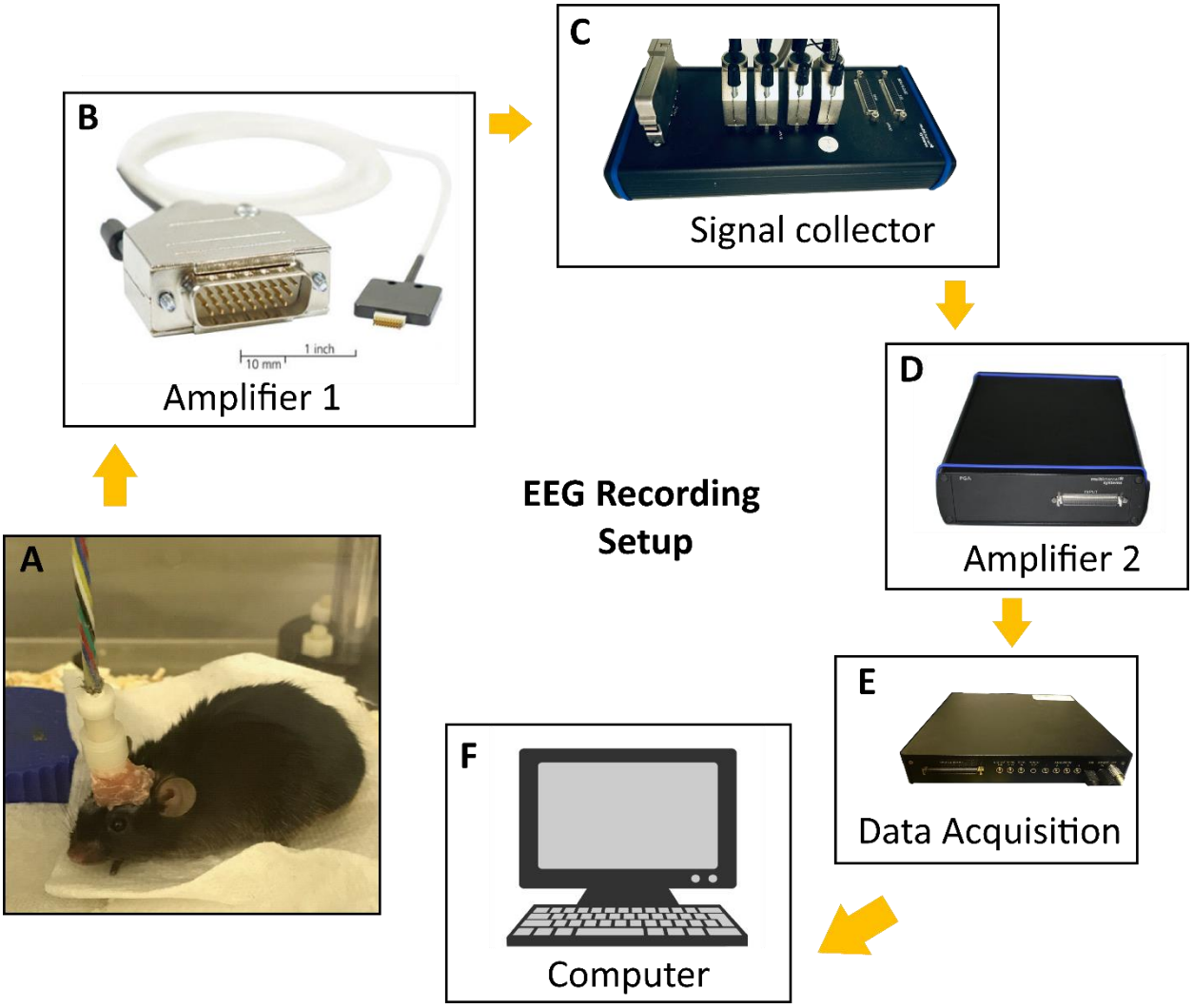

Figure 27. Scheme of the experimental EEG recording system setup.

Mouse implanted with EEG/EMG electrodes is connected to the recording cable (A). The recording signals are pre-amplified (B), before gathered by signal collector (C). Signals are amplified again within a flexible range by the programmable amplifier (D). The data acquisition station (E) processes the signals and data is transferred to the computer (F) equipped with MC_Rack software.

4.7 Sleep deprivation by gentle handling

The SD experiment is immediately following the BSL recording, sleep-deprive the animals for 6 h from the light onset and subsequently followed by 2 consecutive days of recovery recording. Gentle handling means that the animal is kept in its home cage attached to the recording cable and left undisturbed as long as it does not display behavioral or EEG signs of sleep. When needed, sleep is prevented by introducing novel objects (e.g. paper tissue, wooden cubes) brushing the whiskers or fur, gently tapping the cage.

4.7 EEG data acquisition and analysis

All signals are amplified and the reference signals are subtracted from the recording signals before analog-to-digital conversion. Signals were acquired by a computer equipped with MC_Rack software. The raw files (MCD files) are transferred into EDF files by Multi Channel DataManager software. Please refer to my publication here [119] for the method of EEG data analysis.

4.8 Generating ISH probe template

Probe template for GAD67 was generated by PCR. E15.5 brain cDNA which contains high expression of the target gene served as DNA template in the following PCR reaction. Prepare the premix buffer with 5 µl of 10 x Buffer; 10 µl of Q buffer; 5 µl of dNTPs; 0.5 µl of Taq polymerase. Divide 42.5 µl of premix in each PCR tube (3 tubes for 3 annealing temperature). Add 5 µl of primer mix and 2.5µl cDNA to each tube. The run protocol for probe generation is in **Table. 3**.

Table 3. Probe PCR Run protocol

Temperature (°C)	Time	
94°C	3min	
94°C	25"	35cycles
50°C GRADIENT *	25"	
72°C	1min 15"	
72°C	9min	
4°C	pause	

*Make sure at least 3 temperatures are included and used: 53,2°C 57,8°C 62,0°C.

4.9 RNA Probe synthesis for *in situ hybridization*

In vitro transcription is carried out in a cocktail of

(1) 3µl of 10× transcription buffer
(2) 3 µl of 10X DIG / FITC mix (Roche Applied Science)
(3) 0.5 µl of RNAse Ribolocinhibitor
(4) 1 µg of probe template
(5) µl of RNA polymerase (T7 or SP6 New England Biolabs)

Add DEPC water to a final volume of 30 µl

The reaction mix is incubated at 37 °C for at least 2.5 hrs followed by a 15-min incubation with a DNase1 (1.5 µl) to remove the residues from DNA template. After incubation, add 110µl Ammonium acetate (4M) and 800µl of 100% Ethanol (both pre-chilled at -20 deg. C). Incubate the mix at -80 deg.

C overnight. Centrifuge the mix at highest rpm (> 13,000 rpm) for 20 min at 4 deg. C. Discard the supernatant carefully not to disturb the pellet / RNA (RNA will be invisible). Add 900 µl of 70% Ethanol (pre-chilled at -20 deg. C) to the pellet and flick the tube thoroughly. Centrifuge the mix at highest rpm (> 13,000 rpm) for 20 min at 4 deg. C. Discard the supernatant carefully. RNA will be now visible as a small pellet. Air-dry the pellet. Dissolve the pellet in 44 µl of DEPC water. Mix well. Take 2 µl and check the concentration on Nanodrop Spectrophotometer. Dissolve the remaining in Hybridization mix (Ambion) at the final concentration of 100 ng/µl.

4.10 Fluorescent TSA-amplification on standard non-radiometric ISH for adult mouse brain

4.10.1 Preparation of stock solutions

(1) Proteinase K buffer 2X stock (1 L)

Tris 12.1 g

EDTA 2.9 g

Make up the volume to 1L and adjust the pH to 8.

(2) 10X TN buffer (1 L)

Tris 121.15 g

NaCl 87.95 g

Make up the volume to 1L and adjust the pH to 7.5.

(3) 20X SSC buffer (1 L)

Sodium citrate 88.2 g

NaCl 175.3 g

Make up the volume to 1L and adjust the pH to 7.

(4) 0.2N HCl (1 L)

Add 16.6mL of 37%HCl to sterilized ddH2O to make 1L solution.

(5) TNB buffer

Add 2.5g of Perkin Elmer TSA blocking powder (FP1020) to 500mL 1xTN buffer.

Turn on the stirrer and set heated platform to 55ºC. Set oven temperature to 65ºC. Stir moderately for 2 hours (not more than 3 hours). Needs to be degassed. store at -20 ºC. Thaw and warm up to RT before adding primary antibody (It's recommended to thaw the buffer in 4°C overnight until ice-out before sitting at RT).

(6) DAPI stock solution (5mg/ml , 5000X)

Dissolve DAPI (sigma-aldrich, D9542-10MG) with 2ml distilled water.

Store in dark at 4 ºC for half a year or -20 ºC for at least one year. Dilute with PBS to make 1X working solution.

4.10.2 Working solutions to be prepared in advance

1X PBS, 1X Proteinase K buffer, 4% PFA (prepare fresh), 2X SSC, 0.2X SSC, 1X PBST (PBS + 1ml Tween20 to make it 0.1%), 1X TNT (TN + 1ml Tween20 to make it 0.1%), Fluorophore Tyramide working solution (1:50 / prepare fresh), bring TNB buffer at RT.

4.10.3 ISH fluorescence staining procedure

Table 4. ISH fluorescence single staining

Step	Procedure	Reagents and solutions	Time/ Temperature
1	Incubation	5% H_2O_2 in Methanol (prepare fresh)	20min / RT
2	Washing	PBS	2 x 5min / RT
3	Denaturation	0.2N HCL	10min / RT
4	Washing	PBS	2 x 5min / RT
5	Deproteinization	PK buffer+35ul per 100ml proteinase K	2 x 10min / RT
6	Washing	PBS	2 x 5min / RT
7	Fixation	4% PFA in PBS	10min / RT
8	Washing	PBS	2 x 5min / RT
9	Pre-hybridization	Hyb-buffer (+1mg/ml DTT)	30min / 60°C
10	Hybridization	Hyb-buffer + 1.5 ug/ml GAD67 probe (4ul per 250ul) + same amount of tRNA	Overnight / 60°C
11	Washing	2 x SSC buffer	15min / 60°C
12	Washing	2 x SSC buffer	5min / RT
13	Washing	0.2 x SSC buffer	2 x 30min / 60°C
14	Washing	0.2 x SSC buffer	2min / RT
15	Washing	PBST (0.1%)	2 x 20min / RT
16	Blocking	10% inactivated sheep serum in TNB buffer	30min / RT
17	Antibody incubation	Anti-FITC-antibody (1:500) in blocking buffer	30min / RT
18	Washing	TNT (0.1%) buffer	3 x 5min / RT
19	TSA amplification	Incubate in tyramide working solution (1:50)	7min / RT
20	Washing	TNT (0.1%) buffer	3 x 5min / RT
21	DAPI	~300ul per slide	2min / RT
22	Washing	PBS	3 x 5min / RT
23	Mounting	Vectashield with DAPI	Store at 4°C

4.11 Imaging

Brain slides were sealed with transparent nail polish and examined under Nikon microscopy equipped with spinning DISK. The sleep active GABAergic neurons were identified by Anaclet et al in the medullary parafacial zone dorsal lateral of the 7th facial nerve. GAD67 positive stained pe rkenje cells and the 7th facial nerve (**Fig. 6**) was recognized to anchor the focus. The cluster of GAD67 positive cells dorsal-lateral the 7th facial nerve was marked as the center. A 5-by-5 area around the center was scanned for each hemisphere using 405/488 lasers. 25 tiles per channel were montaged and projected by maximum intensity (MIP).

4.12 ISH data analysis

The number and intensity of positively stained cell nuclei (DAPI) and GAD67 expressed GABAergic neurons were quantified using ImageJ 1.53f51. A cluster of neurons identified in the PZ using GAD67 probe was selected to mark the region of interest (ROI-PZ). The ROI-PZs of the same size were selected for each hemisphere per brain section and all neurons from the cluster were include d in this selected region. The ROI-PZs were merged and saved as JPEG. The merged image was first transferred into a binary image (16-bit) and then filtered with the Gaussian blur (Radius = 6.00). The positively double stained cells were distinguished by the classic watershed plugin (MorphoLibJ) under "Bright Objects/Dark Background" with the setting of a value = 200, mask = none. Subsequently, the threshold the watershed-conducted image was adjusted to include the most of the distinguished cells. "Analyze Particles" was conducted on the threshold-adjusted image and the ROIs of the particles (ROI-Ps) were saved in the ROI manager. All of the ROI-Ps were redirected and shown on the MIP image of the two channels, respectively. Measurements were taken and results of mean gray values and areas were exported as csv files respectively for each channel. The grey values of larger than 80% (or 20% for on pair of control and mutant specimen) of the baseline gray value and the area of larger than 0.006.

4.13 Statistics

Statistics analysis and graph plotting were performed using GraphPad Prism 8 or Rstudio. Shapiro-Wilk Normality test was used to analyze the distribution of data. Levene's test was adopted to test whether variances were equal. Parametric tests were performed for the datasets showed a Gaussian distribution. Specifically, for comparisons between two groups, two-tailed paired/unpaired t-test was performed. As for multi-group comparisons, ANOVA followed by Sidak's multiple comparisons was performed. Nonparametric tests were used for the dataset that was not normally distributed or the variances were not equal. In such circumstances, Mann-Whitney test or Wilcoxon signed-rank were used for two-group comparison, or Friedman test followed by Dunn's multiple comparisons test was performed for multi-group comparisons. Linear regression analysis was performed to plaot accumulative spectral power, and equality of slopes or intercepts was calculate to examine the difference between genotypes. ClueGO [165] was used to network anlaysis of DE genes from RNA-analysis.

Acknowledgements

I would like to thank my parents for their full support of my pursuing the PHD degree in Germany. For that I also thank Prof. Dr. Henrik Bringmann for providing this great opportunity to study sleep in mice. As I started a life in Germany, I thank Dr. Yin Wu for helping me find my first apartment. Meanwhile, I started my project with mouse models, I thank Dr. Alejandra Korovaichuk for introducing me to the research. I enjoyed the extra hours that I spent at the institute, because Dr. Anastasios Koutsoumparis told me that the "Steinway & Sons" in the Manfred Eigen hall was inviting me to play. Then Dr. Queen. Elisabeth Maluck came in and said, "You would have to come and see my horses." Thank you for the invitation and I'm looking forward. Later, Dr. Inka Busack asked me "Ni Xiang He Jiu Ma?" (Would you like to drink some wine?), I replied "Ja, warum nicht?" Thank you for asking, that sounded really like home. When I felt that was enough for today's German, Dr. Marina Sinner taught me that there was a "Innerer Schweinehund" greeting me. Thank you for your explanation, that was truly impressive. When I was ready for challenge again, I saw my EEG files renamed by Dr. Jan Konietzka. Thank you, Jan, but wait, what is "Löwenmäulchen"? What does the lion say?

One and half years later, the royal worm force had moved to Marburg. I stayed in Göttingen with hundreds of mice. Here, I have joined the group of Prof. Dr. Gregor Eichele where I spent the remaining almost 3 years of my PhD life. I am grateful to Prof. Dr. Gregor Eichele for helping me get through these years in the most generous way. Without him it would not be possible to finish this project. I thank Dr. Shoba Kapoor for sharing Tom & Jerry stories with me and I enjoyed the good walks we took in the mountains. I thank Dr. Parth Joshi who always have solutions to the difficulties I encountered.

I thank all staff from animal facility where help was always given immediately to those who ask for it. For colony management and animal experiment, I thank Dr. Ulrike Teichmann and Dr. Sara Kimmina for advice on obtaining permits and EEG experiments. I also thank the staff from microscopy facility: Dr. Antonio Politi and Dr. Peter Lenart, who helped me with imaging using the best camera they have.

I am grateful to all my friends in Göttingen. They help me get through this difficult time under Covid-19. Last but not least, I thank my cute Marzipan, who filled my apartment with joy and small gadgets he borrowed from my neighbor.

Abbreviations

EOG	Electrooculogram
REM	Rapid eye movement
NREM	Non-REM
SWS	Slow-wave sleep
EEG	Electroencephalogram
EMG	Electromyogram
SWA	Slow wave activity
SD	Sleep deprivation
BSL	Baseline
GH	Gentle handling
ADHD	Attention-Deficit Hyperactivity Disorder
GWAS	Genome-wide association studies
FNSS	Familial natural short sleepers
NE	Norepinephrine
POA	Preoptic area
VLPO	Ventrolateral preoptic nucleus
TMN	Tuberomammilary nucleus
GAD	Glutamic acid decarboxylase

PZ	Parafacial zone
MPB	Medial parabrachial nucleus
VTA	Ventrolateral tegmental nucleus
NAc	Nucleus accumbens
LHA	Lateral hypothalamus
SLD	Sublaterodorsal nucleus
CTX	Cortex
HP	Hippocampus
HY	Hypothalamus
STR	Striatum
BS	Brainstem
CB	Cerebellum
PCA	Principle component analysis
SP	Secondary prosencephalon
DMH	Diencephalon / midbrain / hindbrain
DE	Differentially expressed
Slc	Solute carrier family
MIP	Maximum intensity projection

List of figures

List of tables

References

1. Blumberg, M.S., Lesku, J.A., Libourel, P.A., Schmidt, M.H., and Rattenborg, N.C. (2020). What Is REM Sleep? Current Biology *30*, R38-R49.
2. Yamazaki, R., Toda, H., Libourel, P.A., Hayashi, Y., Vogt, K.E., and Sakurai, T. (2020). Evolutionary Origin of Distinct NREM and REM Sleep. Front Psychol *11*, 567618.
3. Keene, A.C., and Duboue, E.R. (2018). The origins and evolution of sleep. J Exp Biol *221*.
4. Nagy, S., Tramm, N., Sanders, J., Iwanir, S., Shirley, I.A., Levine, E., and Biron, D. (2014). Homeostasis in C. elegans sleep is characterized by two behaviorally and genetically distinct mechanisms. Elife *3*, e04380.
5. Huber, R., Deboer, T., and Tobler, I. (2000). Effects of sleep deprivation on sleep and sleep EEG in three mouse strains: empirical data and simulations. Brain Res *857*, 8-19.
6. Turek, M., Lewandrowski, I., and Bringmann, H. (2013). An AP2 transcription factor is required for a sleep-active neuron to induce sleep-like quiescence in C. elegans. Curr Biol *23*, 2215-2223.
7. Aserinsky, E., and Kleitman, N. (1953). Regularly occurring periods of eye motility, and concomitant phenomena, during sleep. Science *118*, 273-274.
8. Vasconcelos-Duenas, I., and Ayala-Gerrero, F. (1983). [The phylogeny of sleep: birds]. Bol Estud Med Biol *32*, 83-90.
9. Klein, M., Michel, F., and Jouvet, M. (1964). [Polygraphic Study of Sleep in Birds]. C R Seances Soc Biol Fil *158*, 99-103.
10. Tobler, I.I., Franken, P., Trachsel, L., and Borbely, A.A. (1992). Models of sleep regulation in mammals. J Sleep Res *1*, 125-127.
11. Webb, J.M., and Fu, Y.H. (2021). Recent advances in sleep genetics. Curr Opin Neurobiol *69*, 19-24.
12. Malafeev, A., Laptev, D., Bauer, S., Omlin, X., Wierzbicka, A., Wichniak, A., Jernajczyk, W., Riener, R., Buhmann, J., and Achermann, P. (2018). Automatic Human Sleep Stage Scoring Using Deep Neural Networks. Front Neurosci *12*, 781.
13. Patel, A.K., Reddy, V., and Araujo, J.F. (2021). Physiology, Sleep Stages. In StatPearls. (Treasure Island (FL)).
14. Wang, C., Guerriero, L.E., Huffman, D.M., Ajwad, A.A., Brooks, T.C., Sunderam, S., Seifert, A.W., and O'Hara, B.F. (2020). A comparative study of sleep and diurnal patterns in house mouse (Mus musculus) and Spiny mouse (Acomys cahirinus). Sci Rep *10*, 10944.
15. Hiyoshi, H., Terao, A., Okamatsu-Ogura, Y., and Kimura, K. (2014). Characteristics of sleep and wakefulness in wild-derived inbred mice. Exp Anim *63*, 205-213.
16. Grieger, N., Schwabedal, J.T.C., Wendel, S., Ritze, Y., and Bialonski, S. (2021). Automated scoring of pre-REM sleep in mice with deep learning. Sci Rep *11*, 12245.
17. Yamabe, M., Horie, K., Shiokawa, H., Funato, H., Yanagisawa, M., and Kitagawa, H. (2019). MC-SleepNet: Large-scale Sleep Stage Scoring in Mice by Deep Neural Networks. Sci Rep *9*, 15793.
18. Mang, G.M., and Franken, P. (2012). Sleep and EEG Phenotyping in Mice. Curr Protoc Mouse Biol *2*, 55-74.
19. Campbell, I.G. (2009). EEG recording and analysis for sleep research. Curr Protoc Neurosci *Chapter 10*, Unit10 12.

20. Shein-Idelson, M., Ondracek, J.M., Liaw, H.P., Reiter, S., and Laurent, G. (2016). Slow waves, sharp waves, ripples, and REM in sleeping dragons. Science *352*, 590-595.

21. Nath, R.D., Bedbrook, C.N., Abrams, M.J., Basinger, T., Bois, J.S., Prober, D.A., Sternberg, P.W., Gradinaru, V., and Goentoro, L. (2017). The Jellyfish Cassiopea Exhibits a Sleep-like State. Curr Biol *27*, 2984-2990 e2983.

22. Rattenborg, N.C., Amlaner, C.J., and Lima, S.L. (2001). Unilateral eye closure and interhemispheric EEG asymmetry during sleep in the pigeon (Columba livia). Brain Behav Evol *58*, 323-332.

23. Rattenborg, N.C., Lima, S.L., and Amlaner, C.J. (1999). Half-awake to the risk of predation. Nature *397*, 397-398.

24. Soltani, S., Chauvette, S., Bukhtiyarova, O., Lina, J.M., Dube, J., Seigneur, J., Carrier, J., and Timofeev, I. (2019). Sleep-Wake Cycle in Young and Older Mice. Front Syst Neurosci *13*, 51.

25. Marzano, C., Moroni, F., Gorgoni, M., Nobili, L., Ferrara, M., and De Gennaro, L. (2013). How we fall asleep: regional and temporal differences in electroencephalographic synchronization at sleep onset. Sleep Med *14*, 1112-1122.

26. Werth, E., Achermann, P., and Borbely, A.A. (1996). Brain topography of the human sleep EEG: antero-posterior shifts of spectral power. Neuroreport *8*, 123-127.

27. Borbely, A.A. (1982). A two process model of sleep regulation. Hum Neurobiol *1*, 195-204.

28. Dijk, D.J., Brunner, D.P., Beersma, D.G., and Borbely, A.A. (1990). Electroencephalogram power density and slow wave sleep as a function of prior waking and circadian phase. Sleep *13*, 430-440.

29. Werth, E., Dijk, D.J., Achermann, P., and Borbely, A.A. (1996). Dynamics of the sleep EEG after an early evening nap: experimental data and simulations. Am J Physiol *271*, R501-510.

30. Kopp, C., Albrecht, U., Zheng, B., and Tobler, I. (2002). Homeostatic sleep regulation is preserved in mPer1 and mPer2 mutant mice. Eur J Neurosci *16*, 1099-1106.

31. Vyazovskiy, V.V., Ruijgrok, G., Deboer, T., and Tobler, I. (2006). Running wheel accessibility affects the regional electroencephalogram during sleep in mice. Cereb Cortex *16*, 328-336.

32. Skorucak, J., Arbon, E.L., Dijk, D.J., and Achermann, P. (2018). Response to chronic sleep restriction, extension, and subsequent total sleep deprivation in humans: adaptation or preserved sleep homeostasis? Sleep *41*.

33. Leemburg, S., Vyazovskiy, V.V., Olcese, U., Bassetti, C.L., Tononi, G., and Cirelli, C. (2010). Sleep homeostasis in the rat is preserved during chronic sleep restriction. Proc Natl Acad Sci U S A *107*, 15939-15944.

34. Akerstedt, T., Kecklund, G., Ingre, M., Lekander, M., and Axelsson, J. (2009). Sleep homeostasis during repeated sleep restriction and recovery: support from EEG dynamics. Sleep *32*, 217-222.

35. Trautmann, N., Foo, J.C., Frank, J., Witt, S.H., Streit, F., Treutlein, J., von Heydendorff, S.C., Gilles, M., Forstner, A.J., Ebner-Priemer, U., et al. (2018). Response to therapeutic sleep deprivation: a naturalistic study of clinical and genetic factors and post-treatment depressive symptom trajectory. Neuropsychopharmacology *43*, 2572-2577.

36. Riemann, D., and Berger, M. (1990). The effects of total sleep deprivation and subsequent treatment with clomipramine on depressive symptoms and sleep electroencephalography in patients with a major depressive disorder. Acta Psychiatr Scand *81*, 24-31.

37. Hombali, A., Seow, E., Yuan, Q., Chang, S.H.S., Satghare, P., Kumar, S., Verma, S.K., Mok, Y.M., Chong, S.A., and Subramaniam, M. (2019). Prevalence and correlates of sleep disorder symptoms in psychiatric disorders. Psychiatry Res *279*, 116-122.

38. Van der Heijden, K.B., Smits, M.G., Van Someren, E.J., and Gunning, W.B. (2005). Idiopathic chronic sleep onset insomnia in attention-deficit/hyperactivity disorder: a circadian rhythm sleep disorder. Chronobiol Int *22*, 559-570.

39. Partinen, M. (1997). Sleep disorder related to Parkinson's disease. J Neurol *244*, S3-6.

40. Sare, R.M., Levine, M., Hildreth, C., Picchioni, D., and Smith, C.B. (2016). Chronic sleep restriction during development can lead to long-lasting behavioral effects. Physiol Behav *155*, 208-217.

41. da Costa Souza, A., and Ribeiro, S. (2015). Sleep deprivation and gene expression. Curr Top Behav Neurosci *25*, 65-90.

42. Daniele, T., de Bruin, P.F.C., Rios, E.R.V., and de Bruin, V.M.S. (2017). Effects of exercise on depressive behavior and striatal levels of norepinephrine, serotonin and their metabolites in sleep-deprived mice. Behav Brain Res *332*, 16-22.

43. Lemons, A., Sare, R.M., and Beebe Smith, C. (2018). Chronic Sleep Deprivation in Mouse Pups by Means of Gentle Handling. J Vis Exp.

44. Serchov, T., Clement, H.W., Schwarz, M.K., Iasevoli, F., Tosh, D.K., Idzko, M., Jacobson, K.A., de Bartolomeis, A., Normann, C., Biber, K., et al. (2015). Increased Signaling via Adenosine A1 Receptors, Sleep Deprivation, Imipramine, and Ketamine Inhibit Depressive-like Behavior via Induction of Homer1a. Neuron *87*, 549-562.

45. Havekes, R., Park, A.J., Tudor, J.C., Luczak, V.G., Hansen, R.T., Ferri, S.L., Bruinenberg, V.M., Poplawski, S.G., Day, J.P., Aton, S.J., et al. (2016). Sleep deprivation causes memory deficits by negatively impacting neuronal connectivity in hippocampal area CA1. Elife *5*.

46. Dauvilliers, Y., Maret, S., and Tafti, M. (2005). Genetics of normal and pathological sleep in humans. Sleep Med Rev *9*, 91-100.

47. Shi, G., Xing, L., Wu, D., Bhattacharyya, B.J., Jones, C.R., McMahon, T., Chong, S.Y.C., Chen, J.A., Coppola, G., Geschwind, D., et al. (2019). A Rare Mutation of beta1-Adrenergic Receptor Affects Sleep/Wake Behaviors. Neuron *103*, 1044-1055 e1047.

48. He, Y., Jones, C.R., Fujiki, N., Xu, Y., Guo, B., Holder, J.L., Jr., Rossner, M.J., Nishino, S., and Fu, Y.H. (2009). The transcriptional repressor DEC2 regulates sleep length in mammals. Science *325*, 866-870.

49. McGinty, D.J., and Sterman, M.B. (1968). Sleep suppression after basal forebrain lesions in the cat. Science *160*, 1253-1255.

50. Laposky, A., Easton, A., Dugovic, C., Walisser, J., Bradfield, C., and Turek, F. (2005). Deletion of the mammalian circadian clock gene BMAL1/Mop3 alters baseline sleep architecture and the response to sleep deprivation. Sleep *28*, 395-409.

51. Sheward, W.J., Naylor, E., Knowles-Barley, S., Armstrong, J.D., Brooker, G.A., Seckl, J.R., Turek, F.W., Holmes, M.C., Zee, P.C., and Harmar, A.J. (2010). Circadian control of mouse heart rate and blood pressure by the suprachiasmatic nuclei: behavioral effects are more significant than direct outputs. PLoS One *5*, e9783.

52. Xu, Y., Padiath, Q.S., Shapiro, R.E., Jones, C.R., Wu, S.C., Saigoh, N., Saigoh, K., Ptacek, L.J., and Fu, Y.H. (2005). Functional consequences of a CKIdelta mutation causing familial advanced sleep phase syndrome. Nature *434*, 640-644.

53. Wisor, J.P., Pasumarthi, R.K., Gerashchenko, D., Thompson, C.L., Pathak, S., Sancar, A., Franken, P., Lein, E.S., and Kilduff, T.S. (2008). Sleep deprivation effects on circadian clock gene expression in the cerebral cortex parallel electroencephalographic differences among mouse strains. J Neurosci *28*, 7193-7201.

54. Shiromani, P.J., Xu, M., Winston, E.M., Shiromani, S.N., Gerashchenko, D., and Weaver, D.R. (2004). Sleep rhythmicity and homeostasis in mice with targeted disruption of mPeriod genes. Am J Physiol Regul Integr Comp Physiol *287*, R47-57.

55. Naylor, E., Bergmann, B.M., Krauski, K., Zee, P.C., Takahashi, J.S., Vitaterna, M.H., and Turek, F.W. (2000). The circadian clock mutation alters sleep homeostasis in the mouse. J Neurosci *20*, 8138-8143.

56. Franken, P., Dudley, C.A., Estill, S.J., Barakat, M., Thomason, R., O'Hara, B.F., and McKnight, S.L. (2006). NPAS2 as a transcriptional regulator of non-rapid eye movement sleep: genotype and sex interactions. Proc Natl Acad Sci U S A *103*, 7118-7123.

57. Hu, W.P., Li, J.D., Zhang, C., Boehmer, L., Siegel, J.M., and Zhou, Q.Y. (2007). Altered circadian and homeostatic sleep regulation in prokineticin 2-deficient mice. Sleep *30*, 247-256.

58. Frank, M.G., Stryker, M.P., and Tecott, L.H. (2002). Sleep and sleep homeostasis in mice lacking the 5-HT2c receptor. Neuropsychopharmacology *27*, 869-873.

59. Popa, D., Lena, C., Fabre, V., Prenat, C., Gingrich, J., Escourrou, P., Hamon, M., and Adrien, J. (2005). Contribution of 5-HT2 receptor subtypes to sleep-wakefulness and respiratory control, and functional adaptations in knock-out mice lacking 5-HT2A receptors. J Neurosci *25*, 11231-11238.

60. Dzirasa, K., Ribeiro, S., Costa, R., Santos, L.M., Lin, S.C., Grosmark, A., Sotnikova, T.D., Gainetdinov, R.R., Caron, M.G., and Nicolelis, M.A. (2006). Dopaminergic control of sleep-wake states. J Neurosci *26*, 10577-10589.

61. Wisor, J.P., Nishino, S., Sora, I., Uhl, G.H., Mignot, E., and Edgar, D.M. (2001). Dopaminergic role in stimulant-induced wakefulness. J Neurosci *21*, 1787-1794.

62. Ouyang, M., Hellman, K., Abel, T., and Thomas, S.A. (2004). Adrenergic signaling plays a critical role in the maintenance of waking and in the regulation of REM sleep. J Neurophysiol *92*, 2071-2082.

63. Anaclet, C., Parmentier, R., Ouk, K., Guidon, G., Buda, C., Sastre, J.P., Akaoka, H., Sergeeva, O.A., Yanagisawa, M., Ohtsu, H., et al. (2009). Orexin/hypocretin and histamine: distinct roles in the control of wakefulness demonstrated using knock-out mouse models. J Neurosci *29*, 14423-14438.

64. Parmentier, R., Ohtsu, H., Djebbara-Hannas, Z., Valatx, J.L., Watanabe, T., and Lin, J.S. (2002). Anatomical, physiological, and pharmacological characteristics of histidine decarboxylase knock-out mice: evidence for the role of brain histamine in behavioral and sleep-wake control. J Neurosci *22*, 7695-7711.

65. Cueni, L., Canepari, M., Lujan, R., Emmenegger, Y., Watanabe, M., Bond, C.T., Franken, P., Adelman, J.P., and Luthi, A. (2008). T-type Ca2+ channels, SK2 channels and SERCAs gate sleep-related oscillations in thalamic dendrites. Nat Neurosci *11*, 683-692.

66. Beuckmann, C.T., Sinton, C.M., Miyamoto, N., Ino, M., and Yanagisawa, M. (2003). N-type calcium channel alpha1B subunit (Cav2.2) knock-out mice display hyperactivity and vigilance state differences. J Neurosci *23*, 6793-6797.

67. Lee, J., Kim, D., and Shin, H.S. (2004). Lack of delta waves and sleep disturbances during non-rapid eye movement sleep in mice lacking alpha1G-subunit of T-type calcium channels. Proc Natl Acad Sci U S A *101*, 18195-18199.

68. Frank, M.G. (2006). The mystery of sleep function: current perspectives and future directions. Rev Neurosci *17*, 375-392.

69. Fang, J., Wang, Y., and Krueger, J.M. (1998). Effects of interleukin-1 beta on sleep are mediated by the type I receptor. Am J Physiol *274*, R655-660.

70. Laposky, A.D., Bradley, M.A., Williams, D.L., Bass, J., and Turek, F.W. (2008). Sleep-wake regulation is altered in leptin-resistant (db/db) genetically obese and diabetic mice. Am J Physiol Regul Integr Comp Physiol *295*, R2059-2066.

71. Obal, F., Jr., Alt, J., Taishi, P., Gardi, J., and Krueger, J.M. (2003). Sleep in mice with nonfunctional growth hormone-releasing hormone receptors. Am J Physiol Regul Integr Comp Physiol *284*, R131-139.

72. Graves, L.A., Hellman, K., Veasey, S., Blendy, J.A., Pack, A.I., and Abel, T. (2003). Genetic evidence for a role of CREB in sustained cortical arousal. J Neurophysiol *90*, 1152-1159.

73. Economo, C.V. (1930). Sleep as a problem of localization. J Nerv Ment Dis *71*, 249-259.

74. Saper, C.B., Chou, T.C., and Scammell, T.E. (2001). The sleep switch: hypothalamic control of sleep and wakefulness. Trends Neurosci *24*, 726-731.

75. Saper, C.B., Scammell, T.E., and Lu, J. (2005). Hypothalamic regulation of sleep and circadian rhythms. Nature *437*, 1257-1263.

76. Gong, H., McGinty, D., Guzman-Marin, R., Chew, K.T., Stewart, D., and Szymusiak, R. (2004). Activation of c-fos in GABAergic neurones in the preoptic area during sleep and in response to sleep deprivation. J Physiol *556*, 935-946.

77. Sherin, J.E., Shiromani, P.J., McCarley, R.W., and Saper, C.B. (1996). Activation of ventrolateral preoptic neurons during sleep. Science *271*, 216-219.

78. Sherin, J.E., Elmquist, J.K., Torrealba, F., and Saper, C.B. (1998). Innervation of histaminergic tuberomammillary neurons by GABAergic and galaninergic neurons in the ventrolateral preoptic nucleus of the rat. J Neurosci *18*, 4705-4721.

79. Saito, Y.C., Maejima, T., Nishitani, M., Hasegawa, E., Yanagawa, Y., Mieda, M., and Sakurai, T. (2018). Monoamines Inhibit GABAergic Neurons in Ventrolateral Preoptic Area That Make Direct Synaptic Connections to Hypothalamic Arousal Neurons. J Neurosci *38*, 6366-6378.

80. Takahashi, K., Lin, J.S., and Sakai, K. (2009). Characterization and mapping of sleep-waking specific neurons in the basal forebrain and preoptic hypothalamus in mice. Neuroscience *161*, 269-292.

81. Gaus, S.E., Strecker, R.E., Tate, B.A., Parker, R.A., and Saper, C.B. (2002). Ventrolateral preoptic nucleus contains sleep-active, galaninergic neurons in multiple mammalian species. Neuroscience *115*, 285-294.

82. Chung, S., Weber, F., Zhong, P., Tan, C.L., Nguyen, T.N., Beier, K.T., Hormann, N., Chang, W.C., Zhang, Z., Do, J.P., et al. (2017). Identification of preoptic sleep neurons using retrograde labelling and gene profiling. Nature *545*, 477-481.

83. Kroeger, D., Absi, G., Gagliardi, C., Bandaru, S.S., Madara, J.C., Ferrari, L.L., Arrigoni, E., Munzberg, H., Scammell, T.E., Saper, C.B., et al. (2018). Galanin neurons in the ventrolateral preoptic area promote sleep and heat loss in mice. Nat Commun *9*, 4129.

84. Reichert, S., Pavon Arocas, O., and Rihel, J. (2019). The Neuropeptide Galanin Is Required for Homeostatic Rebound Sleep following Increased Neuronal Activity. Neuron *104*, 370-384 e375.

85. Lu, J., Greco, M.A., Shiromani, P., and Saper, C.B. (2000). Effect of lesions of the ventrolateral preoptic nucleus on NREM and REM sleep. J Neurosci *20*, 3830-3842.

86. Anaclet, C., Lin, J.S., Vetrivelan, R., Krenzer, M., Vong, L., Fuller, P.M., and Lu, J. (2012). Identification and characterization of a sleep-active cell group in the rostral medullary brainstem. J Neurosci *32*, 17970-17976.

87. Fuller, P.M., Sherman, D., Pedersen, N.P., Saper, C.B., and Lu, J. (2011). Reassessment of the structural basis of the ascending arousal system. J Comp Neurol *519*, 933-956.

88. Anaclet, C., Ferrari, L., Arrigoni, E., Bass, C.E., Saper, C.B., Lu, J., and Fuller, P.M. (2014). The GABAergic parafacial zone is a medullary slow wave sleep-promoting center. Nat Neurosci *17*, 1217-1224.

89. Anaclet, C., Griffith, K., and Fuller, P.M. (2018). Activation of the GABAergic Parafacial Zone Maintains Sleep and Counteracts the Wake-Promoting Action of the Psychostimulants Armodafinil and Caffeine. Neuropsychopharmacology *43*, 415-425.

90. Oishi, Y., Suzuki, Y., Takahashi, K., Yonezawa, T., Kanda, T., Takata, Y., Cherasse, Y., and Lazarus, M. (2017). Activation of ventral tegmental area dopamine neurons produces wakefulness through dopamine D2-like receptors in mice. Brain Struct Funct *222*, 2907-2915.

91. Dahan, L., Astier, B., Vautrelle, N., Urbain, N., Kocsis, B., and Chouvet, G. (2007). Prominent burst firing of dopaminergic neurons in the ventral tegmental area during paradoxical sleep. Neuropsychopharmacology *32*, 1232-1241.

92. Qiu, M.H., Zhong, Z.G., Chen, M.C., and Lu, J. (2019). Nigrostriatal and mesolimbic control of sleep-wake behavior in rat. Brain Struct Funct *224*, 2525-2535.

93. Yu, X., Li, W., Ma, Y., Tossell, K., Harris, J.J., Harding, E.C., Ba, W., Miracca, G., Wang, D., Li, L., et al. (2019). GABA and glutamate neurons in the VTA regulate sleep and wakefulness. Nat Neurosci *22*, 106-119.

94. Chowdhury, S., Matsubara, T., Miyazaki, T., Ono, D., Fukatsu, N., Abe, M., Sakimura, K., Sudo, Y., and Yamanaka, A. (2019). GABA neurons in the ventral tegmental area regulate non-rapid eye movement sleep in mice. Elife *8*.

95. Takata, Y., Oishi, Y., Zhou, X.Z., Hasegawa, E., Takahashi, K., Cherasse, Y., Sakurai, T., and Lazarus, M. (2018). Sleep and Wakefulness Are Controlled by Ventral Medial Midbrain/Pons GABAergic Neurons in Mice. J Neurosci *38*, 10080-10092.

96. Honda, T., Takata, Y., Cherasse, Y., Mizuno, S., Sugiyama, F., Takahashi, S., Funato, H., Yanagisawa, M., Lazarus, M., and Oishi, Y. (2020). Ablation of Ventral Midbrain/Pons GABA Neurons Induces Mania-like Behaviors with Altered Sleep Homeostasis and Dopamine D2R-mediated Sleep Reduction. iScience *23*, 101240.

97. Oishi, Y., Xu, Q., Wang, L., Zhang, B.J., Takahashi, K., Takata, Y., Luo, Y.J., Cherasse, Y., Schiffmann, S.N., de Kerchove d'Exaerde, A., et al. (2017). Slow-wave sleep is controlled by a subset of nucleus accumbens core neurons in mice. Nat Commun *8*, 734.

98. Yuan, X.S., Wang, L., Dong, H., Qu, W.M., Yang, S.R., Cherasse, Y., Lazarus, M., Schiffmann, S.N., d'Exaerde, A.K., Li, R.X., et al. (2017). Striatal adenosine A2A receptor neurons control active-period sleep via parvalbumin neurons in external globus pallidus. Elife *6*.

99. Liu, K., Kim, J., Kim, D.W., Zhang, Y.S., Bao, H., Denaxa, M., Lim, S.A., Kim, E., Liu, C., Wickersham, I.R., et al. (2017). Lhx6-positive GABA-releasing neurons of the zona incerta promote sleep. Nature *548*, 582-+.

100. Yang, S.R., Hu, Z.Z., Luo, Y.J., Zhao, Y.N., Sun, H.X., Yin, D., Wang, C.Y., Yan, Y.D., Wang, D.R., Yuan, X.S., et al. (2018). The rostromedial tegmental nucleus is essential for non-rapid eye movement sleep. PLoS Biol *16*, e2002909.

101. Ma, C., Zhong, P., Liu, D., Barger, Z.K., Zhou, L., Chang, W.C., Kim, B., and Dan, Y. (2019). Sleep Regulation by Neurotensinergic Neurons in a Thalamo-Amygdala Circuit. Neuron *103*, 323-334 e327.

102. Xu, M., Chung, S., Zhang, S., Zhong, P., Ma, C., Chang, W.C., Weissbourd, B., Sakai, N., Luo, L., Nishino, S., et al. (2015). Basal forebrain circuit for sleep-wake control. Nat Neurosci *18*, 1641-1647.

103. Gompf, H.S., and Anaclet, C. (2020). The neuroanatomy and neurochemistry of sleep-wake control. Curr Opin Physiol *15*, 143-151.

104. Eckert, D., Buhl, S., Weber, S., Jager, R., and Schorle, H. (2005). The AP-2 family of transcription factors. Genome Biol *6*, 246.

105. Nitta, K.R., Jolma, A., Yin, Y., Morgunova, E., Kivioja, T., Akhtar, J., Hens, K., Toivonen, J., Deplancke, B., Furlong, E.E., et al. (2015). Conservation of transcription factor binding specificities across 600 million years of bilateria evolution. Elife *4*.

106. Hoffman, T.L., Javier, A.L., Campeau, S.A., Knight, R.D., and Schilling, T.F. (2007). Tfap2 transcription factors in zebrafish neural crest development and ectodermal evolution. J Exp Zool B Mol Dev Evol *308*, 679-691.

107. DuBuc, T.Q., Schnitzler, C.E., Chrysostomou, E., McMahon, E.T., Febrimarsa, Gahan, J.M., Buggie, T., Gornik, S.G., Hanley, S., Barreira, S.N., et al. (2020). Transcription factor AP2 controls cnidarian germ cell induction. Science *367*, 757-762.

108. Mitchell, P.J., Timmons, P.M., Hebert, J.M., Rigby, P.W., and Tjian, R. (1991). Transcription factor AP-2 is expressed in neural crest cell lineages during mouse embryogenesis. Genes Dev *5*, 105-119.

109. Zhao, F., Lufkin, T., and Gelb, B.D. (2003). Expression of Tfap2d, the gene encoding the transcription factor Ap-2 delta, during mouse embryogenesis. Gene Expr Patterns *3*, 213-217.

110. Feng, W., and Williams, T. (2003). Cloning and characterization of the mouse AP-2 epsilon gene: a novel family member expressed in the developing olfactory bulb. Mol Cell Neurosci *24*, 460-475.

111. Hesse, K., Vaupel, K., Kurt, S., Buettner, R., Kirfel, J., and Moser, M. (2011). AP-2delta is a crucial transcriptional regulator of the posterior midbrain. PLoS One *6*, e23483.

112. Moser, M., Pscherer, A., Roth, C., Becker, J., Mucher, G., Zerres, K., Dixkens, C., Weis, J., Guay-Woodford, L., Buettner, R., et al. (1997). Enhanced apoptotic cell death of renal epithelial cells in mice lacking transcription factor AP-2beta. Genes Dev *11*, 1938-1948.

113. Zhang, J., Hagopian-Donaldson, S., Serbedzija, G., Elsemore, J., Plehn-Dujowich, D., McMahon, A.P., Flavell, R.A., and Williams, T. (1996). Neural tube, skeletal and body wall defects in mice lacking transcription factor AP-2. Nature *381*, 238-241.

114. Mani, A., Radhakrishnan, J., Farhi, A., Carew, K.S., Warnes, C.A., Nelson-Williams, C., Day, R.W., Pober, B., State, M.W., and Lifton, R.P. (2005). Syndromic patent ductus arteriosus: evidence for haploinsufficient TFAP2B mutations and identification of a linked sleep disorder. Proc Natl Acad Sci U S A *102*, 2975-2979.

115. Rothstein, M., and Simoes-Costa, M. (2020). Heterodimerization of TFAP2 pioneer factors drives epigenomic remodeling during neural crest specification. Genome Res *30*, 35-48.

116. Satoda, M., Zhao, F., Diaz, G.A., Burn, J., Goodship, J., Davidson, H.R., Pierpont, M.E., and Gelb, B.D. (2000). Mutations in TFAP2B cause Char syndrome, a familial form of patent ductus arteriosus. Nat Genet *25*, 42-46.

117. Kucherenko, M.M., Ilangovan, V., Herzig, B., Shcherbata, H.R., and Bringmann, H. (2016). TfAP-2 is required for night sleep in Drosophila. BMC Neurosci *17*, 72.

118. Chazaud, C., Oulad-Abdelghani, M., Bouillet, P., Decimo, D., Chambon, P., and Dolle, P. (1996). AP-2.2, a novel gene related to AP-2, is expressed in the forebrain, limbs and face during mouse embryogenesis. Mech Dev *54*, 83-94.

119. Hu, Y., Korovaichuk, A., Astiz, M., Schroeder, H., Islam, R., Barrenetxea, J., Fischer, A., Oster, H., and Bringmann, H. (2020). Functional Divergence of Mammalian TFAP2a and TFAP2b Transcription Factors for Bidirectional Sleep Control. Genetics *216*, 735-752.

120. Yang, N., Chanda, S., Marro, S., Ng, Y.H., Janas, J.A., Haag, D., Ang, C.E., Tang, Y., Flores, Q., Mall, M., et al. (2017). Generation of pure GABAergic neurons by transcription factor programming. Nat Methods *14*, 621-628.

121. Hori, K., Cholewa-Waclaw, J., Nakada, Y., Glasgow, S.M., Masui, T., Henke, R.M., Wildner, H., Martarelli, B., Beres, T.M., Epstein, J.A., et al. (2008). A nonclassical bHLH Rbpj transcription factor complex is required for specification of GABAergic neurons independent of Notch signaling. Genes Dev *22*, 166-178.

122. Letinic, K., Zoncu, R., and Rakic, P. (2002). Origin of GABAergic neurons in the human neocortex. Nature *417*, 645-649.

123. Zainolabidin, N., Kamath, S.P., Thanawalla, A.R., and Chen, A.I. (2017). Distinct Activities of Tfap2A and Tfap2B in the Specification of GABAergic Interneurons in the Developing Cerebellum. Front Mol Neurosci *10*, 281.

124. Holland, P.W., and Takahashi, T. (2005). The evolution of homeobox genes: Implications for the study of brain development. Brain Res Bull *66*, 484-490.

125. Reichert, H., and Bello, B. (2010). Hox genes and brain development in Drosophila. Adv Exp Med Biol *689*, 145-153.

126. Tumpel, S., Wiedemann, L.M., and Krumlauf, R. (2009). Hox genes and segmentation of the vertebrate hindbrain. Curr Top Dev Biol *88*, 103-137.

127. Narita, Y., and Rijli, F.M. (2009). Hox genes in neural patterning and circuit formation in the mouse hindbrain. Curr Top Dev Biol *88*, 139-167.

128. Pearson, J.C., Lemons, D., and McGinnis, W. (2005). Modulating Hox gene functions during animal body patterning. Nat Rev Genet *6*, 893-904.

129. Graham, A., Maden, M., and Krumlauf, R. (1991). The murine Hox-2 genes display dynamic dorsoventral patterns of expression during central nervous system development. Development *112*, 255-264.

130. Drgonova, J., Liu, Q.R., Hall, F.S., Krieger, R.M., and Uhl, G.R. (2007). Deletion of v7-3 (SLC6A15) transporter allows assessment of its roles in synaptosomal proline uptake, leucine uptake and behaviors. Brain Res *1183*, 10-20.

131. Iversen, L.L. (1963). The Uptake of Noradrenaline by the Isolated Perfused Rat Heart. Br J Pharmacol Chemother *21*, 523-537.

132. Kim, C.H., Waldman, I.D., Blakely, R.D., and Kim, K.S. (2008). Functional gene variation in the human norepinephrine transporter: association with attention deficit hyperactivity disorder. Ann N Y Acad Sci *1129*, 256-260.

133. Ramoz, N., Boni, C., Downing, A.M., Close, S.L., Peters, S.L., Prokop, A.M., Allen, A.J., Hamon, M., Purper-Ouakil, D., and Gorwood, P. (2009). A haplotype of the norepinephrine transporter (Net) gene Slc6a2 is associated with clinical response to atomoxetine in attention-deficit hyperactivity disorder (ADHD). Neuropsychopharmacology *34*, 2135-2142.

134. Son, W.Y., Lee, H.J., Yoon, H.K., Kang, S.G., Park, Y.M., Yang, H.J., Choi, J.E., An, H., Seo, H.K., and Kim, L. (2014). Gaba transporter SLC6A11 gene polymorphism associated with tardive dyskinesia. Nord J Psychiatry *68*, 123-128.

135. Broer, A., Tietze, N., Kowalczuk, S., Chubb, S., Munzinger, M., Bak, L.K., and Broer, S. (2006). The orphan transporter v7-3 (slc6a15) is a Na+-dependent neutral amino acid transporter (B0AT2). Biochem J *393*, 421-430.

136. Takanaga, H., Mackenzie, B., Peng, J.B., and Hediger, M.A. (2005). Characterization of a branched-chain amino-acid transporter SBAT1 (SLC6A15) that is expressed in human brain. Biochem Biophys Res Commun *337*, 892-900.

137. Kohli, M.A., Lucae, S., Saemann, P.G., Schmidt, M.V., Demirkan, A., Hek, K., Czamara, D., Alexander, M., Salyakina, D., Ripke, S., et al. (2011). The neuronal transporter gene SLC6A15 confers risk to major depression. Neuron *70*, 252-265.

138. Santarelli, S., Wagner, K.V., Labermaier, C., Uribe, A., Dournes, C., Balsevich, G., Hartmann, J., Masana, M., Holsboer, F., Chen, A., et al. (2016). SLC6A15, a novel stress vulnerability candidate, modulates anxiety and depressive-like behavior: involvement of the glutamatergic system. Stress *19*, 83-90.

139. Romero, M.F., Chen, A.P., Parker, M.D., and Boron, W.F. (2013). The SLC4 family of bicarbonate (HCO(3)(-)) transporters. Mol Aspects Med *34*, 159-182.

140. Groger, N., Vitzthum, H., Frohlich, H., Kruger, M., Ehmke, H., Braun, T., and Boettger, T. (2012). Targeted mutation of SLC4A5 induces arterial hypertension and renal metabolic acidosis. Hum Mol Genet *21*, 1025-1036.

141. Jacobs, S., Ruusuvuori, E., Sipila, S.T., Haapanen, A., Damkier, H.H., Kurth, I., Hentschke, M., Schweizer, M., Rudhard, Y., Laatikainen, L.M., et al. (2008). Mice with targeted Slc4a10 gene disruption have small brain ventricles and show reduced neuronal excitability. Proc Natl Acad Sci U S A *105*, 311-316.

142. Sinning, A., Liebmann, L., and Hubner, C.A. (2015). Disruption of Slc4a10 augments neuronal excitability and modulates synaptic short-term plasticity. Front Cell Neurosci *9*, 223.

143. Tulen, J.H., Man in't Veld, A.J., Mechelse, K., and Boomsma, F. (1990). Sleep patterns in congenital dopamine beta-hydroxylase deficiency. J Neurol *237*, 98-102.

144. Robertson, D., Haile, V., Perry, S.E., Robertson, R.M., Phillips, J.A., 3rd, and Biaggioni, I. (1991). Dopamine beta-hydroxylase deficiency. A genetic disorder of cardiovascular regulation. Hypertension *18*, 1-8.

145. Hunsley, M.S., and Palmiter, R.D. (2003). Norepinephrine-deficient mice exhibit normal sleep-wake states but have shorter sleep latency after mild stress and low doses of amphetamine. Sleep *26*, 521-526.

146. Yamaguchi, H., Hopf, F.W., Li, S.B., and de Lecea, L. (2018). In vivo cell type-specific CRISPR knockdown of dopamine beta hydroxylase reduces locus coeruleus evoked wakefulness. Nat Commun *9*, 5211.

147. Eban-Rothschild, A., Rothschild, G., Giardino, W.J., Jones, J.R., and de Lecea, L. (2016). VTA dopaminergic neurons regulate ethologically relevant sleep-wake behaviors. Nat Neurosci *19*, 1356-1366.

148. Singh, C., Oikonomou, G., and Prober, D.A. (2015). Norepinephrine is required to promote wakefulness and for hypocretin-induced arousal in zebrafish. Elife *4*, e07000.

149. Dlugos, A.M., Hamidovic, A., Palmer, A.A., and de Wit, H. (2009). Further evidence of association between amphetamine response and SLC6A2 gene variants. Psychopharmacology (Berl) *206*, 501-511.

150. Ohtoshi, A., and Behringer, R.R. (2004). Neonatal lethality, dwarfism, and abnormal brain development in Dmbx1 mutant mice. Mol Cell Biol *24*, 7548-7558.

151. Ohtoshi, A., Nishijima, I., Justice, M.J., and Behringer, R.R. (2002). Dmbx1, a novel evolutionarily conserved paired-like homeobox gene expressed in the brain of mouse embryos. Mech Dev *110*, 241-244.

152. Wong, L., Weadick, C.J., Kuo, C., Chang, B.S., and Tropepe, V. (2010). Duplicate dmbx1 genes regulate progenitor cell cycle and differentiation during zebrafish midbrain and retinal development. BMC Dev Biol *10*, 100.

153. Fujimoto, W., Shiuchi, T., Miki, T., Minokoshi, Y., Takahashi, Y., Takeuchi, A., Kimura, K., Saito, M., Iwanaga, T., and Seino, S. (2007). Dmbx1 is essential in agouti-related protein action. Proc Natl Acad Sci U S A *104*, 15514-15519.

154. Petryniak, M.A., Potter, G.B., Rowitch, D.H., and Rubenstein, J.L. (2007). Dlx1 and Dlx2 control neuronal versus oligodendroglial cell fate acquisition in the developing forebrain. Neuron *55*, 417-433.

155. Barretto, N., Zhang, H., Powell, S.K., Fernando, M.B., Zhang, S., Flaherty, E.K., Ho, S.M., Slesinger, P.A., Duan, J., and Brennand, K.J. (2020). ASCL1- and DLX2-induced GABAergic neurons from hiPSC-derived NPCs. J Neurosci Methods *334*, 108548.

156. de Melo, J., Du, G., Fonseca, M., Gillespie, L.A., Turk, W.J., Rubenstein, J.L., and Eisenstat, D.D. (2005). Dlx1 and Dlx2 function is necessary for terminal differentiation and survival of late-born retinal ganglion cells in the developing mouse retina. Development *132*, 311-322.

157. Colasante, G., Collombat, P., Raimondi, V., Bonanomi, D., Ferrai, C., Maira, M., Yoshikawa, K., Mansouri, A., Valtorta, F., Rubenstein, J.L., et al. (2008). Arx is a direct target of Dlx2 and thereby contributes to the tangential migration of GABAergic interneurons. J Neurosci *28*, 10674-10686.

158. Robledo, R.F., Rajan, L., Li, X., and Lufkin, T. (2002). The Dlx5 and Dlx6 homeobox genes are essential for craniofacial, axial, and appendicular skeletal development. Genes Dev *16*, 1089-1101.

159. Kuwajima, T., Nishimura, I., and Yoshikawa, K. (2006). Necdin promotes GABAergic neuron differentiation in cooperation with Dlx homeodomain proteins. J Neurosci *26*, 5383-5392.

160. Nakai, A., Fujiyama, T., Nagata, N., Kashiwagi, M., Ikkyu, A., Takagi, M., Tatsuzawa, C., Tanaka, K., Kakizaki, M., Kanuka, M., et al. (2020). Sleep Architecture in Mice Is Shaped by the Transcription Factor AP-2beta. Genetics *216*, 753-764.

161. Veraksa, A., Del Campo, M., and McGinnis, W. (2000). Developmental patterning genes and their conserved functions: from model organisms to humans. Mol Genet Metab *69*, 85-100.

162. Turek, M., Besseling, J., Spies, J.P., Konig, S., and Bringmann, H. (2016). Sleep-active neuron specification and sleep induction require FLP-11 neuropeptides to systemically induce sleep. Elife *5*.

163. Borbely, A.A., Daan, S., Wirz-Justice, A., and Deboer, T. (2016). The two-process model of sleep regulation: a reappraisal. J Sleep Res *25*, 131-143.

164. Fukumoto, K., Tamada, K., Toya, T., Nishino, T., Yanagawa, Y., and Takumi, T. (2018). Identification of genes regulating GABAergic interneuron maturation. Neurosci Res *134*, 18-29.

165. Bindea, G., Mlecnik, B., Hackl, H., Charoentong, P., Tosolini, M., Kirilovsky, A., Fridman, W.H., Pages, F., Trajanoski, Z., and Galon, J. (2009). ClueGO: a Cytoscape plug-in to decipher functionally grouped gene ontology and pathway annotation networks. Bioinformatics *25*, 1091-1093.

Curriculum Vitae

Yang Hu **E-mail:** yang.hu@mpibpc.mpg.de

EDUCATION

Max Planck Institute for Biophysical Chemistry, Goettingen, Germany Sep, 2017- Present

PhD Candidate

Sun Yat-sen University, Guangzhou, China Sep, 2012- Jun, 2015

M.S. in Pharmacology

Wuhan University of Science and Technology, Wuhan, China Sep, 2008- Jun, 2012

B.S. in Pharmacy

JOURNAL PUBLICATIONS

Hu, Y., Korovaichuk, A., Astiz, M., Schroeder, H., Islam, R., Barrenetxea, J., Fischer, A., Oster, H., and Bringmann, H. (2020). Functional Divergence of Mammalian TFAP2a and TFAP2b Transcription Factors for Bidirectional Sleep Control. Genetics 216, 735-752.

Danyang Liu, **Yang Hu** (co-first author), Zhuzhu, Juncheng Pan, Yijun Huang. (2017) Microorganism-induced multidrug resistance of hepatocarcinoma requires the interaction of P37 and Annexin A2. PLoS ONE 12(10).

Yang Hu, Wenting Ding, Xiaonan Zhu, Ruzhu Chen, Xuelan Wang. (2015) Olfactory dysfunctions and decreased nitric oxide production in the brain of human P301L tau transgenic mice. Neurochem Res; 41: 722.

RESEARCH EXPERIENCE

Sleep and Waking Group, MPI for Biophysical Chemistry Sep, 2017- Present

PhD Candidate

Thesis adviser: Prof. Dr. Henrik Bringmann

- Sleep and waking characterization of transcription factor mutants in mice.

Department of Pharmacology, Sun Yat-sen University

Research assistant Jun, 2015- 2017

Research Adviser: Dr. Yijun Huang

- Investigate drug resistance of chemotherapeutic agents and identification of cancer stem cells.

Department of Pharmacology, Sun Yat-sen University

Master training Sep, 2012- Jun, 2015

Research Adviser: Dr. Xuelan Wang

- Investigate the relationship between spatial and olfactory behavioral changes and the alternations of nitric oxide levels in different brain areas of the tau transgenic mice.

TECHNICAL SKIILS

Programming: MATLAB and R studio

EEG surggery and recordings in mouse models

Xenograft model antitumor assays: build and experiment on human tumor xenograft in nude mice

Molecular and Cellular Biology skills: PCR; Western Blot; Immunofluorescence (Confocal Microscopy); Bielschowsky Silver Staining (Frozen Sectioning Technique); Flow Cytometry.

Cell culture: primary neuron culture (usually from hippocampus/cerebellum of newborn mice or rats), primary mouse bone marrow cell culture, cancer cell lines (e.g. SH-SY5Y).

Behavioral tests: Morris Water Maze (Spatial learning and memory); Buried Food Test (Olfactory detection); Odor discrimination test (Olfactory discrimination); Depressive-like behavior test; Fear conditioning; Open field test.

CONFERENCE PRESENTATIONS

Oral presentation: Sleep and waking characterization of transcription factor mutants in mice. Retreat of Göttingen Graduate School for Neurosciences, Biophysics, and Molecular Biosciences, February 23, 2018.